NASA CR- 143716

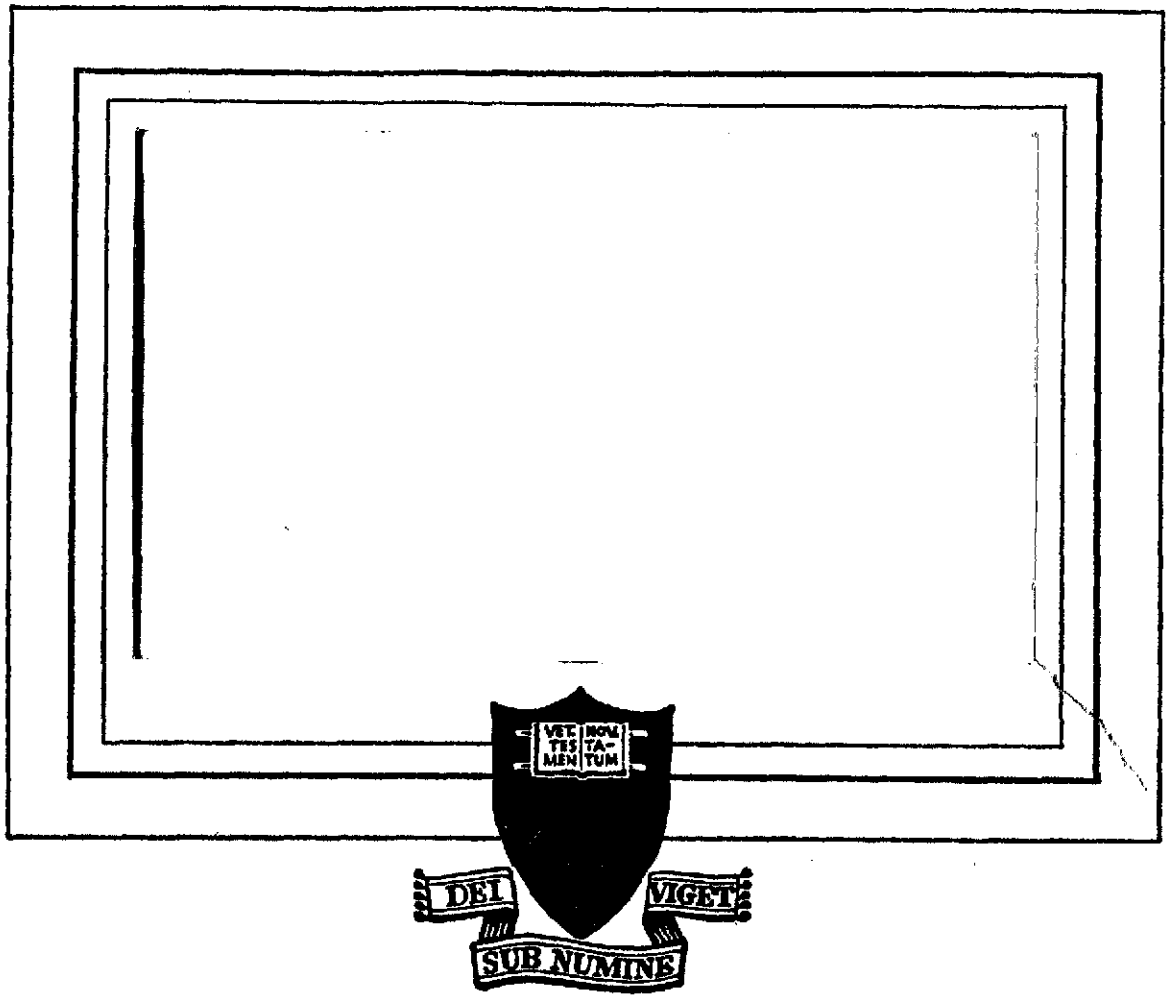

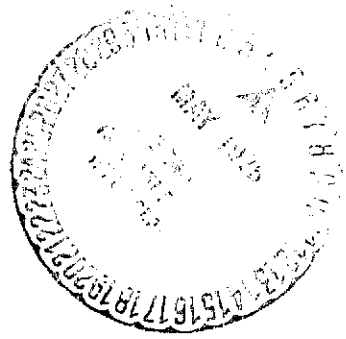

PRINCETON UNIVERSITY

(NASA-CR-143716) STUDY OF PERMANENT MAGNET FOCUSING FOR ASTRONOMICAL CAMERA TUBES Final Report (Princeton Univ.) 109 p HC $5.25 CSCL 03A

N75-22218

Unclas
G3/89 18629

PRINCETON UNIVERSITY
Department of Astrophysical Sciences
Princeton, New Jersey
08540

STUDY OF PERMANENT MAGNET FOCUSING FOR ASTRONOMICAL CAMERA TUBES

FINAL REPORT

NATIONAL AERONAUTICS AND SPACE ADMINISTRATION
Contract No.: NAS 5-20507

By: D.C. Long
J.L. Lowrance

February 28, 1975

ABSTRACT

This study is devoted to developing a design of a permanent magnet assembly (PMA) useful as the magnetic focusing unit for the 35 and 70 mm (diagonal) format SEC tubes. Detailed PMA designs for both tubes are given, and all data on their magnetic configuration, size, weight and structure of magnetic shields adequate to screen the camera tube from the earth's magnetic field are presented. A digital computer is used for the PMA design simulations. The expected operational performance of the PMA is ascertained through the calculation of a series of photoelectron trajectories. Their determined performance appears to be excellent.

A large volume where the magnetic field uniformity is greater than 0.5% appears obtainable, as shown in Figures 12 through 15. The point spread function (PSF) and modulation transfer function (MTF) shown in Figures 28-30 indicate nearly ideal performance. The MTF at 20 cycles per mm exceeds 90%. The weight and volume appear tractable for the Large Space Telescope and ground based applications. In a follow on program, a prototype of the 35 mm format design will be fabricated and evaluated.

TABLE OF CONTENT

LIST OF FIGURES

LIST OF TABLES

I. INTRODUCTION

The SEC tube is a television camera tube sometimes referred to as the SEC-vidicon or SEC-orthicon. It is shown schematically in Figure 1. Light falling on the photocathode produces photoelectrons that are accelerated by a uniform electric field and focused by the electric field and a parallel magnetic field on a target. The photoelectrons penetrate the thin dielectric membrane target where they are multiplied via secondary electron generation. An electric field across the thin dielectric target membrane sweeps the secondary electrons out of the dielectric region. The stored image consists of the positive charge left by the removal of the secondary electrons released by the incident photoelectrons. The stored charge is read out by scanning the target with a focused electron beam.

The optimum accelerating voltage to maximize the target multiplication is in the order of 7 to 10 thousand volts. With the usual target to photocathode spacing of 11.4 cm the magnetic focus field must be approximately 80 gauss. The relationship between these parameters is:

$$\ell = 10.59\, n\, B^{-1} V^{1/2}$$

where ℓ is the photocathode to target spacing in centimeters, B is the focus field in gauss, V is the accelerating potential in volts, and n is the number of Larmor loops made by electrons as they move from the photocathode to the target. The electron gun used for reading out the target is normally operated at the same magnetic field but lower voltage so the gun electrons execute 4 loops as they move between the gun aperture and the target.

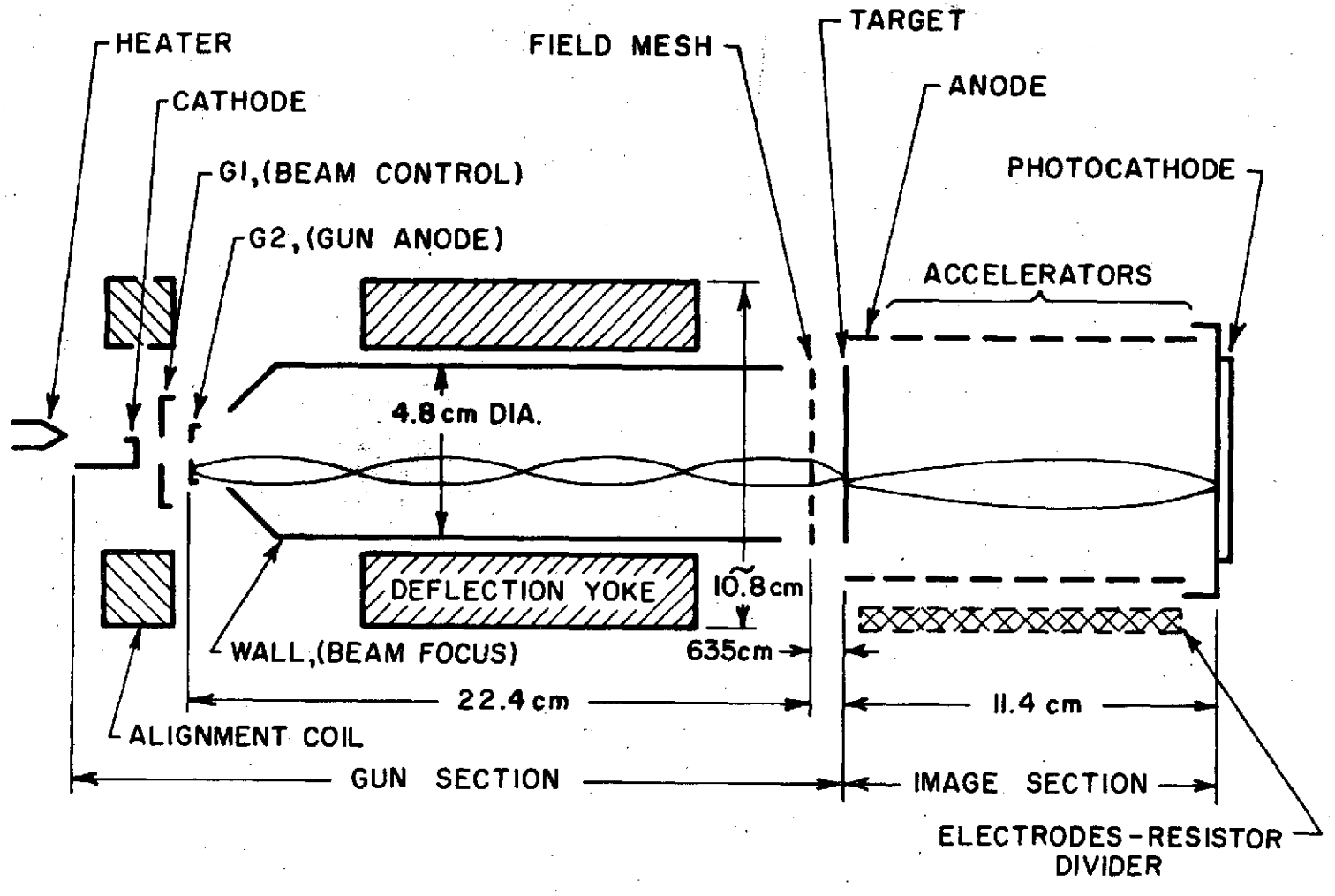

Fig. 1 - SEC and Readout Coils Schematic

Permanent magnets have been used to generate the focus field for image intensifier and traveling wave tubes in numerous applications. They have not been used to focus television camera tubes except on an experimental basis. A main incentive for using permanent magnets for focusing TV tubes is the elimination of the heating caused by the power dissipation within the solenoid electromagnet that is usually used as the focusing element. For a fixed volume electromagnet the power dissipation is proportional to the square of the magnetic field, i.e., doubling the field takes four times the power. As the magnetic field required to focus television tubes is often lower than that employed for image intensifiers, the thermal problem is relatively minor and television camera designers have preferred to use solenoid electromagnets which are simple to design and manufacture. However, in astronomical applications it is important that the thermal emission from the photocathode of television camera tubes be minimized in order to limit the background signal from that source. Usually the photocathode window is refrigerated in some manner to keep the temperature below 0°C.

Therefore, there is a system design tradeoff between the use of a solenoid or a PMA that depends on the difficulty of refrigerating the window and the difficulty involved in using permanent magnets to generate the focus field. This tradeoff is of considerable interest in low-light level applications of TV tubes as envisioned for the Large Space Telescope (LST), where there is the additional requirement to minimize thermal transients within the instrument compartment while providing the means of cooling the photocathode from the ambient temperature of +20°C down to -10°C.

It should be noted that magnetic focus is employed rather than electrostatic focus because of the aberrations associated with the latter. Also, the spherical photocathode required for electrostatic focus systems is most difficult to accommodate where sensitivity in the far UV is desired.

Prior to this study Princeton had, as a part of its overall astronomical image sensor development program (NSR 31-001-236), designed a permanent magnet focus assembly (PMA). The design concept is shown schematically in Figure 2. This symmetrical assembly consists of two permanent magnets located at opposite ends of the PMA unit, which in addition includes an iron "profile" tube, two outerface iron shunts, and an outer cylinder iron shunt. The tapered wall thickness of the "profile" tube (the inner cylinder), serves to maintain a constant flux density within the focusing region. A computer program was used to calculate the flux density and magnetizing force in the various iron parts and in the inner and outer air space.

A prototype PMA was fabricated. The resultant field came close to that calculated but the region of sufficiently uniform field was found to be too short for the 35 mm format SEC tube. Because of the promising preliminary results, the present study has taken this design as its starting point.

II. PERMANENT MAGNET FOCUS ASSEMBLY DESIGN

K. Wakefield of Princeton University's Plasma Physics Laboratory devised the toroidal PMA concept shown in Figure 2, in order to generate the long, axially symmetric, uniform magnetic field required to focus SEC television tubes. He also developed a special computer program ("FINE") that performs the calculations necessary to delineate the PMA's magnetic qualities.

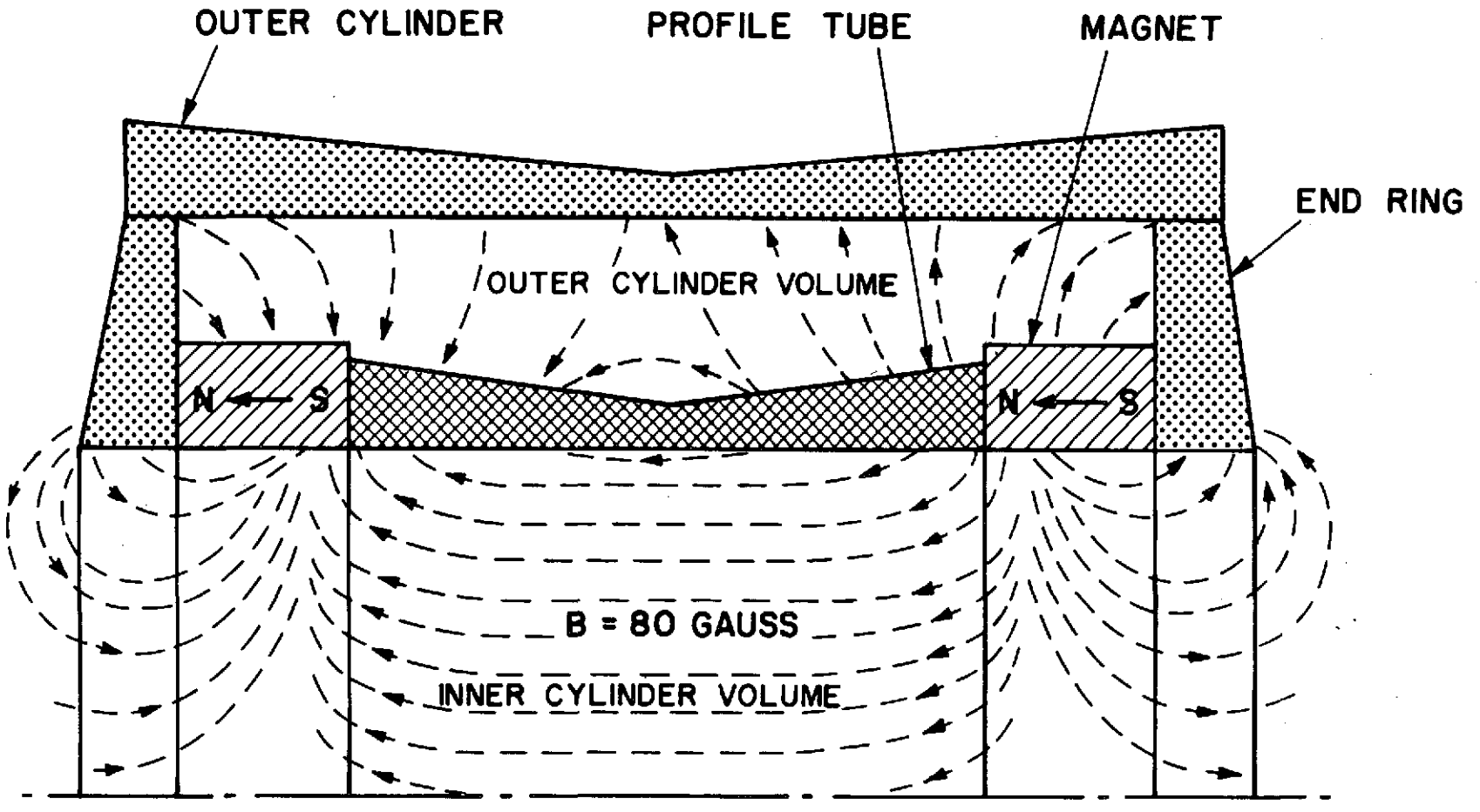

THICKNESS OF PROFILE TUBE IS TAPERED SUCH THAT THE FLUX DENSITY (B) IN THE IRON IS CONSTANT. THE MAGNETIZING FORCE (H) REQUIRED TO SUSTAIN THIS FIELD IS 80, THUS PRODUCING AN AXIAL FIELD OF 80 GAUSS WITHIN THE INTERIOR OF THE CYLINDER.

Fig. 2 - Permanent Magnet Assembly (PMA) Schematic

As the PMA design is cylindrically symmetric, the program works on one quarter of a longitudinal section. The magnetomotive forces (MMFs) are represented in two, two-dimensional arrays; one for the inner cylinder volume, the volume within the profile tube, and the second for the outer cylinder volume, the volume between the profile tube and the outer cylinder. To model the assembly in three dimensions, it is only necessary to have the columns of the arrays represent radial cross-sections and rows represent co-axial cylinders. MMF is defined as the magnetic "pressure" required so that magnetic flux can flow, analogous to voltage as the electric "pressure" required for current flow.

The program accepts the following input parameters: values representing the relation between the magnetizing forces and flux density for the material used for the profile tube, end rings, and outer cylinder; the thickness of the profile tube; the desired flux density, B_o; values of MMF along the boundaries between the outer cylinder volume and the outer cylinder and end ring; and the dimensions of the assembly, including the inner radii of the profile and magnet, the spacing between the profile tube and the outer cylinder, the length of the profile, the length and thickness of the magnet, and the number of points in the MMF arrays.

The outer cylinder array is initialized in the following manner. No radial components of flux are assumed along the radial axis boundary of the cylindrical assembly, thus the MMFs along this axis are defined to be equal to the outer cylinder boundary MMF. The profile tube edge of the array is calculated by means of a linear interpolation from the radial center to the

point where the tube meets the magnet:

$$\Delta \text{ MMF} = B_o \text{ (DA)}$$

where B_o is the initial flux density and DA is the axial distance separating adjacent columns of the array.

Beyond the magnet the MMF decreases linearly to the value specified for the end ring boundary. With values thus established along the boundaries, the initial values for the remaining points of the array are found by decreasing the MMF proportionately along each column from the profile to the outer cylinder.

The inner cylinder volume array is initialized by setting each radial column of MMFs equal to the profile tube-outer cylinder boundary MMF in the same radial cross-sectional plane, with the exception of the last column on the magnet end of the array where the open-end conditions are taken into account. The two innermost axial rows are assumed to have no radial flux component throughout the program as defined by on-axis conditions.

The values in the two arrays are then subjected to repeated alterations to establish stable inner points. Each iteration of this process includes a readjustment of the inner array's last radial column for open-end effects and a separate recalculation of the two innermost axial row values.

The flux flowing into the profile from both arrays is summed on an element basis from the radial center toward the magnet end of the assembly.

The flux density in the profile is calculated on an element basis.

$$B_j = \phi_j / A_j$$

where ϕ_j is the flux and A_j is the profile cross-section of an element.

From the B/H characteristics of the iron used for the profile tube, the H_j and then the MMF_j are calculated per element.

The MMF_j in the iron profile tube is compared to the MMF_i calculated at the air-profile boundary on a per element basis. If the sum of differences between the MMFs of the profile-tube and air-profile exceed a predetermined values, the MMFs of the air-profile boundary are modified and the cycle of recalculating array values and profile tube MMFs are repeated.

The axial and radial flux densities are calculated from the inner cylinder MMF array.

$$B(\text{axial})_{i,c} = \frac{MMF_{(i+1,\ c)} - MMF_{(i-1,\ c)}}{2\ (DA)}$$

$$B(\text{radial})_{i,c} = \frac{MMF_{(i,\ c+1)} - MMF_{(i,\ c-1)}}{2\ (DR)}$$

where DR = radial element spacing of the inner cylinder rows,

i = array column location, and

c = array row location

From the MMF drop across the magnet, the magnet's flux, cross-sectional area and length, the magnet operating point, B_d and H_d are calculated.

Additional computer programs used for the PMA design are listed below: "VOLWT" calculates the minimum thicknesses for the tapered outer cylinder and end rings required to keep the magnetizing force below a predetermined value. This program also calculates the weight of the PMA given the densities of the various components.

"SHIELD" determines the effect of the leakage flux from the PMA's outer cylinder and end rings on the operating flux density of the earth's magnetic shield as a function of spacing and shield thickness. The shield weight is also calculated.

"DUBLZOOM" uses the inner cylinder MMF array generated in the FINE program to calculate the trajectories of two symmetrically released electrons accelerated from the photocathode through an electric field. Inputs accepted by the program include the vector components of the electric field, location of the photocathode within the PMA and the electron's initial coordinate and velocity components. The program's output includes a succession of three-dimensional positions occupied by each electron (which can be plotted), a three-dimensional components of the PMA's flux density, and the radial distances between the electrons at each position. DUBLZOOM is also equipped to locate the point at which the pair focuses.

"ZOOMPLOT", a special version of DUBLZOOM, gives output plots of radii of the discs of confusion on a target as a function of initial velocity and angles of departure from the photocathode.

"PSFPLOT" utilizes the radius/angle data obtained from ZOOMPLOT, along with the photoelectron velocity distribution information to calculate the point spread function (PSF).

"BESS" uses PSFPLOT's output to calculate the modulation transfer function (MTF).

PMA Dimensional Analysis

The inside radius of the PMA selected is equal to the inside radius of the solenoid focus coil (5.4 cm) currently used with the SEC tubes. As shown in Figure 1, this radius provides room for the readout beam's deflection yoke currently used, and allows sufficient space between the accelerator electrodes-resistor divider and the focus coil bobbin to prevent corona.

The length of the image section (photocathode to target) is 11.4 cm, and the readout electron gun aperture to target distance is 24.2 cm for the 35 mm tube and 30.1 cm for the 70 mm tube.* Thus, a minimum length of 50 cm for a 35 mm PMA is indicated when 14.5 cm is allotted for the magnets and end rings. However, a study of a number of electron trajectories shows that for the maximum MTF the image section must be focused with a magnetic field whose radial component is less than 1% of the axial focus field. The focus of the electron gun is also important, but past experience with solenoid generated fields shows that the magnetic field can be considerably lower at the gun aperture than at the target and still yield good performance. For this reason the tube is positioned such that the photocathode is closer to the center of the assembly than is the gun to ensure the highest possible field uniformity over the full photocathode-to-target distance. Further trajectory trials indicated that the photocathode should be located approximately 16 cm from the center of an assembly of inside length of about 65 cm for the 35 mm PMA. The weight of a PMA is length dependent, and it is found that a given fractional change in the inside length results in between 2 and 2.7 times that change in overall weight. This is shown by comparing Mod 14 with Mod 7, Mod 0 with Mod 1 and Mod 5 with Mod 4 in Table I.

The remaining major dimension is the outside radius of the assembly. The focus field is essentially independent of the outer cylinder's dimensions, as this cylinder is unsaturated. Therefore, the major design determinant on outside radius is weight. Figure 3 shows the variation in weight of both the

---

*The target dimensions of the tubes are 25 x 25 mm and 51 x 56 mm respectively. They are referred to by their useful diagonals of 35 and 70 mm throughout this report.

TABLE 1

TABLE OF PMA DESIGNS

	Weight-Kilograms-Note 2					Dimensions-cm								Trajectory-Microns Note 1				On-Axis Axial field -gauss		Remarks
	Outer Cyl.	End Ring	Pro-file	Magnet	Total	Inside Radius IR	Outside Radius OR	Inner Outside Radius IOR	Magnet Length	Magnet Thick-ness	1/2 Length 1/2 L	1/2 Inside Length 1/2 IL	PC/ Gun Location Note 3	On-Axis Start ΔX	On-Axis Start ΔY	Off-Axis Start ΔX	Off-Axis Start ΔY	PC	Gun	
1.Mod 0 (Initial Baseline Design	7.95	2.74	3.62	4.05	18.36	6.67	11.17	10.63	4.76	1.27	31.12	30.16	16.5/19.1	2	44	18	34	74.4	56.6	
2.Mod 1	11.26	3.37	4.82	5.57	25.02		11.32		5.36	1.52	35.27	33.98	17.0/18.6	0	4	1	4	79.4	78.0	Increased length of magnet & profile to obtain a more uniform field at photocathode.
3.Mod 2	17.66	2.89	6.87	7.68	35.10		10.32	9.06		2.03	35.82			0	0	1	0	79.8	79.3	Mod 1 except reduced outer cylinder radius.
4.Mod 3	9.32	3.76	4.16	4.56	21.80		12.26	11.75		1.27	35.51			0	6	3	6	79.1	77.0	Mod 1 except increased outer cylinder radius.
5.Mod 4	11.42	2.66	4.69	5.50	24.27	5.40	9.46	8.60		1.78	35.51			0	0	0	0	79.9	79.6	Mod 1 with IR & IOR scaled down equally.
6.Mod 5	9.76	2.43	4.10	4.81	21.10		9.38		5.11	1.65	33.75	32.33		0	2	1	2	78.7	78.6	Mod 4 except reduced inside length.
7.Mod 6	7.52	2.81	3.34	3.91	17.57		10.39	9.87		1.37	33.49			0	4	2	6	79.4	77.7	Mod 5 except increased outer cylinder radius.
8.Mod 7-A	6.35	3.35	2.82	3.20	15.72		11.70	11.50		1.14	33.32			0	6	1	7	79.2	77.2	Mod 5 except increased outer cylinder radius more than Mod 6.
9.Mod 7													16.0/19.6	0	2	1	4	79.7	74.4	Moved PC into more uniform field area.
10.Mod 8-A	5.14	5.09	2.28	2.66	15.17		15.72	15.56		0.965	33.15	32.33	16.0/19.6	0	6	2	8	79.2	71.7	
11.Mod 8													15.0/20.6	0	2	1	5	79.6	65.2	Mod 5, except increased outer cylinder radius as compared to Mod 7.
12.Mod 9	5.19	6.74	2.12	2.52	16.57		18.71	18.61		0.914	33.10	32.33	—	—	—	—	—	—	—	Mod 5, except increased outer cylinder radius as compared to Mod 8.
13.Mod 10	6.36	10.06	2.01	2.28	20.71		23.27	23.18		0.838	33.07	32.33	15.0/20.6	0	6	2	5	79.2	63.0	Mod 5 except increased outer cylinder radius to a maximum.

TABLE 1
(continued)

	Weight-Kilograms-Note 2					Dimensions-cm								Trajectory-Microns Note 1				On-Axis Axial field -gauss		Remarks
	Outer Cyl.	End Ring	Pro-file	Magnet	Total	Inside Radius IR	Outside Radius OR	Inner Outside Radius IOR	Magnet Length	Magnet Thick-ness	1/2 Length 1/2 L	1/2 Inside Length 1/2 IL	PC/Gun Location Note 3	On-Axis Start ΔX	On-Axis Start ΔY	Off-Axis Start ΔX	Off-Axis Start ΔY	PC	Gun	
14.Mod 11	4.60 (+.96) Note 5	3.35	2.82	3.20	14.93	5.40	11.84	11.50	5.11	1.14	33.32	32.33	See	Mod	7					Mod 7 with the outer cylinder material changed to Vanadium Permendur (sheet form). See notes 4 and 5.
15.Mod 12	17.93 (+.96) Note 5				28.26		11.95		See	Mod	7									Mod 11, except the Vanadium Permendur outer cylinder material thickness was increased. See note 6.
16.Mod 13	13.87 (+.96) Note 5				24.20		12.26		See	Mod	7									Mod 12, except outer cylinder material changed to conetic.
17.Mod 14	3.88	2.40	1.77	1.94	9.99		11.72		4.19	0.86	27.27	26.54	$12.0/_{14.7}$	0	4	1	4	79.4	74.6	Shorter version of Mod. 7. 15.3 cm target to gun length used in this design.
18.Mod 15	9.69	5.62	4.38	5.16	24.85	6.60	14.27	14.07	5.97	1.30	38.94	37.84	$18.5/_{23.0}$	0	2	2	3	79.5	72.4	Scaled-up design for 70 mm PMA.
19.Mod 16	11.95	4.70	5.10	6.15	27.90		12.66	12.09		1.50	39.12			0	2	1	2	79.7	73.8	Mod 15, except decreased outer cylinder radius.
20.Mod 17	7.79	11.40	3.29	3.96	26.44		22.92	22.81		1.02	38.70		$17.5/_{24.0}$	0	6	6	4	79.2	62.5	Mod 15, except increased outer cylinder radius to a maximum.
21.Mod 18	8.29	7.89	3.65	4.39	24.22		18.23	18.03		1.12	38.78		$18.0/_{23.5}$	0	4	4	4	79.4	67.4	Mod 15, except increased outer cylinder radius less than Mod 17.

TABLE I (continued)

Notes:

1. Electron trajectories; initial conditions: $V_{xo} = \pm 1$ ev, $V_{zo} = 1$ ev, $V_{yo} = 0$, $Y_o = 0$ cm. The off-axis starting point for Mods 0 thru 14 (35 mm PMA) is 1.8 cm, while for Mods 15 thru 18 (70 mm PMA) the off-axis starting point is 3.5 cm. Electric field: Uniform density over entire PC to target length; Δ X and Δ Y are the X-axis and Y-axis distance between the two electron trajectories at the on-axis best focus Z distance.
2. The weight is based on low-carbon-steel profile, outer cylinder, and end rings unless otherwise noted. The magnet material is Alnico 5. A high permeability shield required to reduce the effect of the earth's field upon the SEC is not included in these weight tabulations.
3. PC/Gun location is the distance from the center of the PMA to the photocathode/electron gun.
4. The thickness of the Vanadium Permendur (VP) outer cylinder in Mod 11 was controlled by the thickness required for the return flux.
5. An aluminum bobbin is required for the VP material and was estimated to weigh 0.96 kilograms.
6. The outer cylinder VP thickness for Mod 12 was increased to give the required attenuation of the earth's magnetic field. End cap shields are still required.

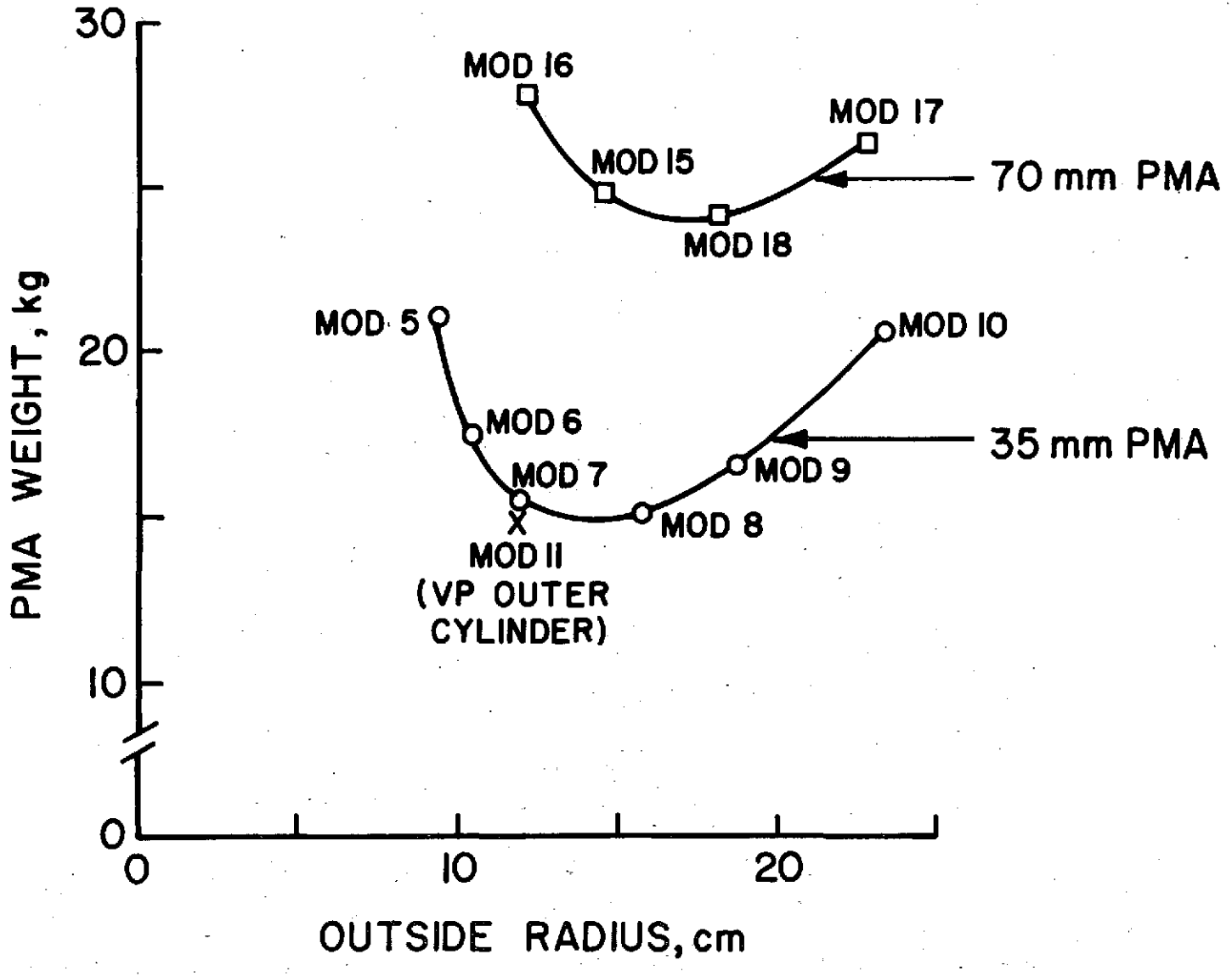

Fig. 3 - PMA Weight vs. Outside Radius.

35 and 70 mm designs as a function of outside radius. These plots show that to minimize the PMA's volume/weight ratio an outside radius of approximately 12 cm is nearly optimum for the 35 tube focus assembly, while 14 or 15 cm is optimum for the 70 mm focus assembly.

PMA Design Variations

Table I tabulates all of the characteristics of the PMA designs studied. The prime objective is to obtain an aberration-free focus at a photocathode to target distance of about 12 cm. In the first design trial the magnetic field was not uniform over a sufficient length. In Mod 1 the design was lengthened. This improved the focus. In Mod 2, 3 and 4 the effect of outside diameter on overall weight was probed. In Mod 5 the length was reduced somewhat. The focus still looked acceptable, and in Mods 6 through 10 the outer radius was varied to determine the minimum weight. Mod 7 appeared to be the optimum design. In Mod 11 the material for the outer cylinder was changed to rolled sheets of Vanadium Permandur, resulting in a modest decrease in weight but at the expense of a more complicated fabrication procedure.

In Mods 12 and 13 the outer cylinder also serves as a magnetic shield against the earth's magnetic field. This proves to be a poor idea from a weight viewpoint. Mod 7 with a separate shield for the earth's field is a more nearly optimum solution (see Section V on shielding).

In Mod 14 the length was reduced to see the weight advantage from developing a shorter SEC tube. This could be done with a tube design employing the readout electron gun that is in the 2-inch Return Beam Vidicon, (developed for the Earth Resources Technology Satellite). With a shorter tube the weight would be reduced by at least 36 percent.

In Mod 15, the Mod 7 design was scaled up to the 70 mm SEC tube dimensions. In Mod 16, 17 and 18 the 70 mm design was probed to determine the minimum weight as a function of the outer radius. From the graphs shown in Figure 3, Mod 15 and 7 appear to have the optimum minimum diameters.

PMA Configuration

Figures 4 and 5 are scale drawings of the Mod 7 and Mod 15 versions of the PMA showing the location of the gun, target and photocathode of the SEC tubes. The photocathodes are deeply recessed within the assembly. In this position the unvignetted optical cone is f/2.7 or slower for the 35 mm design and f/3.9 for the 70 mm design. This could present some difficulty in matching the detector to fast optical systems. An auxillary low power electromagnet located near the photocathode might make the magnetic field more uniform and allow the photocathode to be moved nearer to the end of the assembly.

Figures 6 and 7 are quarter cross-section drawings of the Mod 7 and Mod 15 designs showing the detailed dimensions and assembly details. Table II lists the thicknesses of the profile tube and outer cylinder as a function of axial dimension for both Mod 7 and 15 designs. The terminology is consistent with Table I and one may find these figures helpful in following the design variations listed in Table I. The magnet is Alnico 5. The profile tube, end rings and outer cylinder are low carbon iron. The shield material is Conetic. The long tapered sleeve between the end ring and outer cylinder is also low carbon iron. It is used to facilitate assembly with a minimum air gap. These pieces would be pinned together. There is a non-magnetic ring around the toroidal magnet to hold the magnet, end ring and profile tube in alignment. Small holes in the outer cylinder would be required to allow air to escape easily and also provide means of holding the shield in position. These details have not been worked out but appear easily accommodated in actual application.

CROSS SECTION OF MOD 7 PMA
WITH MAGNETIC SHIELD
FOR 35 mm SEC

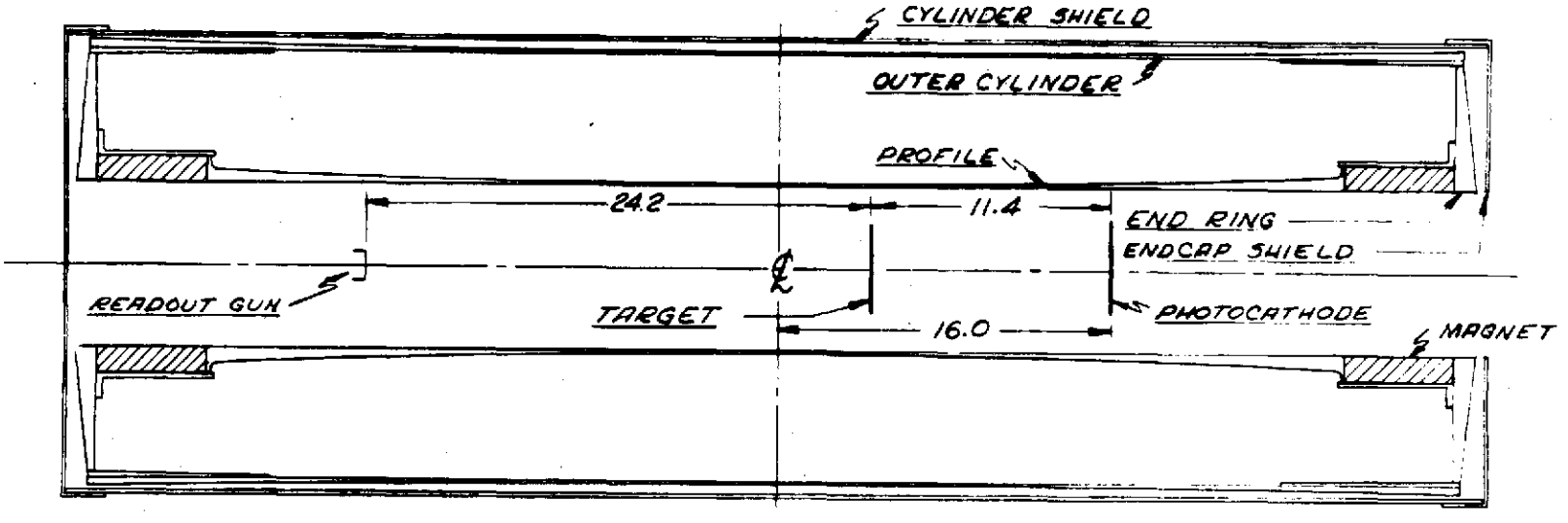

ALL DIMENSIONS ARE IN CENTIMETERS

Fig. 4 - Cross-section for Mod 7 PMA with Magnetic Shield for 35 mm SEC.

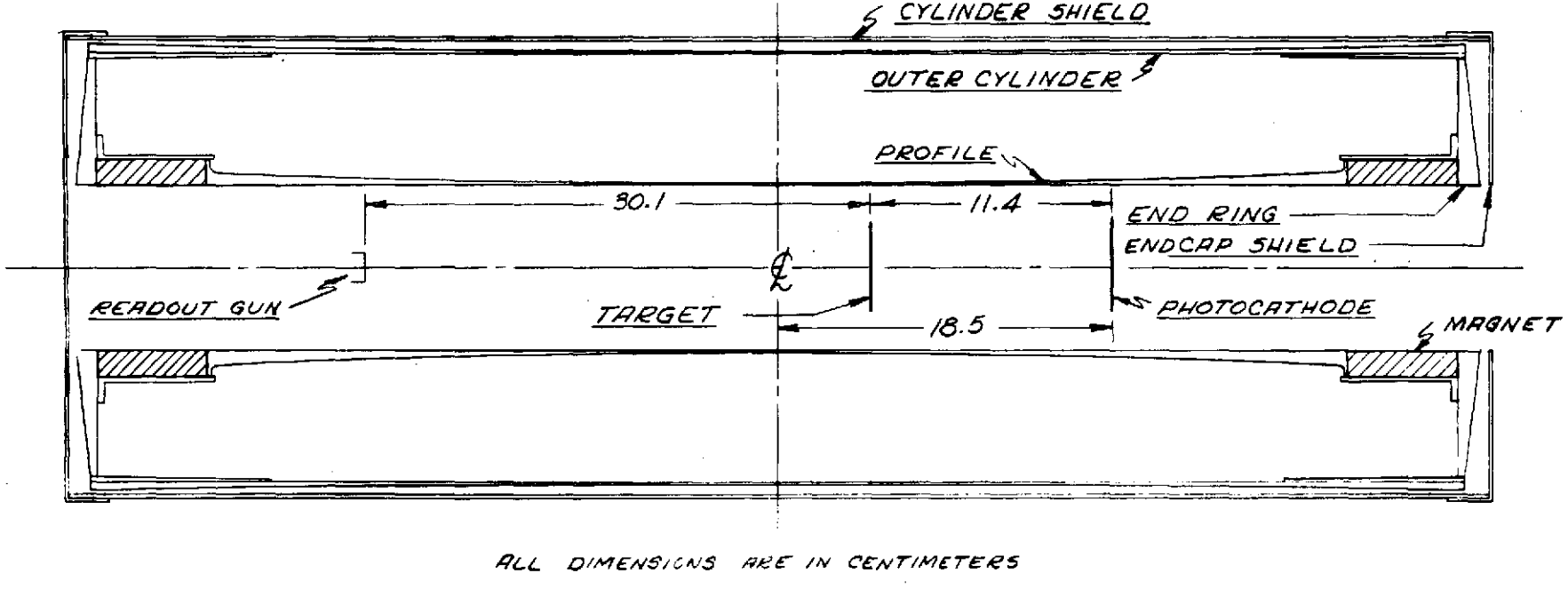

Fig. 5 - Cross-section of Mod 15 PMA with Magnetic Shield for 70 mm SEC.

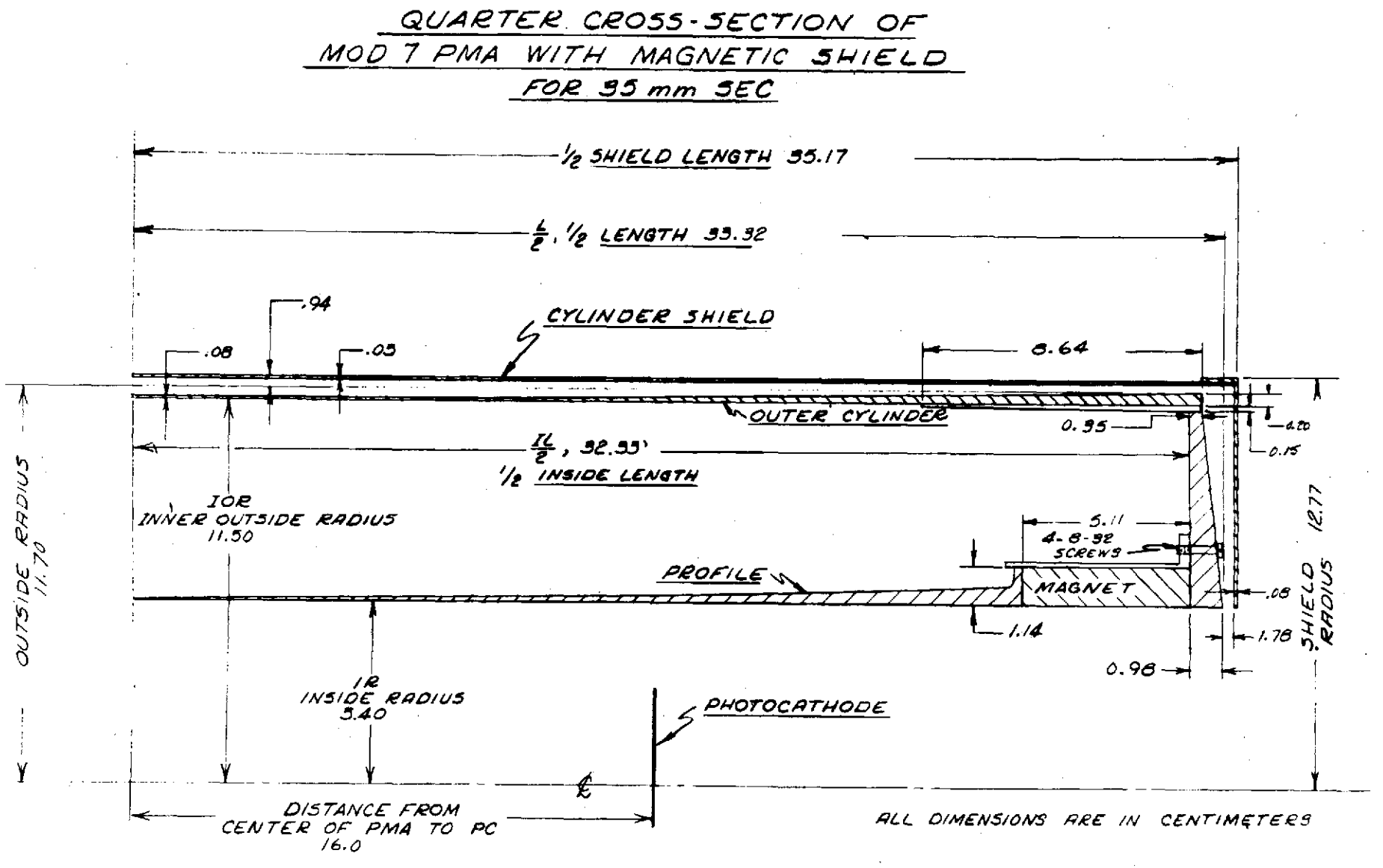

Fig. 6 - Quarter Cross-section of Mod 7 PMA with Magnetic Shield for 35 mm SEC.

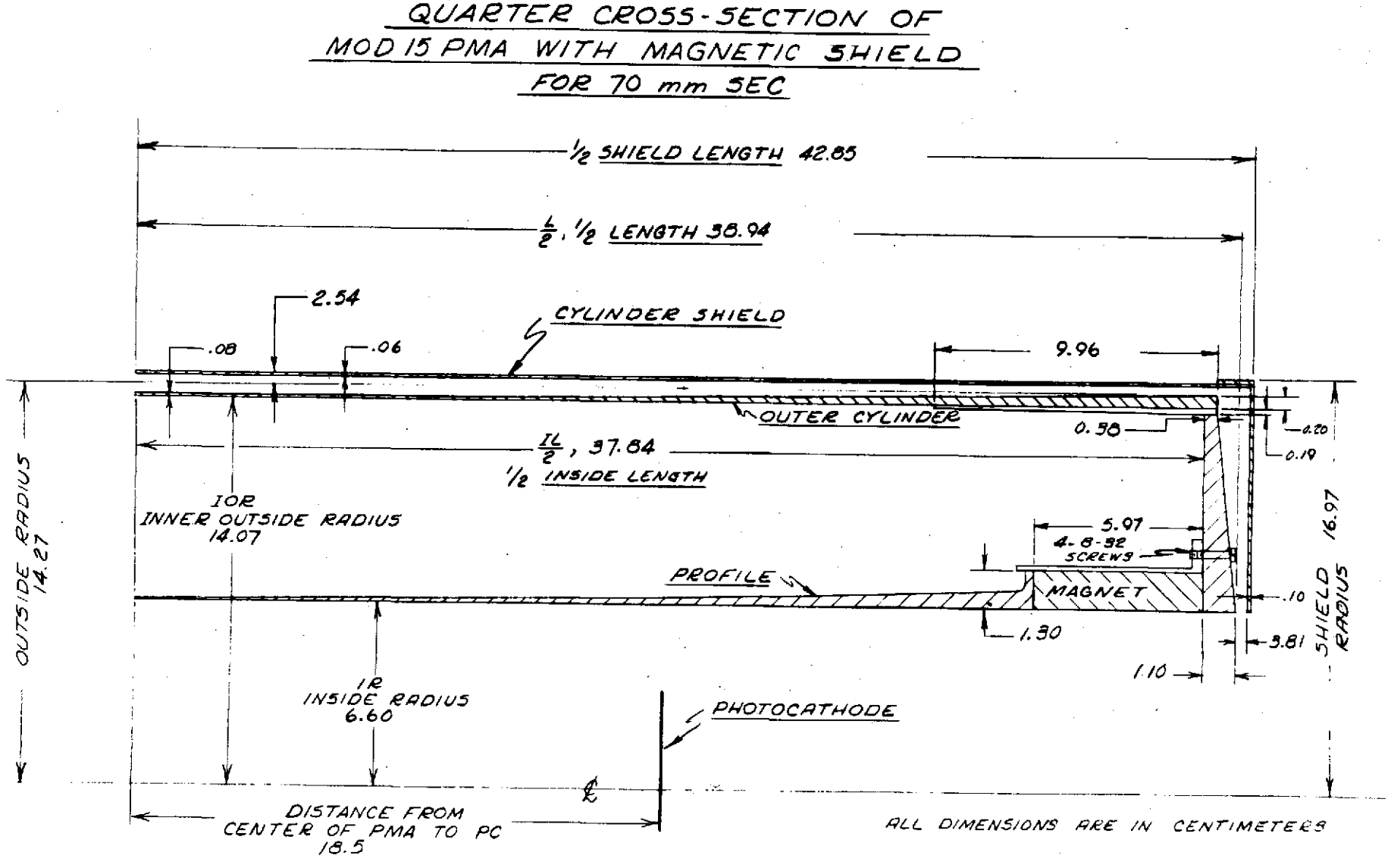

Fig. 7 - Quarter Cross-section of Mod 15 PMA with Magnetic Shield for 70 mm SEC.

TABLE II

TABLE OF PROFILE TUBE AND
OUTER CYLINDER THICKNESSES

Mod 7 PMA			Mod 15 PMA		
Distance from PMA Center cm	Profile Thickness cm	Outer Cylinder Thickness cm	Distance from PMA Center cm	Profile Thickness cm	Outer Cylinder Thickness cm
0	.051	.076	0	.051	.076
.85	.051	.076	.996	.051	.076
1.70	.053	.076	1.99	.053	.076
2.55	.056	.076	2.99	.056	.076
3.40	.056	.076	3.98	.058	.076
4.25	.061	.076	4.98	.064	.076
5.11	.066	.076	5.97	.066	.076
5.96	.071	.076	6.97	.074	.076
6.81	.076	.076	7.97	.079	.076
7.66	.084	.076	8.96	.086	.076
8.51	.091	.076	9.96	.097	.076
9.36	.099	.079	10.95	.104	.079
10.21	.109	.081	11.95	.114	.081
11.06	.119	.084	12.94	.127	.084
11.91	.130	.086	13.94	.137	.086
12.76	.140	.089	14.94	.152	.089
13.61	.152	.091	15.93	.165	.091
14.47	.168	.104	16.93	.180	.107
15.32	.180	.117	17.92	.196	.122
16.17	.196	.130	18.92	.213	.137
17.02	.211	.142	19.91	.229	.152
17.87	.229	.155	20.91	.249	.168
18.72	.244	.168	21.90	.267	.183
19.57	.262	.180	22.90	.287	.198
20.42	.282	.193	23.90	.310	.203
21.27	.302	.203	24.89	.333	.203
22.12	.323	.203	25.89	.356	.203
22.97	.345	.203	26.88	.381	.203
23.83	.368	.203	27.88	.410	.203
24.68	.399	.203	28.87	.442	.203
25.53	.427	.203	29.87	.475	.203
26.38	.472	.203	30.87	.526	.203
27.23	1.14 (.517)*	.203	31.86	1.30 (.579)*	.203
28.08	-	.203	32.86	-	.203
28.93	-	.203	33.85	-	.203
29.78	-	.203	34.85	-	.203
30.63	-	.203	35.84	-	.203
31.48	-	.203	36.84	-	.203
32.33	-	.203	37.84	-	.203

* The profile thickness at the magnet boundry is increased from the design value to the thickness of the magnet. Increasing the contact area reduces the air gap effects. Reference Figures 6 and 7.

The PMA would be assembled with the magnets demagnetized. After the PMA is magnetized, the assembly would be inserted into the magnetic shield and the shield end caps attached.

The PMA is inherently strong and can be expected to withstand the launch environment without impairing its performance in orbit. The shield is much less rigid and may require some simple support between it and the PMA to keep it from deforming under vibration. The method of mounting the PMA to the spacecraft has not been investigated, but from inspection one could envisage using the end plates as the attachment points.

Fine Tuning

There appears to be no requirement to fine tune the magnetic field generated by the PMA. Precise focus of the television tube would be accomplished by adjusting the electrode potentials as is the usual technique with a solenoid electromagnetic generated magnetic focus field.

The interaction of the deflection yoke and gun alignment coils with the PMA is a present concern. The effects on the magnetic focus field uniformity by these readout coils could be investigated during a prototype evaluation.

Azimuthal variations in the magnetic field are expected to be small because of the symmetry of the magnetic circuit design. This is an aspect that should be investigated when a prototype is built. If required, fine tuning of the PMA could be accomplished by symmetric wrapping or stripping of magnetic tape on the profile tube. This procedure would be non-interacting, but very time consuming.

Electromagnetic trimming coils near the photocathode might allow the photocathode to be located nearer the permanent magnet end of the assembly, thereby making the assembly shorter, lighter in weight, and capable of receiving a lower focal ratio optical image. This is an aspect that could be investigated by experimenting with a prototype unit.

PMA Magnetic Field

The computer program prints a tabular listing and also plots a graph of the magnetic field strength. Figures 8 and 9 show the on-axis axial magnetic field for the 35 and 70 mm PMA, (Mod 7 and Mod 15). Figure 10 is a plot of the axial and radial magnetic field 1.8 cm off-axis in the 35 mm format and Figure 11 is a similar plot at 3.5 cm off-axis in the 70 mm format. In each case the photocathode is located in the region where the radial component is less than 0.2% of the axial field. This is necessary to ensure good focus over the full target. Although the electron gun portion of the tube was not studied, it is known from the other work that the magnetic field uniformity is much less critical near the electron gun. For this reason, positioning the tube in an unsymmetrically manner should not degrade the tubes' overall performances. The gun can probably tolerate an even greater field reduction than allowed here. Thus, the PMA can be shorter, resulting in a reduction in weight. The longer length chosen will allow experimentation to verify this, once a PMA is fabricated.

Figure 12 shows the shape of the flux lines near the magnet for the Mod 7 design. Figures 13, 14 and 15 depict the uniformity of the vector magnitude, the axial and the radial components of the magnetic field as a percentage of the field at the center of the PMA. In Mod 7 and Mod 15 the field uniformity at the photocathode is at least 0.5% and improves in the direction of the target. These figures give a qualitative view of the magnetic field generated by the PMA.

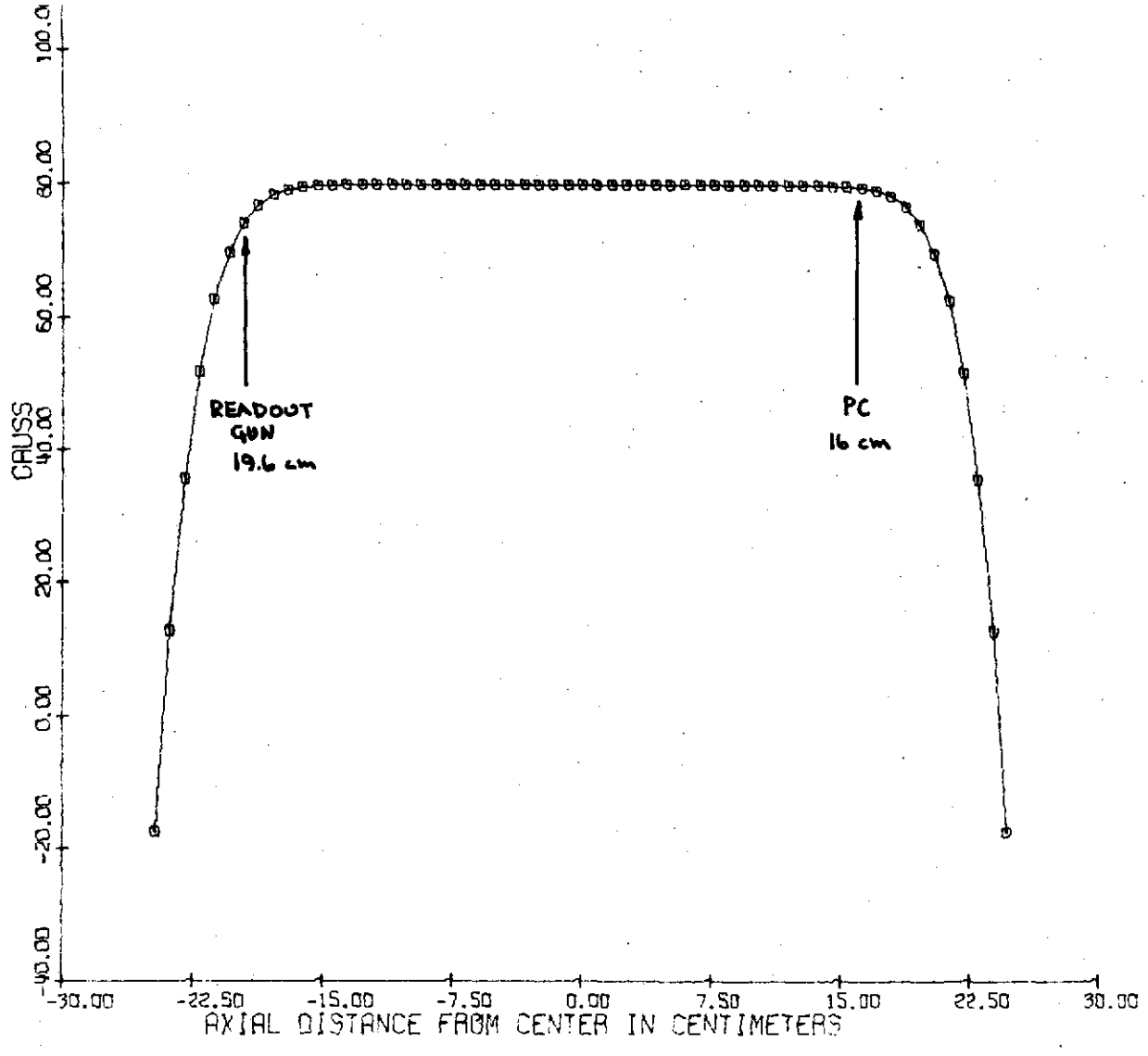

Fig. 8 - On-Axis, Axial Magnetic Field for 35 mm Mod 7 Design

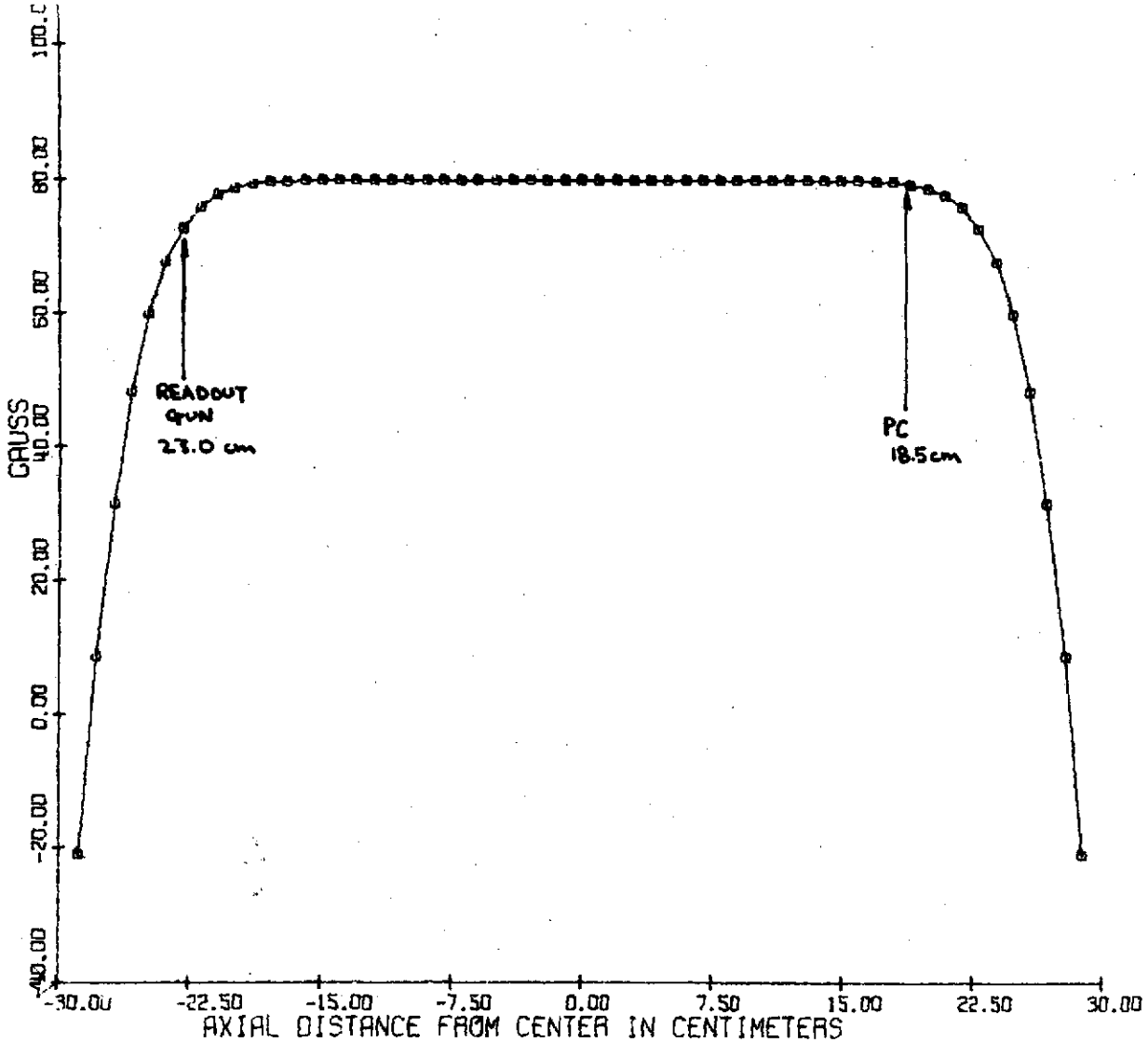

Fig. 9 - On-Axis, Axial Magnetic Field for 70 mm Mod 15 Design

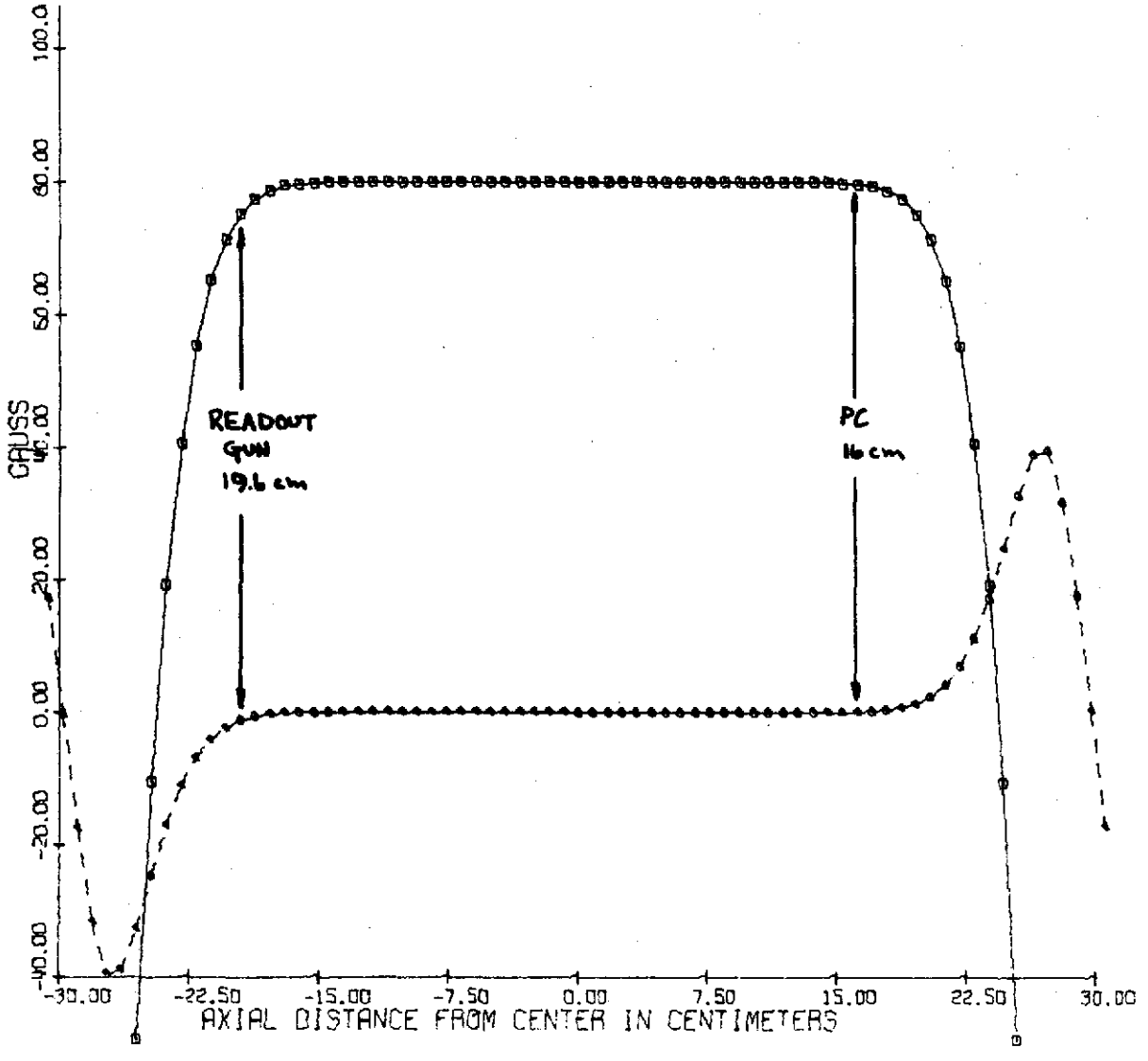

Fig. 10 - Off-Axis, Axial and Radial Magnetic Fields for 35 mm Mod 7 Design
X_o=1.8 cm, Y_o=0 cm

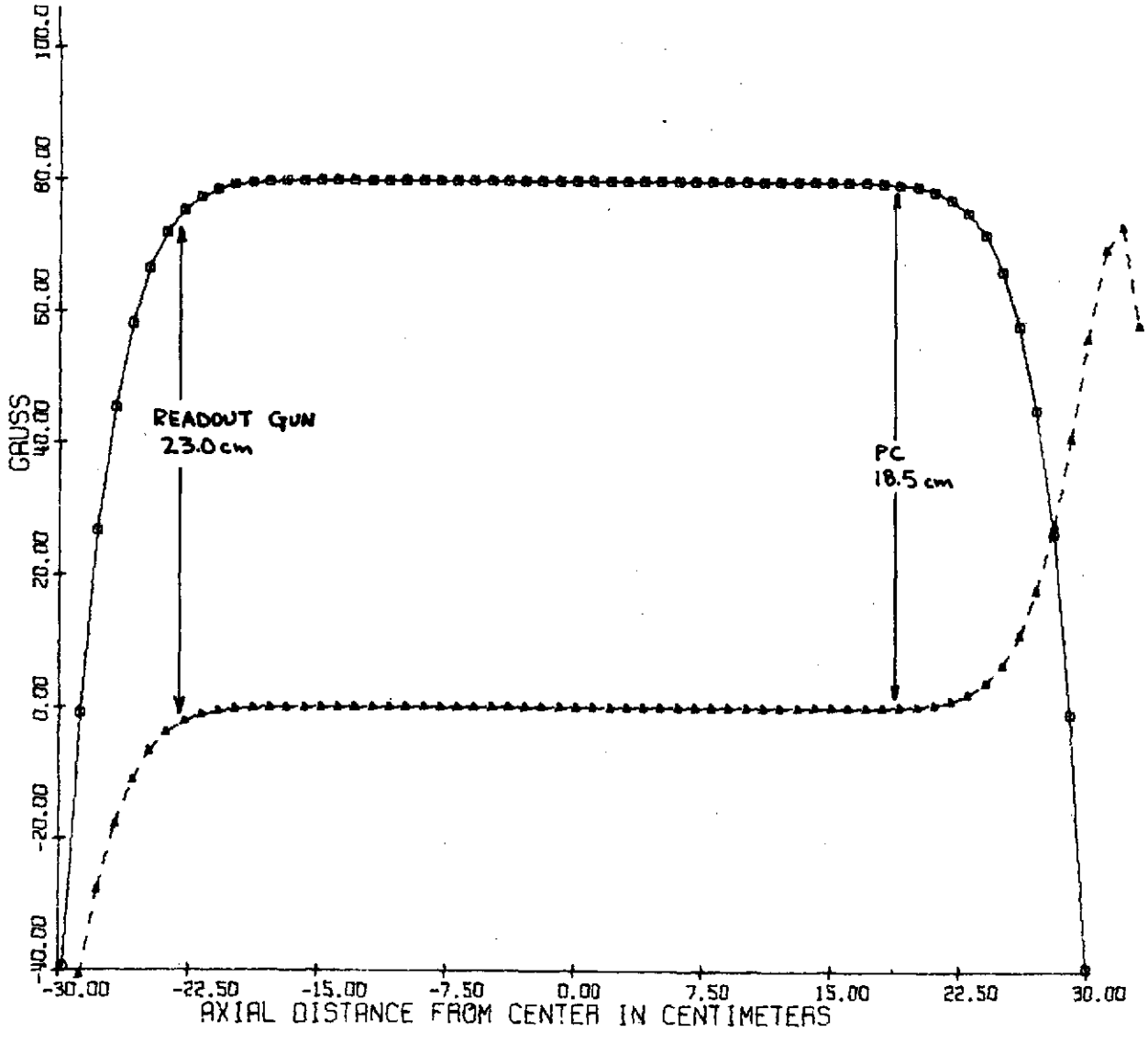

Fig. 11 - Off-Axis, Axial and Radial Magnetic Fields for 70 mm Mod 15 Design
X_o=3.5 cm, Y_o=0 cm

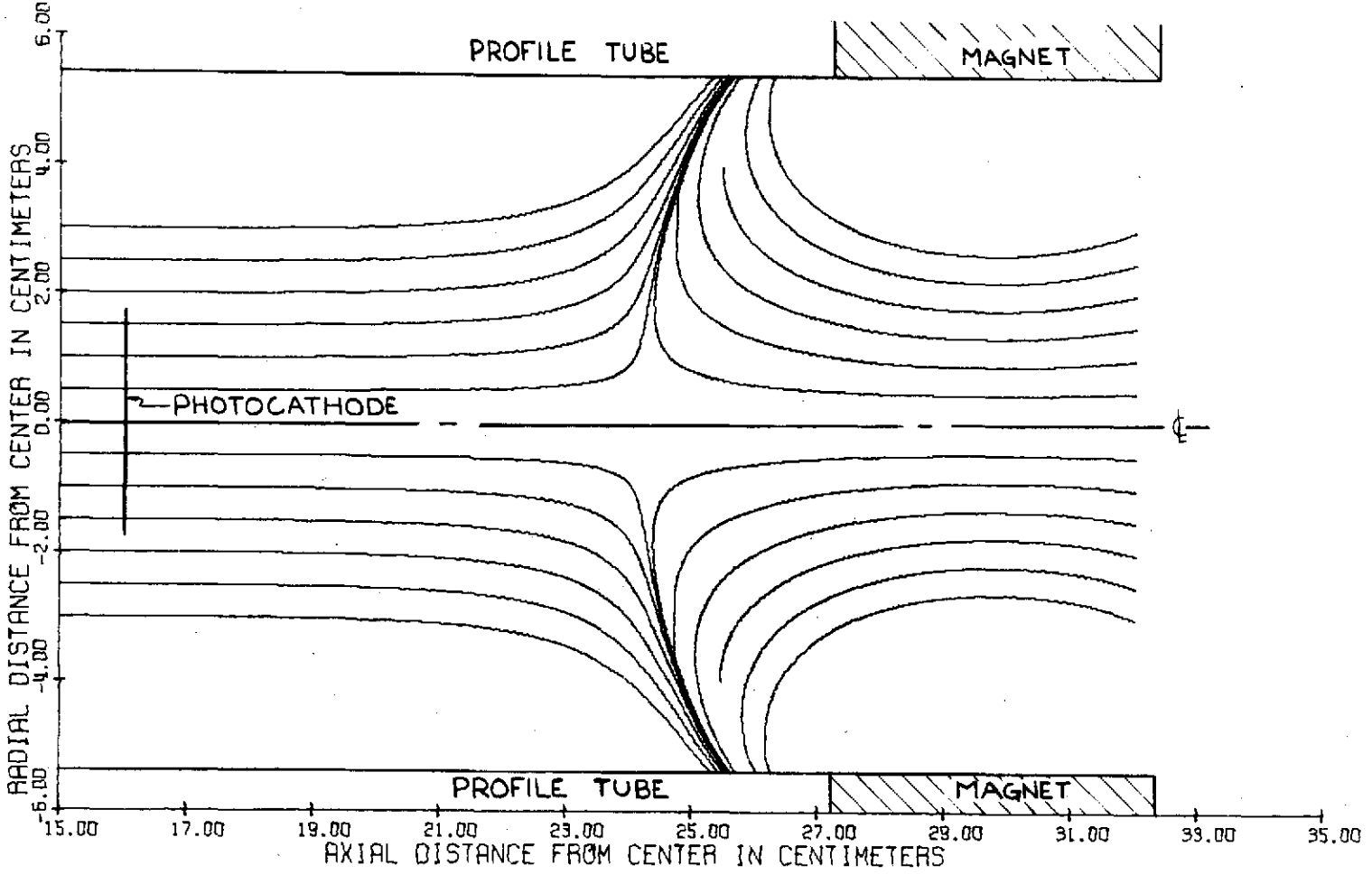

Fig. 12 - Magnetic Flux Lines for Mod 7 PMA

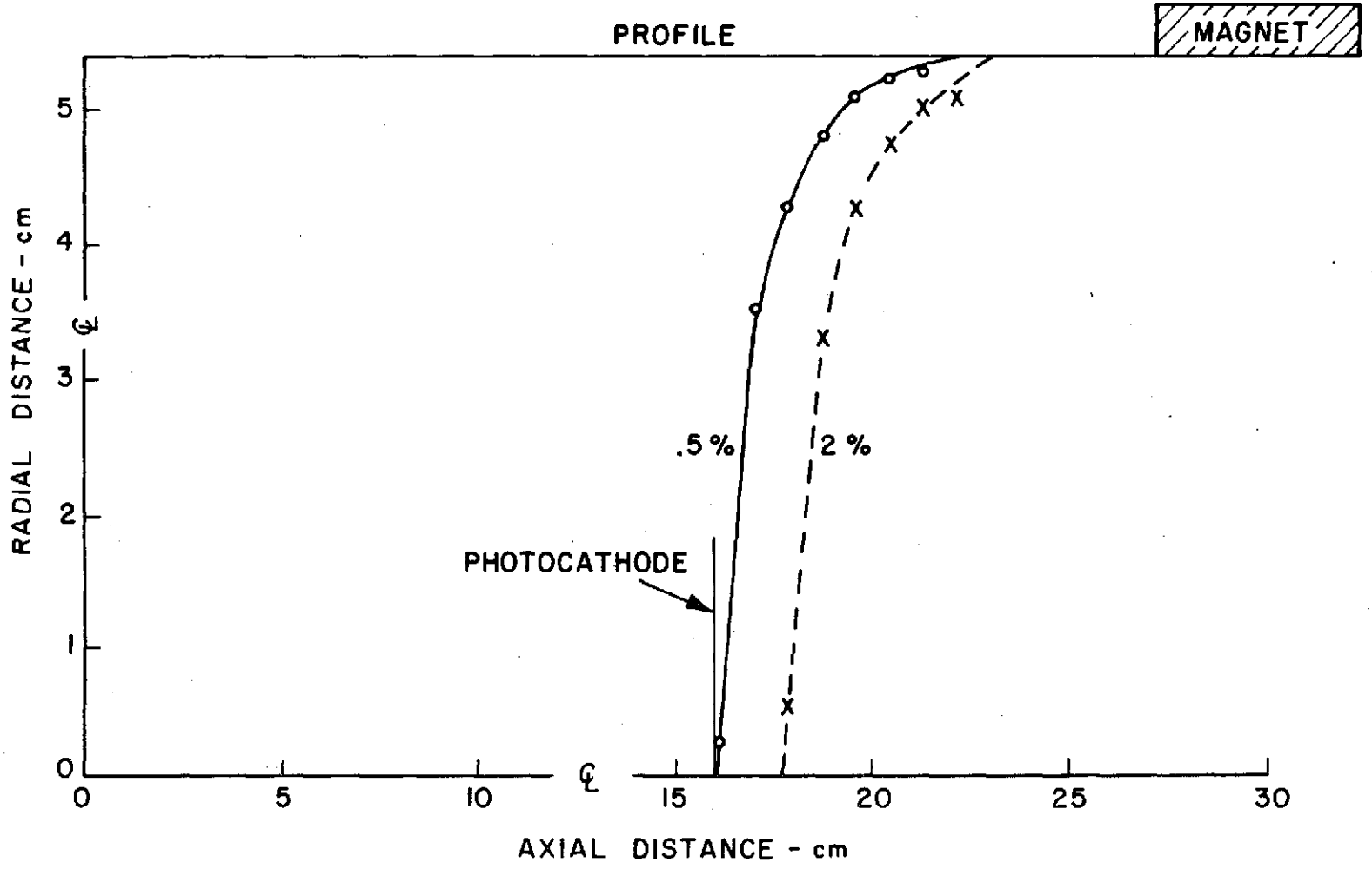

Fig. 13 - Uniformity of the Magnitude of the Magnetic Field as a Percentage of the field of the PMA Center (Mod 7)

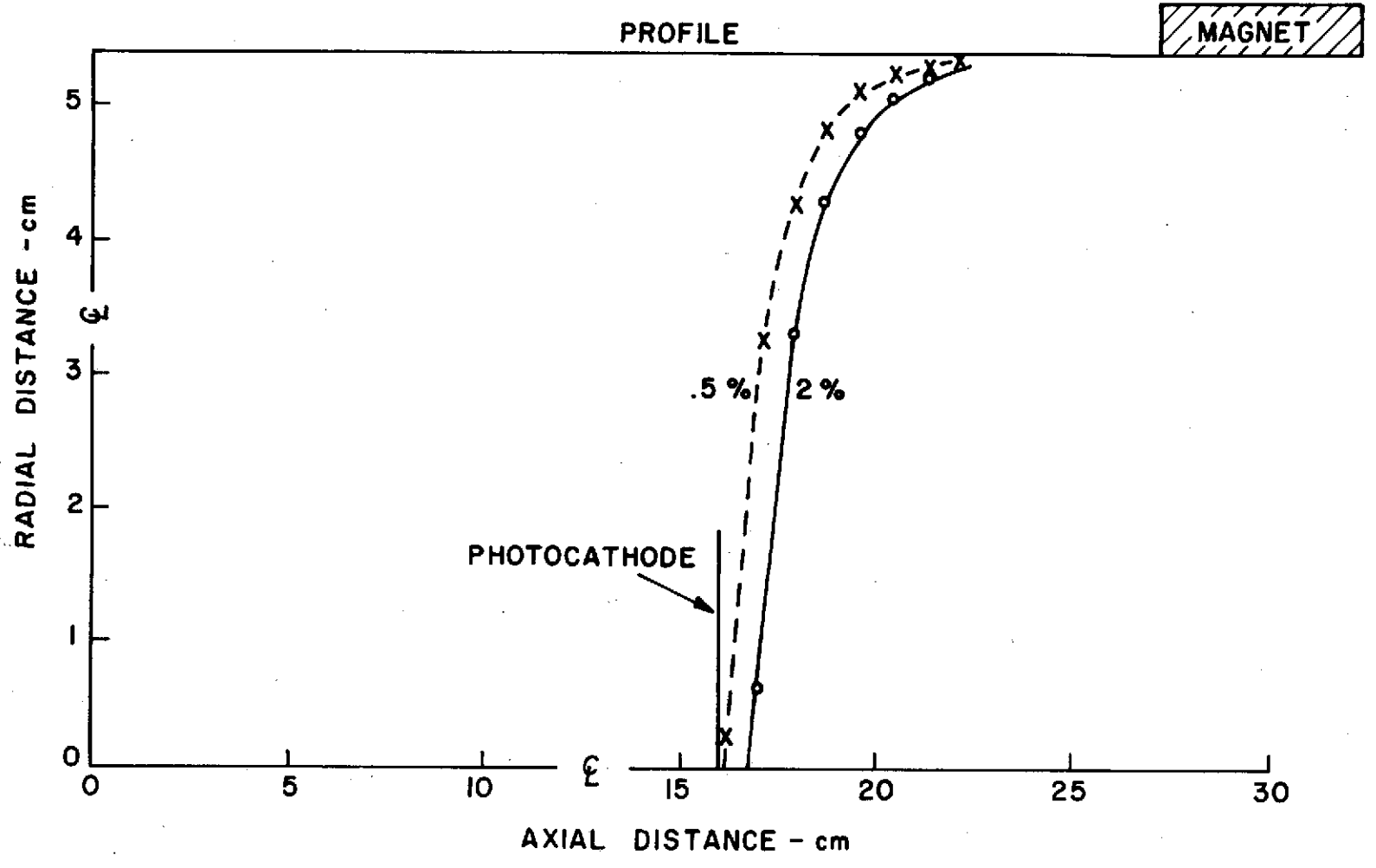

Fig. 14 - Uniformity of the Axial Magnetic Field as a Percentage of the Field at the PMA Center (Mod 7)

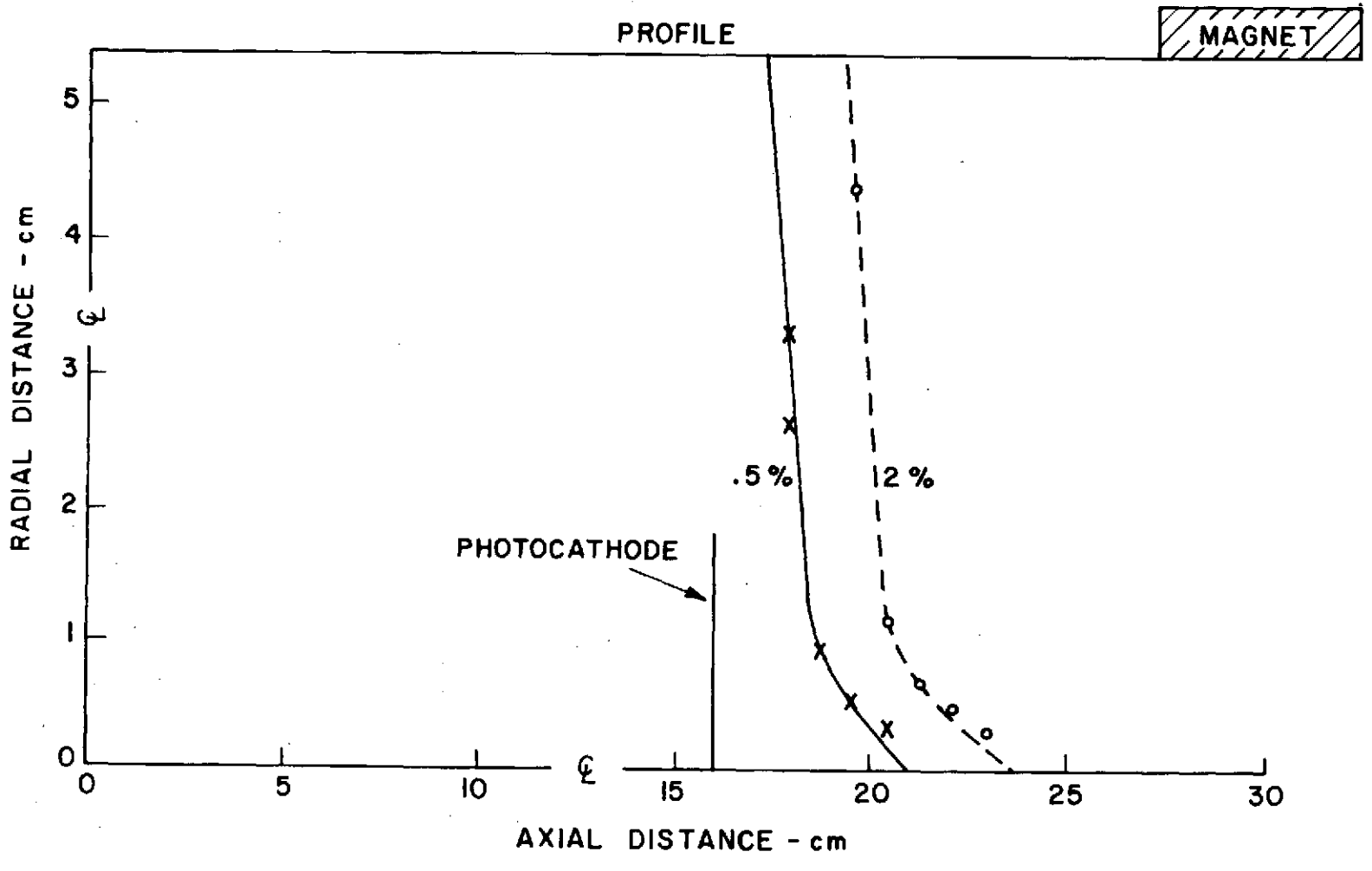

Fig. 15 - Uniformity of the Radial Magnetic Field as a Percentage of the Field at the PMA Center (Mod 7)

Aberration in Magnetic Focus Systems*

In image systems in which a magnetic field is used to focus electrons accelerated from the photocathode onto a target, the distribution of energies and directions of emission of the electrons are such that there is no plane at which all electrons from a given point will focus, but a plane of best focus can be found in which the mean square deviation of radial distance between electrons is a minimum.

Uniform Electric and Magnetic Fields

Uniform parallel fields give unit-magnification imagery. In the parallel field case an electron's parallel and transverse motions can be analyzed separately. The transverse velocity remains at its initial value which results in a transverse motion that is circular, with a period = 2π m/eB. Only the axial velocity is affected by the electrostatic field:

$$u_a = \frac{e}{2m} E t + u_{a0}$$

where e is the charge on the electron, m is its mass, E is the electric field, t is the time, and u_{a0} is the initial value of the axial velocity. As the period for executing the transverse circular motion is independent of the velocity, all electrons regardless of initial axial velocity return to the axis together in a time T equal to the Lamar period. But electrons with different initial axial velocities will transverse different axial distances in any fixed time. Thus, the spread of photoelectrons at a given focal plane distance is the consequence of the different transit times associated with different initial axial velocities and the incompatibility of these times

*Adapted from reference 14

with the Lamar period. Of course, a best plane will be that for which the mean transit time is equal to a Lamar period (or integer multiple thereof).

The difference in the time of arrival in a focal plane for an electron with initial energy ev_o associated with its motion parallel to the axis as compared to the time for an electron with zero initial velocity is given by the integral

$$\Delta T = \int_0^L \left(\frac{1}{u_o} - \frac{1}{u} \right) dz ,$$

where L is the distance from cathode to target in meters, $u = \left[2(e/m)(V + v_o) \right]^{1/2}$ is the axial velocity at any point of an electron emitted with an initial energy ev_o , $u_o = \left[2 (e/m) V \right]^{1/2}$ is the axial velocity of electrons with zero emission velocity and V is the potential at a point distance z along the axis from the cathode. For a uniform electric field E, the accelerating voltage V is equal to E x Z. Thus,

$$\Delta T = 2(e/m)^{1/2} \int_0^L \left[(1/E_z)^{1/2} - \left(\frac{1}{E_z + v_o} \right)^{1/2} \right] dz$$

$$\Delta T = \frac{m}{eE} \left[u_T - \left(u_T^2 + u_z^2 \right)^{1/2} + u_z \right]$$

where u_T is the velocity of electrons with zero initial velocity by the time they reach the target, and u_z is the initial axial velocity of emission corresponding to the energy ev_o.

As u_T is large compared with u_z, the time advance reduces to

$$\Delta T = \frac{u_z}{E e/m}$$

During this time, which is small compared with the total transit time or Lamar period, an electron with transverse velocity u_t will be displaced a distance along its transverse orbit given by:

$$r = u_t \Delta T = \frac{u_z u_t}{E\, e/m}$$

Likewise, in the plane of focus of electrons having initial axial velocity u_1, the transverse displacement will be given by

$$r = \frac{(u_z - u_1) u_t}{E\, e/m}$$

In terms of total velocity of emission u and angle of emission θ this becomes

$$r = \frac{(u \cos\theta - u_1) u \sin\theta}{E\, e/m}$$

$$r = \frac{V}{E}\left[\sin 2\theta - 2\frac{u_1}{u}\sin\theta\right]$$

Photoelectrons

For a Lambertian angular distribution of electrons, the mean square radial aberration is

$$\overline{r}^2 = \int_0^{\pi/2} 2r^2 \sin\theta \cos\theta \, d\theta$$

which reduces to

$$\overline{r}^2 = 2\left(\frac{mu^2}{2eE}\right)^2\left[\frac{1}{3} - \frac{16}{15}\frac{u_1}{u} + \left(\frac{u_1}{u}\right)^2\right]$$

In order to develop a feel for the order of magnitude for the radius of least confusion, it is seen that the above expression takes on a minimum value for $u_1/u = 8/15$ equal to

$$\bar{r}^2 = \frac{22}{225}\left[\frac{mu^2}{2eE}\right]^2$$

Thus, denoting $(\bar{r}^2)^{\frac{1}{2}}$ by $\underline{r}$ and writing $\frac{1}{2}mu^2 = ev$, we obtain:

$$\underline{r} = 0.31\frac{v}{V_T}L$$

where V_T is the target potential.

Using typical SEC operating parameters, the minimum mean square radial aberration may be evaluated. Let B = 80 gauss, L = 0.114 meters, V_T = 7416 volts, and v = 1 volt, then $\underline{r}$ = 4.8 microns. The root mean square radius is a figure of merit often used to describe optical system performance. In this particular case it represents the radius of a circle containing 75% of the energy in the point spread function of a monochromatic point source of photoelectrons.

A more complete analysis of photoelectron focusing with spatially uniform and parallel electric and magnetic fields is presented in Appendix B. This analysis was performed by Thomas Kelsall of Goddard Space Flight Center.

III. PHOTOELECTRON TRAJECTORY ANALYSIS

The preceding analysis yields a good estimate of the performance of an magnetically focused system when the E and H fields are uniform and parallel. As actual magnetic fields are never entirely uniform, it is important to determine how this non-uniformity effects the point spread function in the focal plane and subsequently the television tube's overall MTF. As the non-uniform field case is difficult to handle analytically, photoelectron trajectories through the magnetic field generated by the PMA are explicitly calculated.

The trajectories used are for an electron pair of a given energy released from a common point on the photocathode, each electron of the pair has identical axial velocity but opposing transverse velocity components. Figures 16 and 17 show the X-Y and Z-X projections of a photoelectron pair's paths from the photocathode to focal plane for single loop focus for the 35 PMA. The two photoelectron trajectories plotted are for the cases (electron 1 = $U_{xo} = U_{zo}$, $U_{yo} = 0$; electron 2: $U_{xo} = -U_{zo}$, $U_{yo} = 0$) both with total energy of 1.41 eV. The initial location is on-axis ($X_o = 0$, $Y_o = 0$). The intersection of the two trajectories locates the focal plane. By repeating the calculation for photoelectrons originating off-axis, image rotation and magnification can be obtained from the numerical tabulation of the trajectory data. Comparison of the on-axis trajectory plots (Figures 16 and 17) to the plots for trajectories originating 1.8 cm off-axis (Figures 18 and 19) show them to be indistinguishable from one another. The trajectories of photoelectrons in the 70 mm PMA are shown in Figures 20, 21, and 22, and are identical to the 35 mm trajectories.

As discussed in the section on variable gain, there is interest in operating

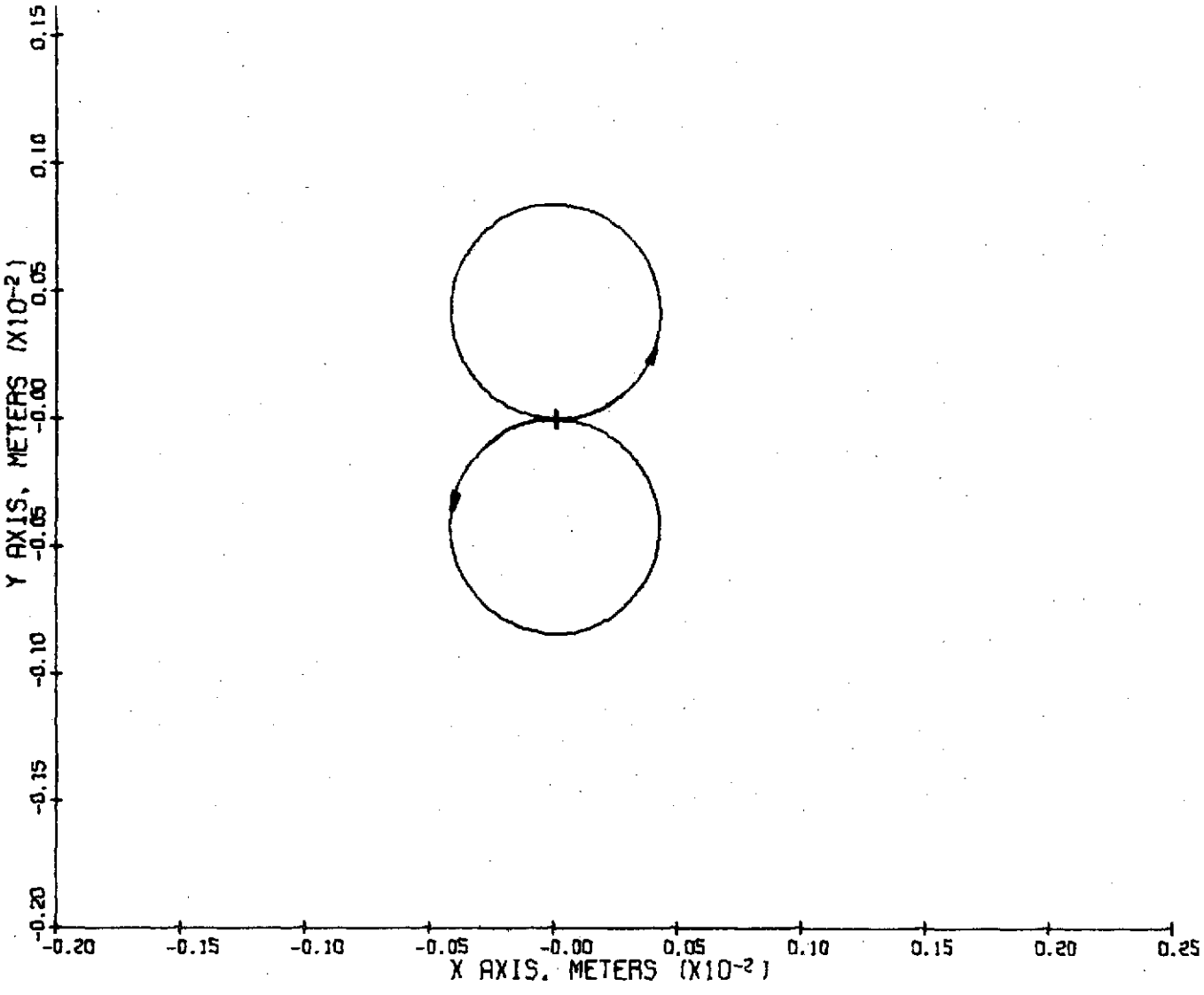

Fig. 16 - X-Y Projection of Photoelectron Trajectories for 35 mm Mod 7 Design
X_o=0, Y_o=0, V_{xo}=±1 ev, V_{yo}=0 and V_{zo}=1 ev

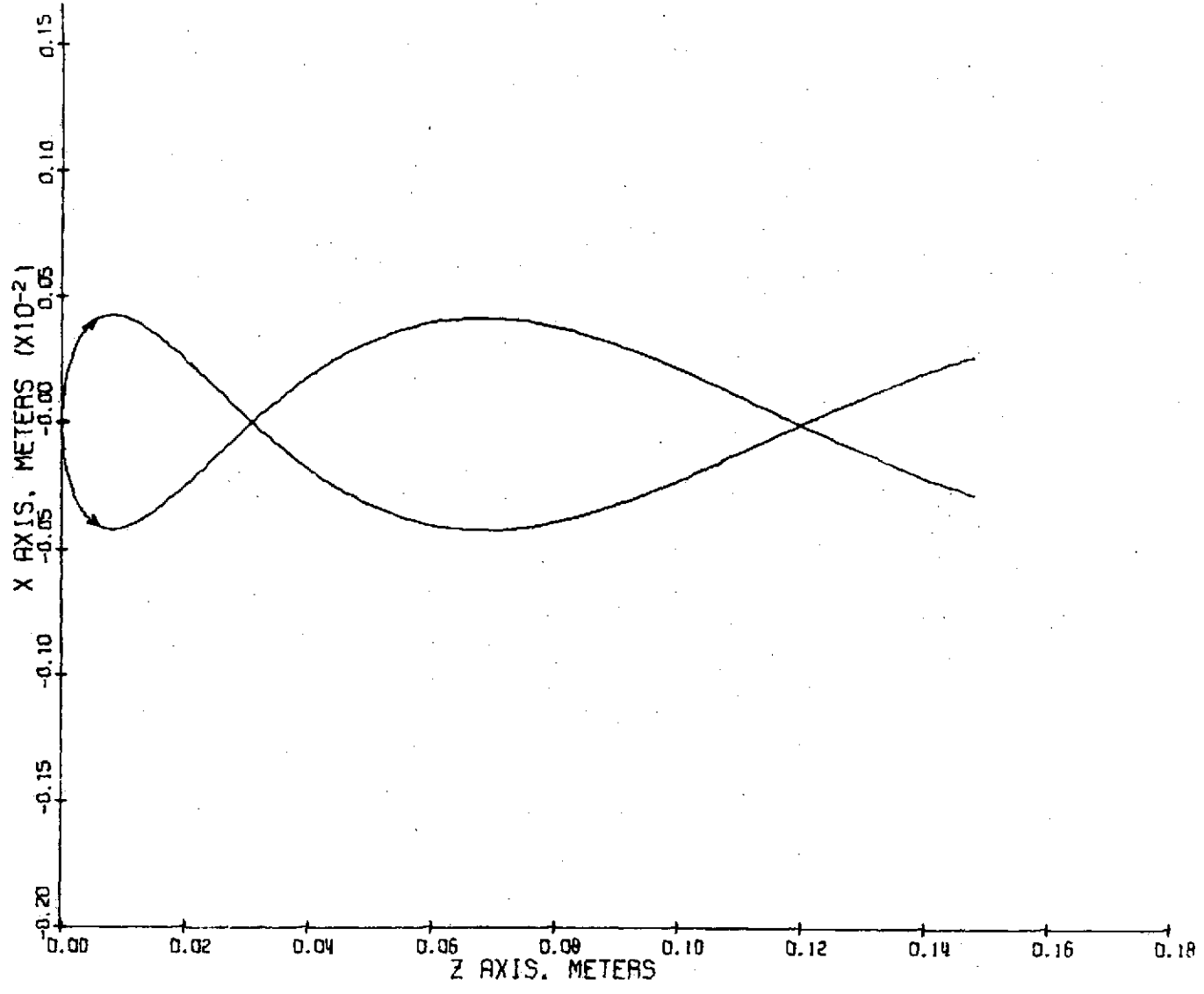

Fig. 17 - Z - X Projection of Photoelectron Trajectories for 35 mm Mod 7 Design
X_o=0, Y_o=0, V_o=±1 ev, V_{yo}=0 and V_{zo}=1 ev

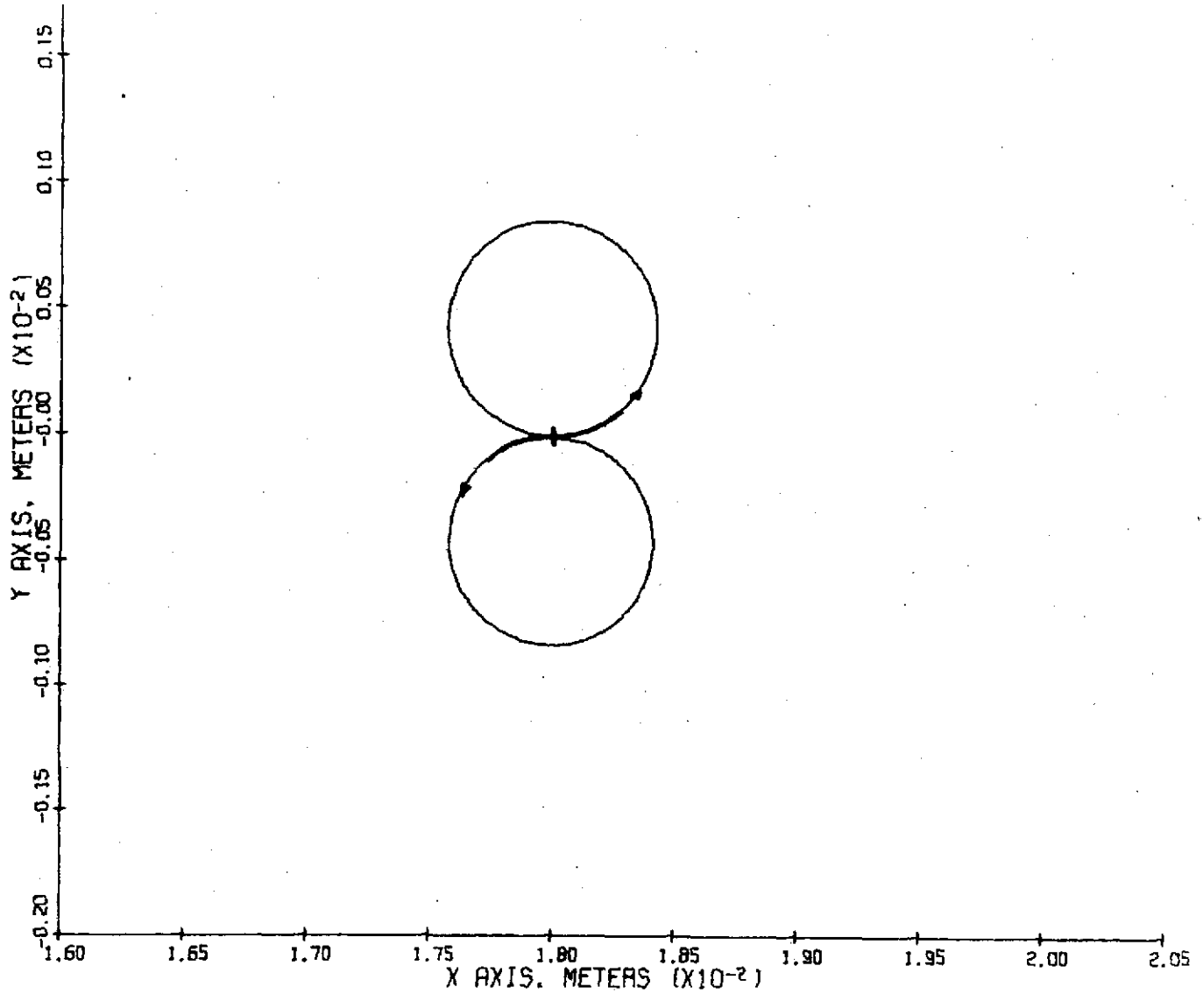

Fig. 18 - X - Y Projection of Photoelectron Trajectories for 35 mm Mod 7 Design
X_o=1.8 cm, Y_o=0, V_{xo}-±1 ev, V_{yo}=0 and V_{zo}=1 ev

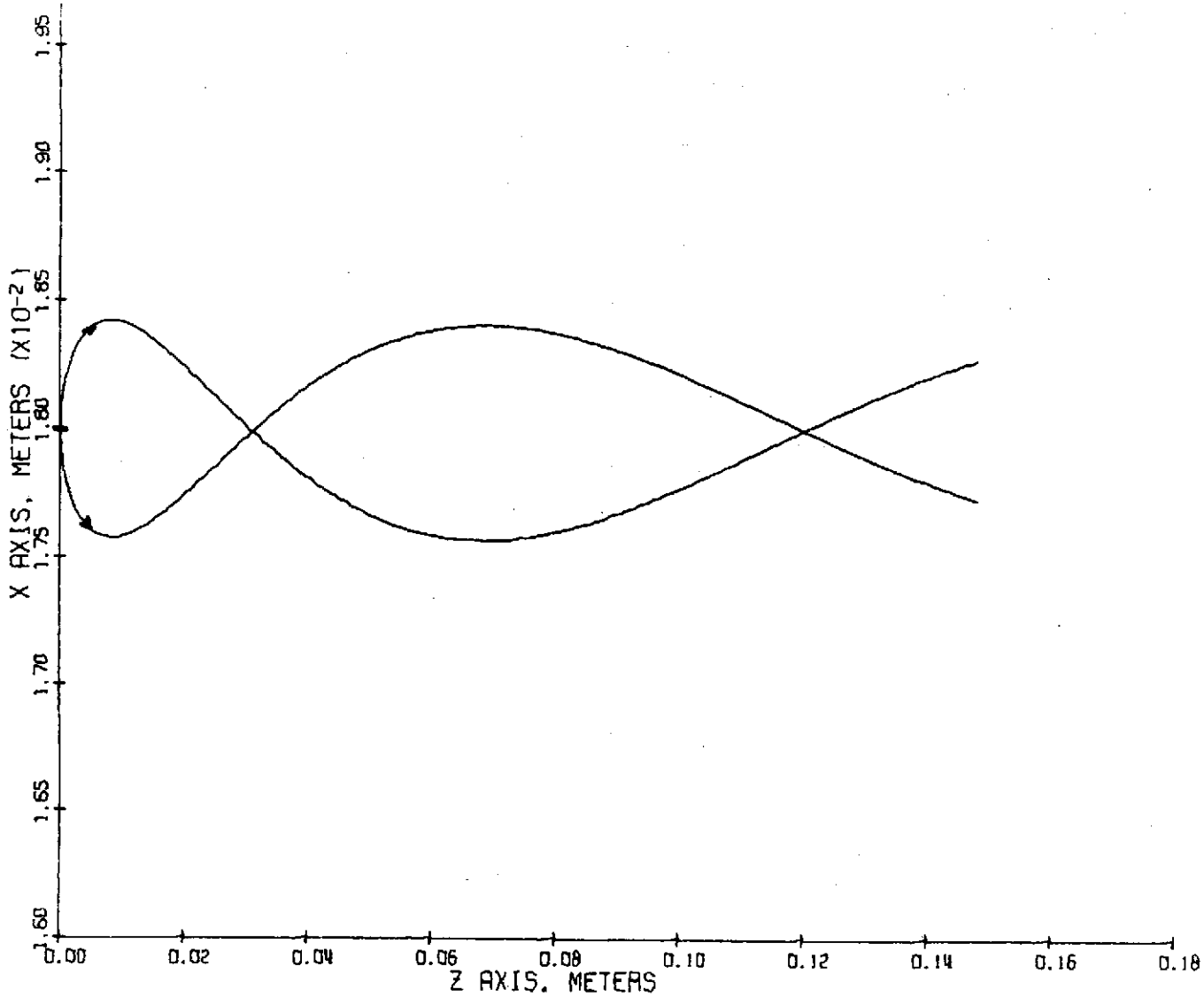

Fig. 19 - Z - X Projection of Photoelectron Trajectories for 35 mm Mod 7 Design.
X_o=1.8 cm, Y_o=0, V_{xo}=±1 ev, V_{yo}=0 and V_{zo}=1 ev

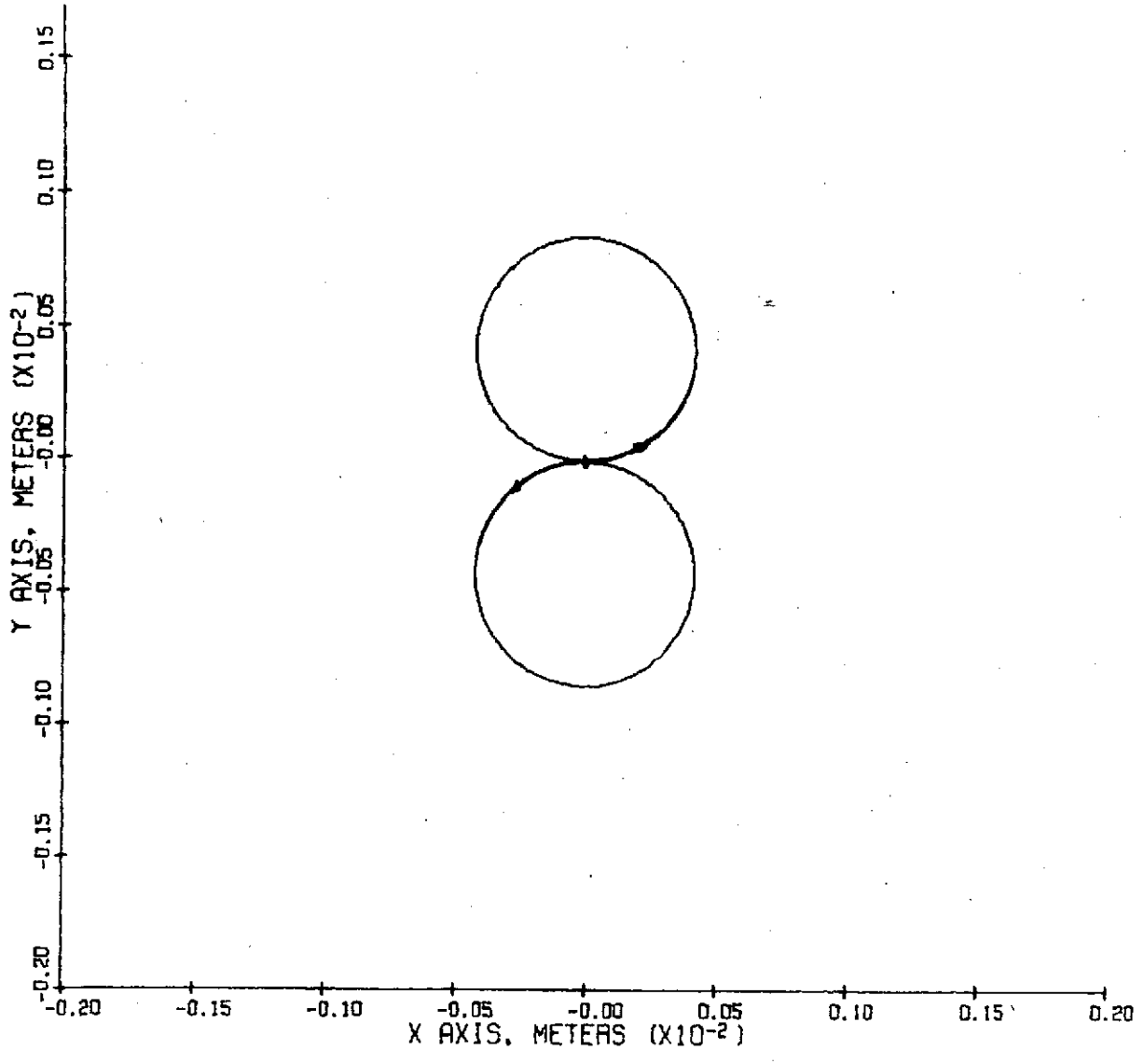

Fig. 20 - X - Y Projection of Photoelectron Trajectories for 70 mm Mod 15 Design.
X_o=0, Y_o=0, V_{xo}=±1 ev, V_{yo}=0 and V_{zo}=1 ev

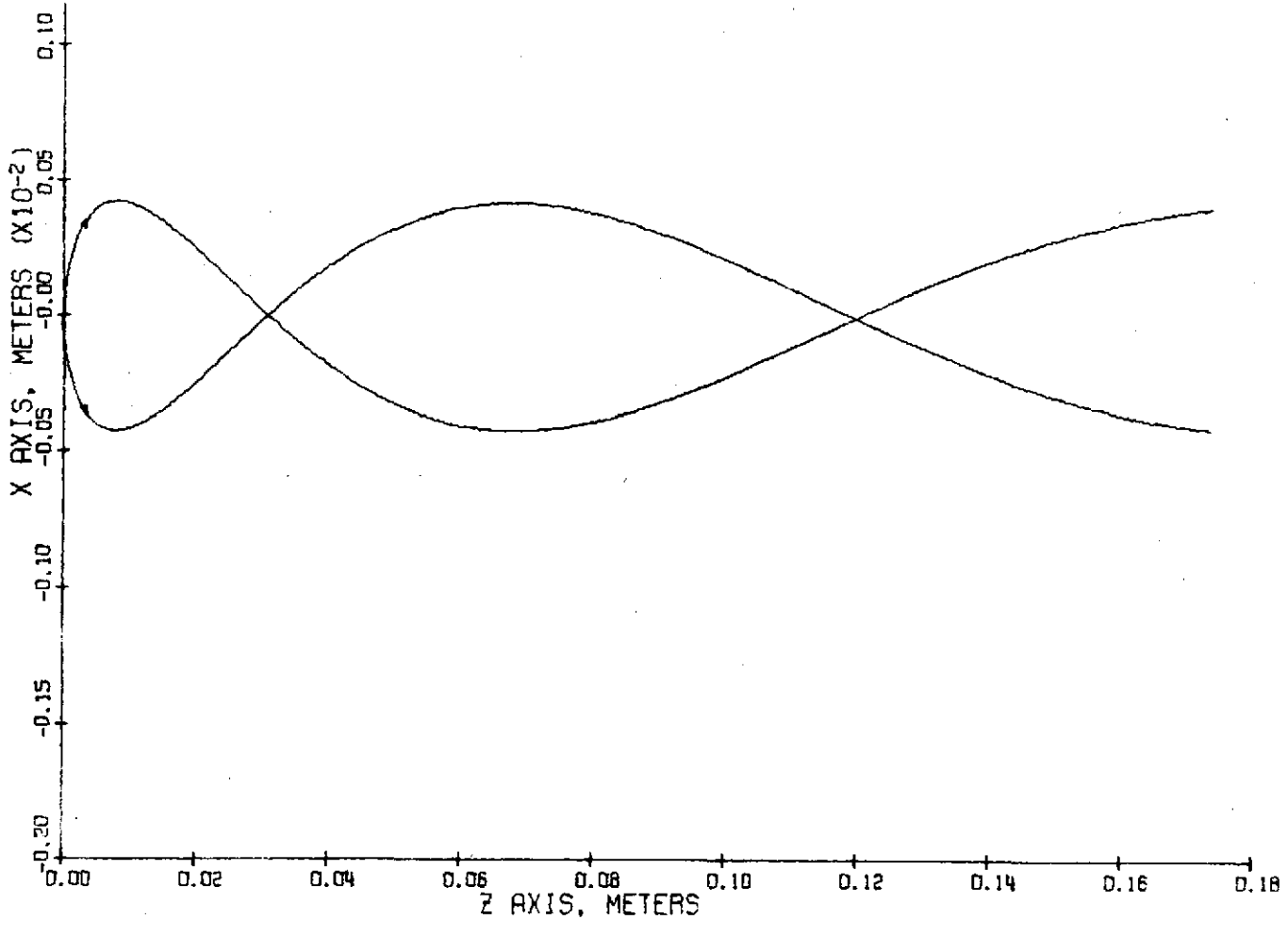

Fig. 21 - Z - X Projection of Photoelectron Trajectories for 70 mm Mod 15 Design.
X_o=0, Y_o=0, V_{xo}=±1 ev, V_{yo}=0 and V_{zo}=1 ev

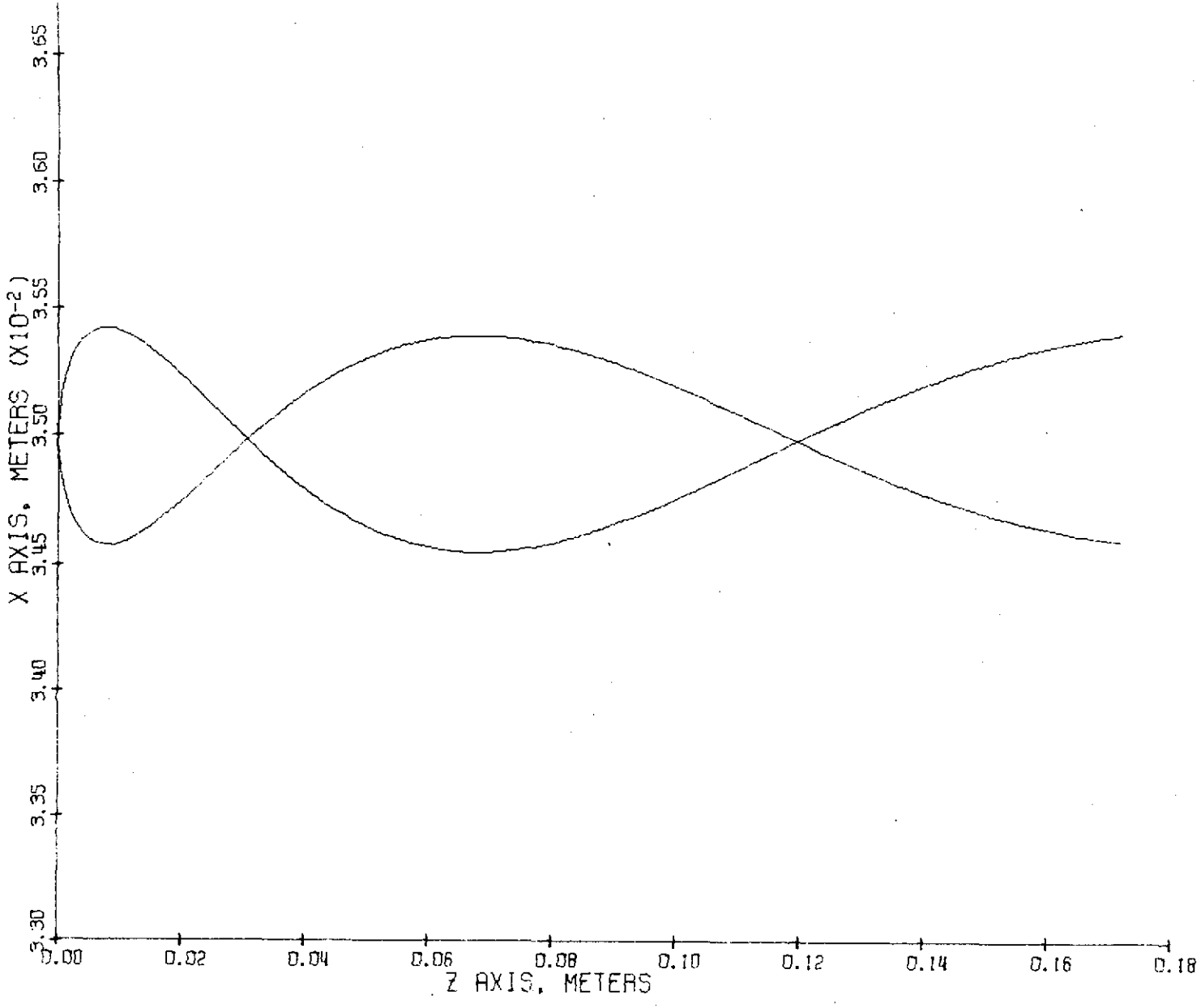

Fig. 22 - Z - X Projection of Photoelectron Trajectories for 70 mm Mod 15 Design.
X_o=3.5 cm, Y_o=0, V_{xo}=±1 ev, V_{yo}=0 and V_{zo}=1 ev

the image section with multi-loop focus. Some examples of the multi-loop orbits are given in Figures 23, 24 and 25, where the voltage is reduced by a factor of 4 for 2 loops and a factor of 9 for three loops, as compared to the single loop case. This is consistent with the analytical conditions for focus, but the graphs do show a shift in the focus evidencing slight field non-uniformities. The X-Y projection is the same in all cases since the radial or transverse component of velocity is unchanged.

Table III lists the focal plane, magnification and rotation for one, two and three loop focus of 1.41 eV electrons emitted at 45° from the photocathode for both the 35 mm and 70 mm formats, using the Mod 7 and Mod 15 PMA magnetic fields, respectively. In all cases the magnification is essentially unity and the rotation is negligible as expected for such uniform axial magnetic fields. (See Figures 8 through 15). Though restricted, these data indicate that the permanent magnet assembly can provide an essentially undistorted image. The shift in focal plane between the one, two and three loop cases is easily corrected in operation by a slight adjustment of the photocathode voltage.

Point Spread Function (PSF) and Modulation Transfer (MTF) Calculations

In the above analysis, only a monoenergetic photoelectron pair are considered as leaving the photocathode. The distribution of photoelectron energies from a real Cs-Na-KSb, (S-20), photocathode excited by 2090Å (5.9 electron volt) photons[11] is shown in Figure 26. Using this energy distribution and assuming a cosine distribution function for the emission angles allows the calculation of a realistic PSF.

To determine the PSF, the number of electrons impacting the target within an annulus of radii r and $r + \Delta r$ must be calculated for the assumed energy and angular distributions discussed.

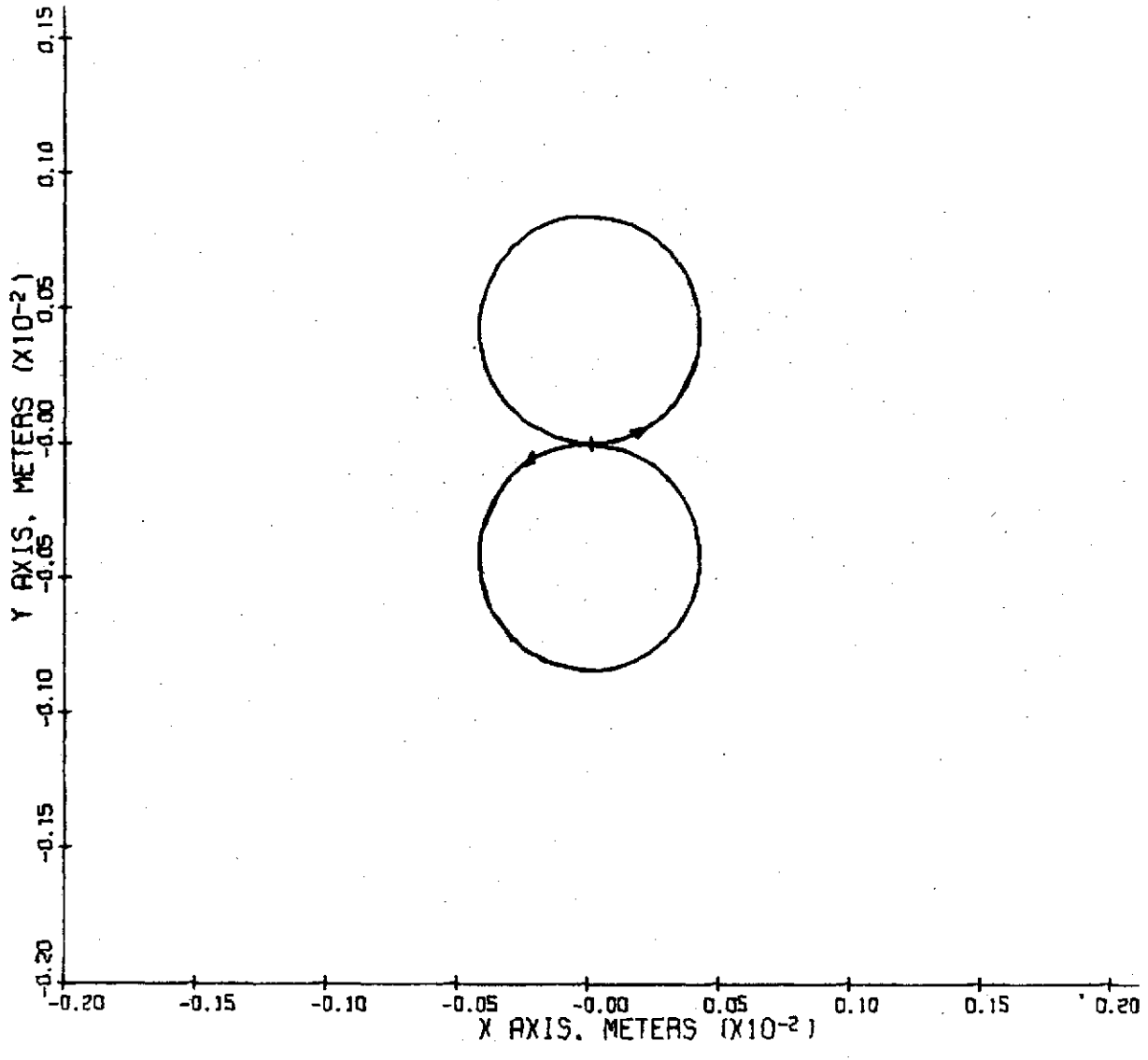

Fig. 23 - X - Y Projection of Photoelectron Trajectories for Electric Field 1/4 Normal. Otherwise, same conditions as Figure 16.

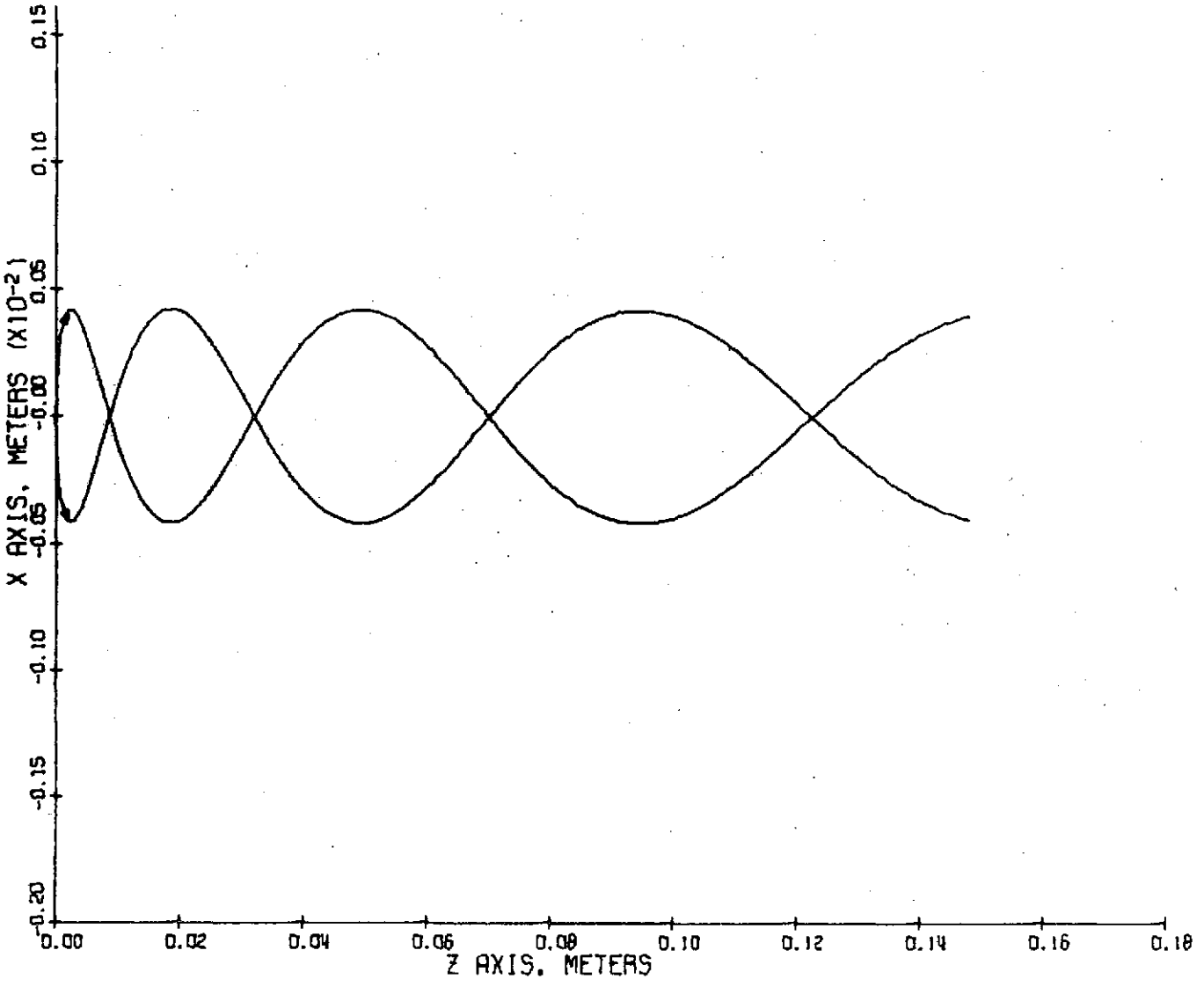

Fig. 24 - Z - X Projection of Photoelectron Trajectories Showing Two Loop Focus with Electric Field 1/4 Normal. Otherwise same conditions as Figure 17.

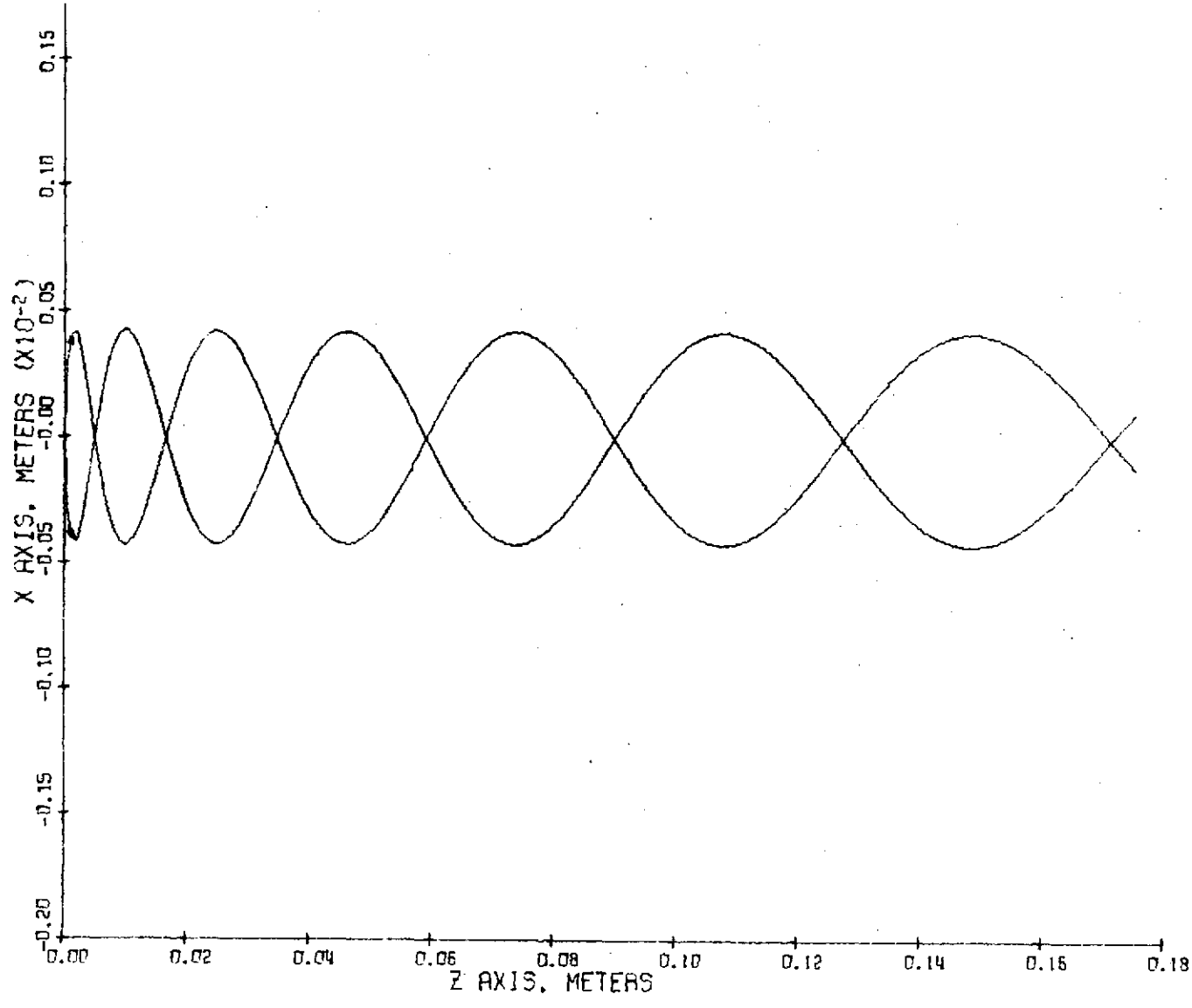

Fig. 25 - Z - X Projection of Photoelectron Trajectories Showing Three Loop Focus with Electric Field 1/9 Normal. Otherwise same conditions as Figure 17

TABLE III

SUMMARY OF PMA IMAGE QUALITY DATA

35 mm, MOD 7 Design

Xo X Axis Starting Point cm	Z Distance from Photocathode meter	E Electric Field Volts/meter	Δ X * microns	Δ Y ** microns	Magnification	Rotation degrees	Comments
0	0.119718	0.6667×10^5	0	2	-	-	Single Loop focus, Yo = 0, $Vy_o = 0$
0.6			0	3	0.9988	0.024	$Vx_o = \pm$ lev, Vz_o = 1 ev
1.2			0	3	0.9995	0.031	
1.8			1	4	0.9999	0.029	
0	0.122465	0.1667×10^5	0	2	-	-	Double Loop focus, Yo = 0, $Vy_o = 0$
0.6			0	2	0.9987	0.010	$Vx_o = \pm$ 1 ev, Vz_o = 1 ev
1.2			6	3	0.9993	0.007	
1.8			3	3	0.9998	0.008	
0	0.125116	0.7407×10^4	0	2	-	-	Triple Loop focus, Yo = 0, $Vy_o = 0$,
0.6			0	3	0.9988	0.014	$Vx_o = \pm$ 1 ev, Vz_o = 1 ev
1.2			1	3	0.9994	0.007	
1.8			3	4	0.9998	0.006	

* X-Axis Distance between two electron trajectories at Z .

** Y-Axis Distance between two electron trajectories at Z .

TABLE III con't

SUMMARY OF PMA IMAGE QUALITY DATA

70 mm, MOD 15 Design

Xo X Axis Starting Point cm	Z Distance from Photocathode meter	E Electric Field Volts/meter	Δ X * microns	Δ Y ** microns	Magnification	Rotation degrees	Comments
0	0.119793	0.6667×10^5	0	2	-	-	Single Loop focus, Yo = 0, Vy_o = 0
1.2			0	2	0.9985	0.029	Vx_o = ± 1 ev, Vz_o = 1 ev
2.3			1	3	0.9989	0.021	
3.5			2	3	0.9995	0.022	
0	0.122568	0.1667×10^5	0	2			Double Loop focus, Yo = 0, Vy_o = 0
1.2			1	3	0.9985	0.002	Vx_o = ± 1 ev, Vz_o = 1 ev
2.3			3	3	0.9989	0.003	
3.5			7	3	0.9995	0.007	
0	0.125216	0.7407×10^4	0	2	-	-	Triple Loop focus, Yo = 0, Vy_o = 0,
1.2			2	3	0.9986	0.002	Vx_o = ± 1 ev, Vz_o = 1 ev
2.3			5	3	0.9990	0.001	
3.5			10	3	0.9996	0.004	

* X-Axis Distance between two electron trajectories at Z.

** Y-Axis Distance between two electron trajectories at Z.

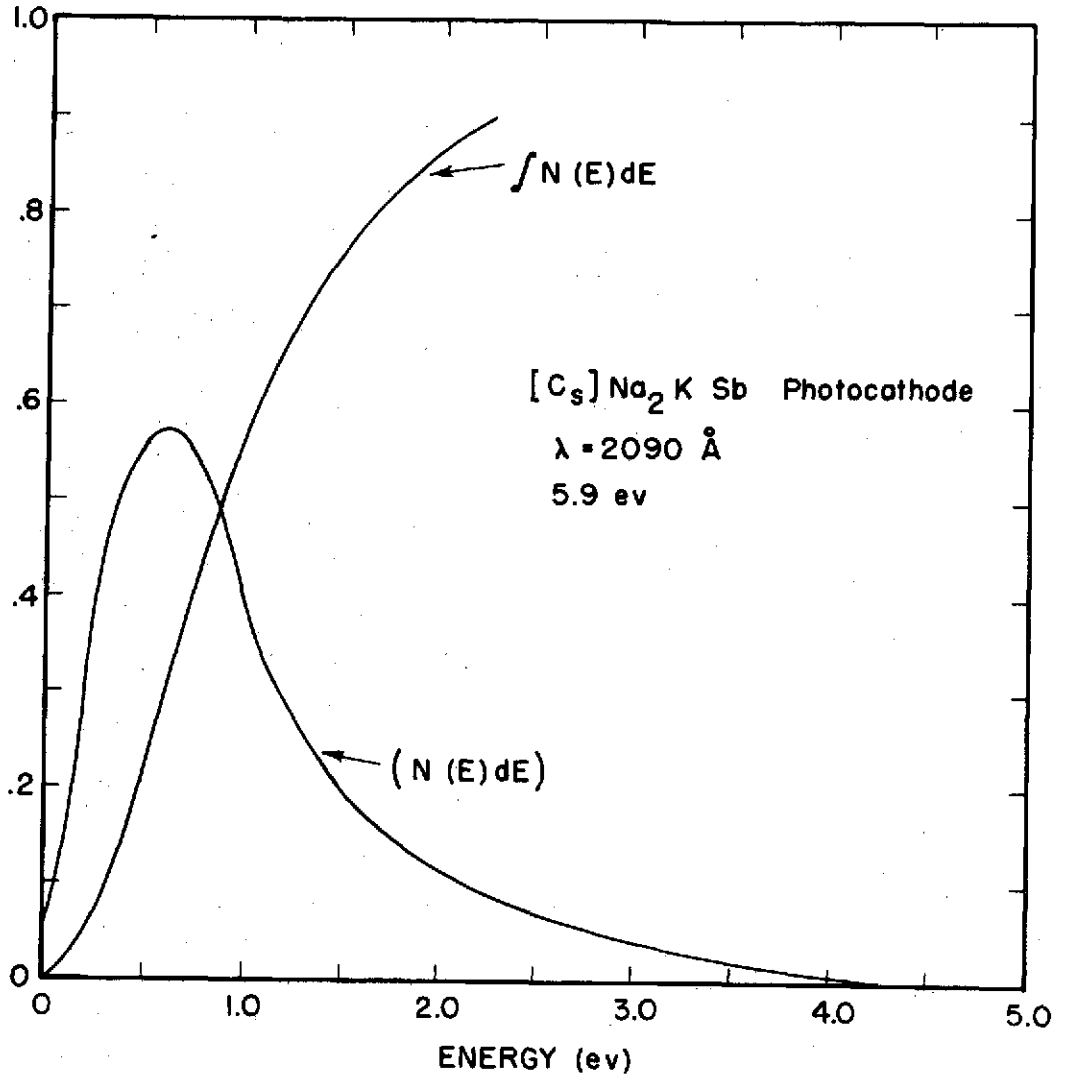

Fig. 26 - Photoelectron Energy Distribution for Cs Na_2 K Sb Photocathode

The number of electrons falling upon an annulus on the target with radii r_i and r_{i+1} is:

$$N'(r_i, r_{i+1}) = \int_{E_1}^{E_2} \left[\int_{\theta_1(E)}^{\theta_2(E)} \cos\theta \, d\theta \right] N(E) \, dE,$$

where E_1 and E_2 are the range of energies of electrons that impact the annulus, θ_1 (E) and θ_2 (E) are the limits on the angles of release from the photocathode for which electrons at energy E strike within the annulus, and N(E) is the energy distribution function.[12]

N' (r_i, r_{i+1}) can be approximated by the following summation:

$$N'(r_i, r_{i+1}) = C' \sum_j N(E_j) \left[\sin\theta_2(E_j) - \sin\theta_1(E_j) \right] \Delta E_j,$$

where $N(E_j)$ is the number of electrons leaving the photocathode with energy E_j, and C' is a normalization constant. As the PMA design creates a near-uniform axially symmetric magnetic field, electrons of equal energies but opposite angles that leave the PC to strike the target within the same radius so it is not necessary to do a double summation.

The N(E) function is represented by eight points (.125 ev, .375 ev, .625 ev, 1.0 ev, 1.5 ev, 2.0 ev, 2.5 ev and 3.0 ev). The computer electron trajectory program, Zoomplot is run for each value of the chosen Es for eighteen initial angular directions.

For a selected focal plane distance, radius (r) for each initial energy-angle (θ) is determined. The θ vs r curves are plotted for each of the photoelectron energies, so for each selected annular ring radii the energy dependent contributing angles can be determined. The full set of $N'(r_i, r_{i+1})$ summation are found. Figure 27 shows a plot of initial trajectory angle vs radius (θ vs r) for the Mod 7 PMA with the initial energy equal to .625 ev and one loop focus conditions.

The electron density for any annulus is proportional to the number of electrons and inversely proportional to annulus area.

$$I(r_i, r_{i+1}) \propto \frac{N'(r_i, r_{i+1})}{\left[(r_{i+1})^2 - r_i^2\right]}$$

A plot of the Point Spread Function, I vs r is shown in Figure 28 for the 35 mm PMA in the single loop focus mode. The ordinate of the PSF curves has been normalized such that $\frac{1}{\pi}\int I \cdot d\,(\text{Area}) = 1$. Figure 28 also shows a plot of $\frac{1}{\pi}\int I \cdot d\,(\text{Area})$ vs radius where $\frac{1}{\pi}\int I \cdot d\,(\text{Area})$ is the normalized sum of electrons falling with an annulus of radius r.

To obtain the MTF, the following transformation is performed:[2]

$$MTF(k) = 2\pi \int_{-\infty}^{+\infty} \left[I(r)\right]\left[J_0(2\pi k r)\right] r\, dr$$

where I(r) is the point spread function,

$J_0\,(2\pi\, k\, r)$ is the Bessell function of the first kind of zero order,

r is the radius,

dr is the increment of radius, and

k is the spatial frequency.

The integral is evaluated on the computer by summations and the MTF for the 35 mm Mod 7 PMA is shown in Figure 30. This is in good

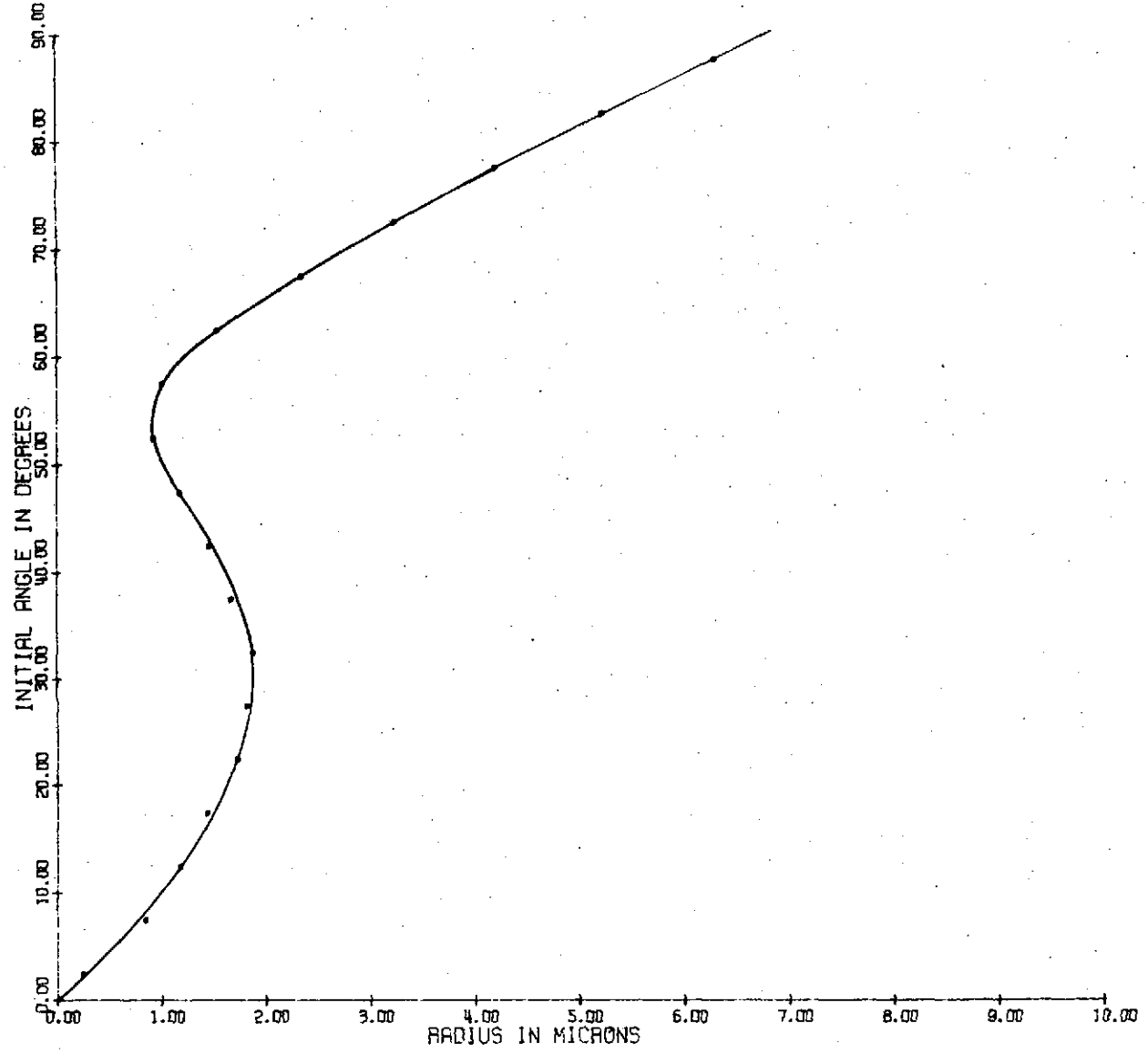

Fig. 27 - Initial Trajectory Angle vs. Radius for Mod 7 (PMA) where the Initial Energy = .625 ev. One Loop Focus Electric Field.

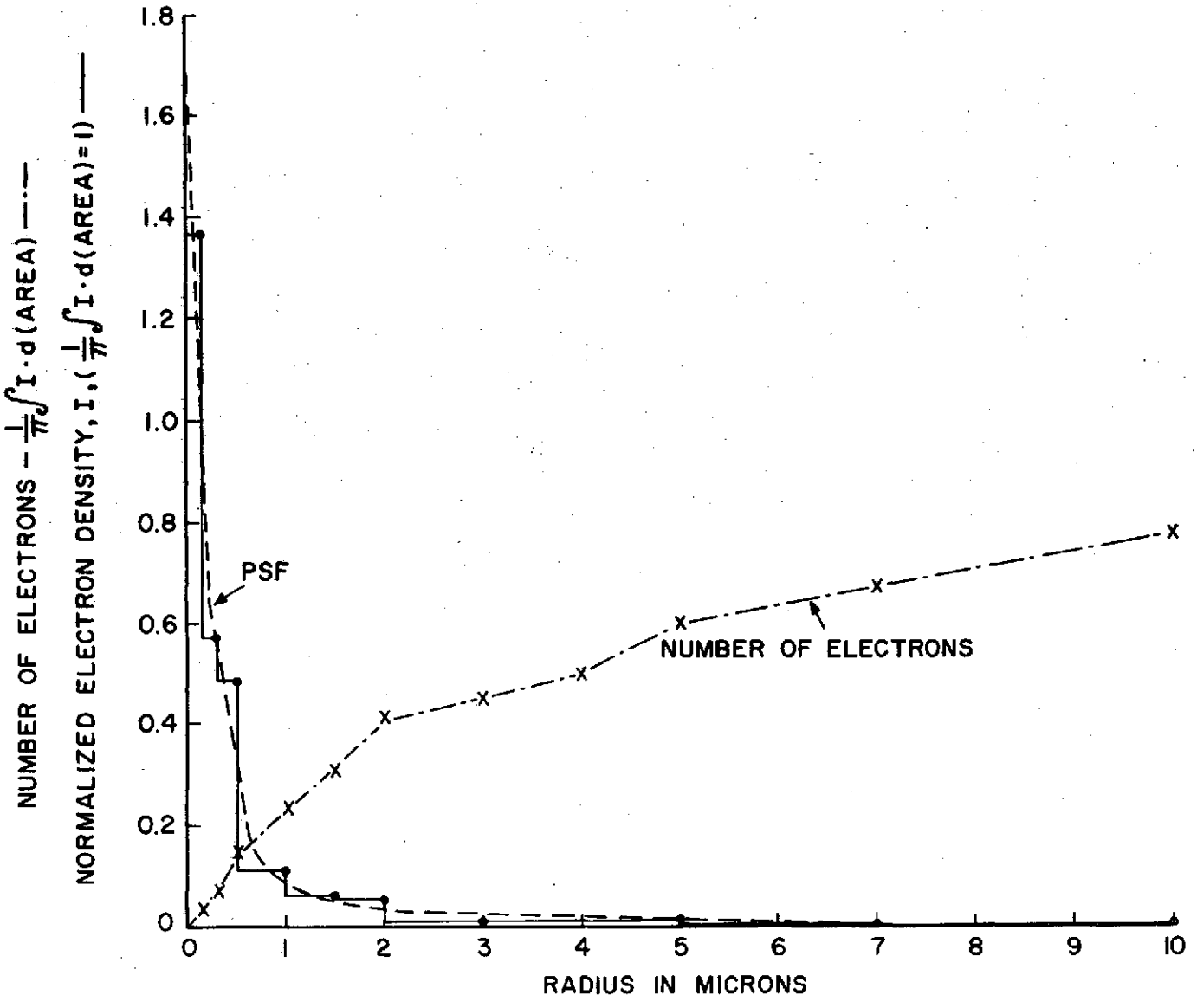

Fig. 28 - Image Section Point Spread Function, (PSF), for Mod 7 Design.
X_o=1.8 cm, Y_o=0.

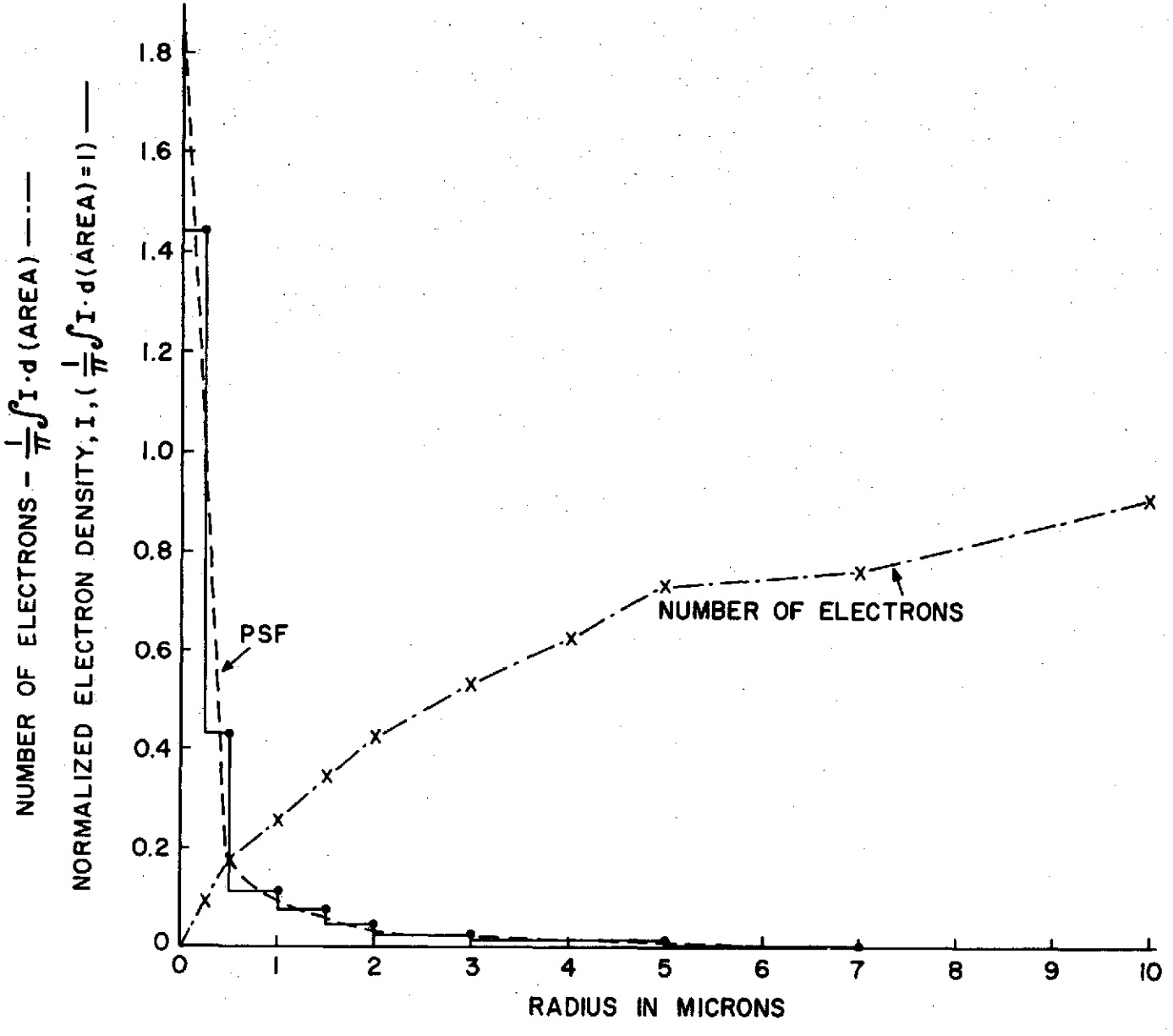

Fig. 29 - Image Section Point Spread Function, (PSF), for Uniform Field Case.

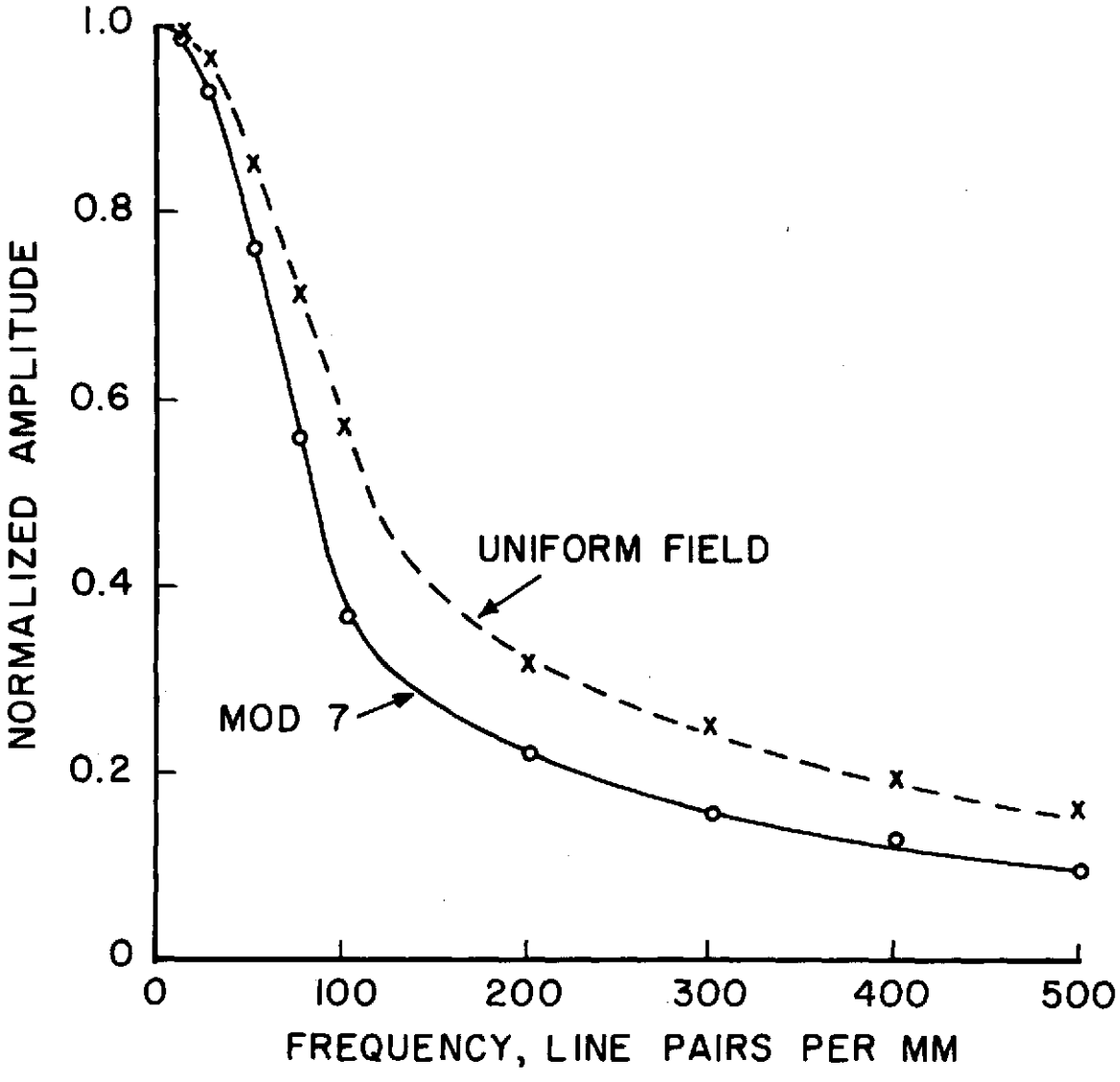

Fig. 30 - Image Section Modulation Transfer Function, (MTF), for Mod 7 Design at X_o=1.8 cm and Uniform Field Case.

agreement with the MTF of a comparable image calculation by Schade.[20]

The Point Spread Function and the integral of intensity for the uniform field case discussed in Appendix B is shown in Figure 29. Also shown in Figure 30 is the MTF for the uniform field case. The MTF of the permanent magnetic focused image section closely approaches the theoretical performance possible with uniform fields in the 0 to 50 $lp/_{mm}$ range, while the performance beyond 50 $lp/_{mm}$ is slightly degraded.

Since the magnetic field uniformity is comparable, the same MTF can be expected at other points in the image for both the 35 and 70 mm designs. This image section MTF is high compared to the MTF of the overall tube which has been measured to be 50% at 20 cycles/mm when focused with an electromagnet. The MTF of the target dominates the overall SEC tube MTF with the gun MTF also contributing a significant factor.

From this analysis one concludes that the permanent magnet focus assembly design is more than adequate to focus the SEC tube.

IV. VARIABLE GAIN

Variable gain in SIT or EBS type detectors is achieved by varying the voltage between photocathode and target. Gain variations in the SEC type detector can be achieved in this same manner, but the SEC gain is usually varied by adjusting the target bias voltage.

Presuming the gain is to be varied by varying the photocathode voltage, there are two possible schemes: simultaneous adjustment of both magnetic and electric fields to maintain single loop focus or, varying the number of loops of focus in the image section by decreasing the electric fields. The focal condition for the multi-loop case is expressed by the equation:

$$\ell = 10.59\, V^{\frac{1}{2}}\, B^{-1},$$

where ℓ is the loop length (cm)

B is the magnetic field (gauss)

and V is the accelerating potential (volts).

Therefore, going from a one loop to a two loop focus requires the voltage to be reduced by a factor of four. As the charge generated in the target is proportional to an electron's impact energy, this would result in a decrease in gain of the order of four fold. However, the gain is less than four as an appreciable amount of an electron's energy is lost as it passes through the Al_2O_3 membrane that is the structural part of the SEC target and the aluminum signal plate before impacting the KCl target. There is a comparable dead layer on the silicon target. Smaller incremental changes in the voltage and resultant gain are possible by starting at two loops and going to three, etc.

The photometric performance of the sensor is degraded for large decreases in gain because of an effect associated with the dead layers of the target. As a large fraction of the photoelectron energy is dissipated in the dead layers, the non-uniformities in the thickness of those layers become increasingly important. For example, consider the case where the dead layer energy loss is 2 kV and the total voltage is 10 kV. For dead layer spatial thickness variations of 10% the gain will be spatially modulated by:

Total potential - dead layer = gain producing potential

10 kV - 2 kV = 8 kV effective potential

Spatial variation:

10% of 2 kV = 0.2 kV

Spatial variation in gain:

$$\frac{0.2\ \text{kV}}{8\ \text{kV}} \times 100 = 2.5 \text{ percent.}$$

As the voltage is reduced by a factor four to go from 1 to 2 loop focus, the modulation becomes:

$$2.5 \text{ kV} - 2 \text{ kV} = 0.5 \text{ kV effective potential}$$

Spatial variations:

$$10\% \text{ of } 2 \text{ kV} = 0.2 \text{ kV}$$

Spatial variation in Gain:

$$\frac{0.2 \text{ kV}}{0.5 \text{ kV}} \times 100 = 40 \text{ percent}$$

The effect on signal to noise when operating at reduced gain with silicon targets has been experimentally investigated and these general results are confirmed.[17,18]

Notwithstanding the argument presented above, it does appear quite feasible from an electro-optical standpoint to operate the image section at multiple loop focus by reducing the accelerating voltage. Figures 17, 24 and 25 shows the Z-X projection of the photoelectron trajectory for 1, 2 and 3 loop focus in the PMA uniform magnetic field of 80 gauss. The results listed in Table II indicate that the image rotation, field flatness, and "S" distortion is negligible in all three cases. However, even for the perfect case of parallel H and E fields the chromatic aberration is much more pronounced in the multiple loop case due to the fact that the differences in initial photoelectron velocities are a larger fraction of the accelerating voltage and, as noted by Beurle and Wreathall,[14] the root mean square radius of the circle of confusion is proportional to $L \frac{U_i}{V}$ (U_i is the initial photoelectron velocity in the axial direction, V the acceleration potential and L is the photocathode-target distance).

The effect is graphically demonstrated by comparing the total number of electrons landing within the first 10 microns and the Point Spread Profiles for the single loop focus and double loop focus shown in Figure 28 and Figure 31. There are approximately twice as many electrons landing within the first 10 microns for the single loop case as compared to the two loop focus.

Therefore, low accelerating voltage operation results in a poorer MTF, poorer point source response and degraded signal to noise ratio. The effects are independent of the permanent magnet assembly per se. They are true for any focus system: magnetic, electrostatic, or proximity.

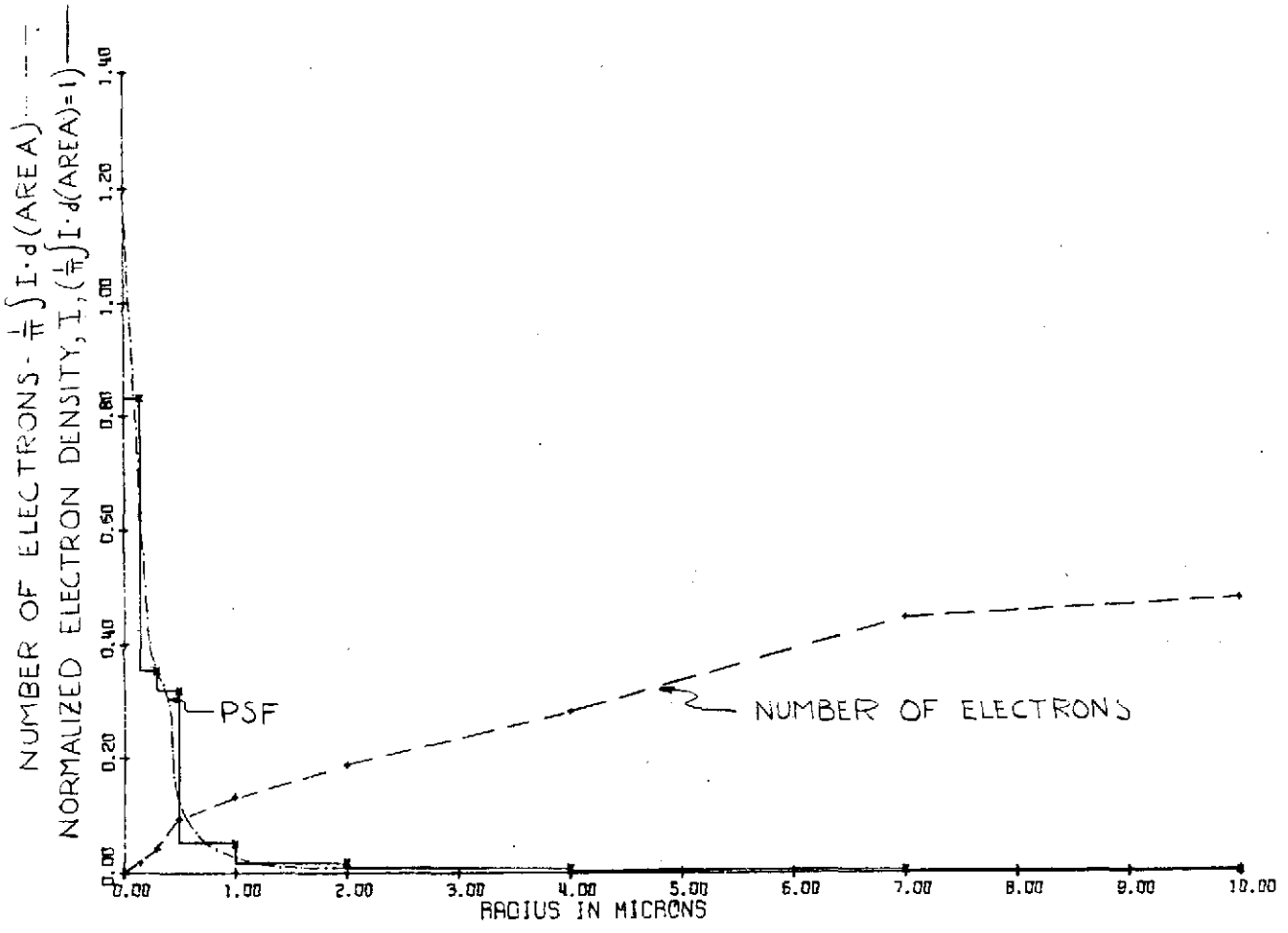

Fig. 31 - Image Section Point Spread Function, (PSF), for Mod 7 Design at X_o=1.8 cm with Two Loop Focus.

V. MAGNETIC SHIELDING

Image Deflection Considerations

Deflection of the photoelectron image by the orbital changes in the earth's magnetic field is an important consideration because of the long exposures expected in the LST mission. The image section deflection transfer function upon application of a transverse field is 0.9 mm per gauss.[10] In order to keep the loss in spatial frequency response (MTF) caused by smearing of the image during exposure to less than 10 percent, the image shift must be less than 1/2 of a picture element. At 20 cycles/mm this is a shift of 12.5 microns which corresponds to a transverse field of 0.014 gauss. Since the orbital change in the earth's magnetic field is 0.7 gauss peak-to-peak, a magnetic shield with an attenuation factor of at least 50 is required.

Deflection in the gun section is 0.5 mm/gauss[10] and not as serious since the readout occurs in less than a minute, too short a time for the earth's field to change significantly. An absolute shift in position of the image on the scanning raster is not a serious problem since it can be corrected during the data processing.

Axial Field Considerations

It is difficult to shield the television tube from magnetic fields aligned with the axis of the tube. The worst case condition would be for the earth's field to be aligned with the tube axis. The maximum magnetic field is ± 0.35 gauss. Presuming that the initial focus is set up with the axial component of the earth's field zero, laboratory experience[10] indicates that a change of 0.35 gauss results in a decrease in the image sections' spatial frequency response at 20 cycles/mm of approximately 8%. It appears advisable to sense the earth's magnetic field and make an appropriate adjustment in the tube electrode potentials. It is also possible to place a magnetic shield in the

axial path, if the optical path includes folding optics.

Shield Design

The magnetic shielding problem is accentuated by the fact that the shield must absorb the external field of the focus magnet without saturating and still provide the required factor of 50 attenuation for external transverse fields. This is also the case when the focus field is provided by a solenoid. However, in most cases the return flux that a solenoid shield has to carry is less than returned flux in a permanent magnet focus assembly's shield for an equivalent internal magnetic field.

The best design for efficient magnetic shielding is the use of multiple cylindrical shields[4] where the thickness required is governed by the attenuation requirements and not the flux carrying requirements. Wadley[4] has shown that it is profitable to have a single layer shield only as long as the shield thickness, t, obeys the relation: $t < 3a_1/2\mu$, where a_1 is the inner shield radius and μ is the permeability of the shielding material. Wadley[4] treated the multilayer shielding subject in detail, but this analysis is not repeated here.

In the permanent magnetic assembly Armco low carbon iron is used to provide the return flux path, as it has a high maximum flux density. An outer shield cylinder of high permeability is used to shunt the earth's field.

The attenuation factor, g, of a single layer shield is:[4]

$$g = \frac{\mu}{4}\left(1 - \frac{a_1}{b_1}\right)$$

where a_1 is the inside and b_1 is the outside radius. Figure 32 shows the permeability curve of Co-Netic (Perfection Mica Company) that is used in the permanent magnet shield. For an attenuation of 50, μ must be high to avoid

a thick heavy shield. To use CO-Netic as a shield the results in Figure 32 show that the ultimate flux density in the shield must be 6000 gauss or less. Presuming a minimum permeability of 10^5, the thickness for an attenuation of 50 is calculated below:

$$50 = \frac{10^5}{4} \left(1 - \frac{a_1}{b_1}\right)$$

$$\frac{a_1}{b_1} = 0.998$$

The outer cylinder shield radius of the 35 mm PMA is approximately 12 cm. Therefore, the minimum thickness is:

$$t \geq b_1 - a_1$$

$$t \geq b_1 - 0.998 b_1 \geq 12\ (0.002) \geq 0.024 \text{ cm}$$

For external transverse fields, the cylindrical shield flux density is approximately:[7]

$$B = \frac{2.5\ a_1\ H_o}{t} \text{ gauss.}$$

With H_o as the Earth's field in oersted

$$B = \frac{2.5 \times 12 \times .4}{24 \times 10^{-3}} = 500 \text{ gauss.}$$

The magnetic flux density in the shield due to the leakage flux from the PMA's low carbon iron outer cylinder is approximately 5000 gauss for a spacing of 1 cm and shield thickness of 0.024 cm. The maximum flux density in the shield occurs near the end caps, but it is not necessarily in the same direction as the earth's magnetic flux density. The sum is less than 6000 gauss in the worst case so that a permeability of 10^5 as originally selected from Figure 32 is adequate. In the shield designs for the 35 mm and 70 mm PMA listed in Table IV, the thickness has been made somewhat thicker than minimum to provide a safety margin on the attenuation and flux density and also to make fabrication easier. Table V shows the result of making the outer cylinder of the PMA thick enough to screen the tube from the earth's field without resorting to a separate shield. This clearly shows the advantage of multi-layer shielding.

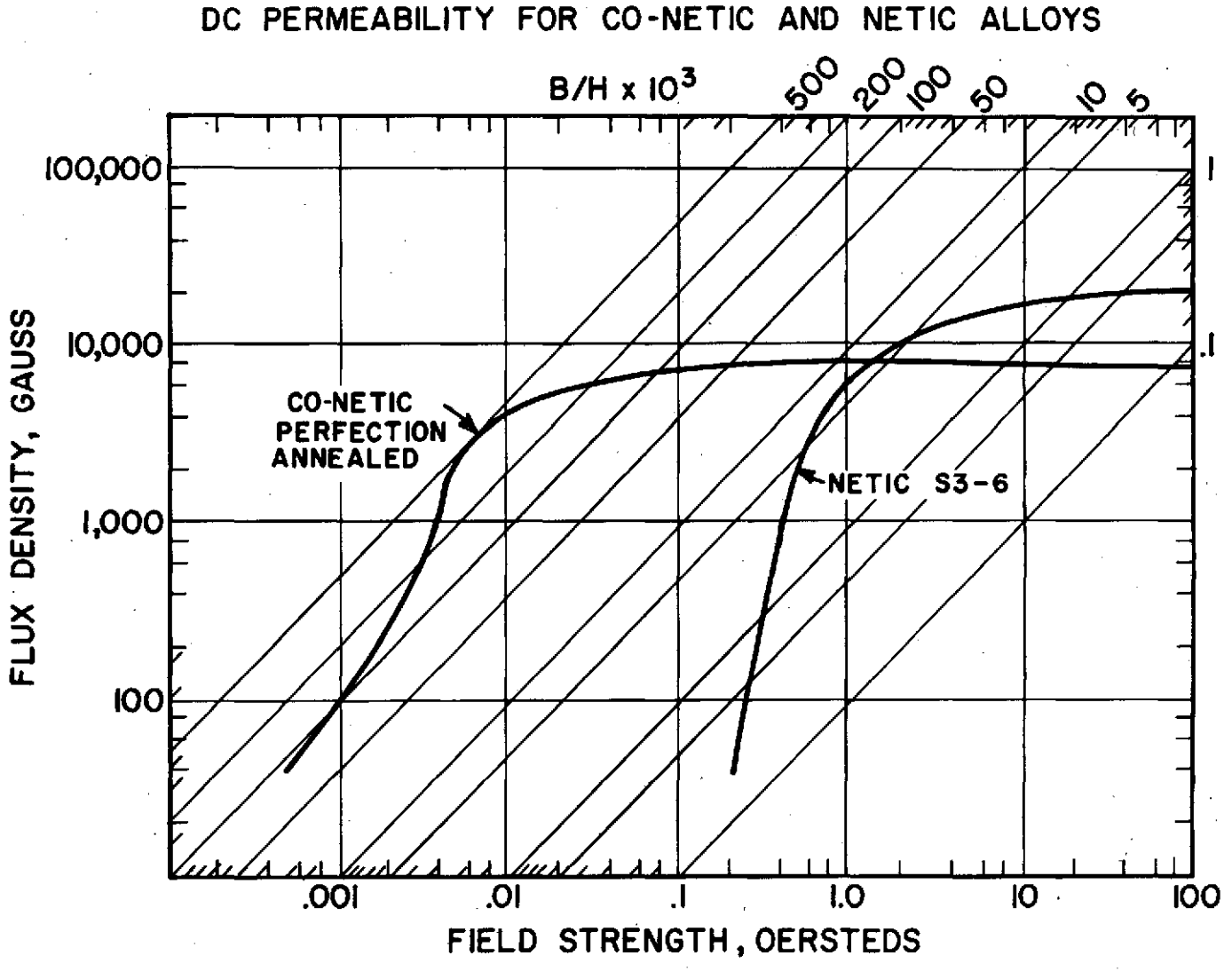

Fig. 32 - Permeability Curve for Conetic Shield Material

TABLE IV

MAGNETIC SHIELD PARAMETERS

For 35 mm and 70 mm PMA Designs

PMA Size	Shield Thickness cm		Minimum Spacing cm		Weight - Kilograms			Outside Dimensions cm	
	Cylinder	End Cap	Outer Cylinder to shield	End Ring To End Cap Shield	Cylinder	End Caps	Total	Radius	Length
35 mm (Mod 7)	0.051	0.079	0.94	1.78	2.36	0.87	3.23	12.85	70.34
70 mm (Mod 15)	0.064	0.102	2.54	3.81	4.78	1.87	6.65	16.97	85.90

TABLE V

PMA WEIGHTS INCLUDING MAGNETIC SHIELDING

	PMA Weight Kilograms	Cylinder Shield Weight Kilograms	End Cap Shield Weight Kilograms	Total Weight Kilograms	Comments
1. Mod 7	15.72	2.36	0.87	19.0	Mod 7 design uses low carbon steel for the outer cylinder and end rings. Conetic shielding material is used for the magnetic shield.
2. Mod 12	28.26	-	0.76	29.0	Mod 12 design uses low carbon steel for the end rings and Vanadium Permendur (VP) for the outer cylinder. The VP outer cylinder serves a dual function, as the PMA's return flux path and as the magnetic shield. Conetic end shields are used for axial shielding. The outside shield radius = 12.03 cm and the outside shield length = 66.34 cm.
3. Mod 13	24.20	-	0.80	25.0	Mod 13 is the same as Mod 12 except conetic material replaced the VP in the outer cylinder. The outside shield radius = 12.34 cm and the outside shield length = 67.56 cm.

VI. STABILITY OF PERMANENT MAGNETS

The magnetic field used to focus the SEC tube must be stable to ±0.1% if the MTF degradation due to field alone is to be less than 10% at 20 cycles/mm.[10] When the other tubes parameter tolerances are taken into consideration so that the overall system deviation is 10% loss at 20 cycles/mm, the error budget for the magnetic field is ±0.035%.[10] In general any change in magnetic field can be compensated for by adjustment of the accelerating voltage (electric field).

In the permanent magnet assembly only slow "steady state" variations exist due to the long thermal time constant of the assembly and its thermal environment. As discussed in the following paragraphs, the effect of shock, stress, vibration, radiation and adverse magnetic fields are expected to be negligible or easily accommodated as part of the normal focus routine for the camera.

Figure 33 shows the change in remanence, B_d , as a function of temperature for Alnico 5, where P is the ratio of B_d to H_d. H_d is the magneto-motive force per unit length at the magnet's operating point. In both the Mod 7 and 15 designs the P factor equals approximately 22. The temperature coefficient is approximately 0.012% per degree Centigrade for a P = 18. If the magnetic field of the PMA were proportional to B_d of the magnets, a ± 3°C temperature variation could be tolerated provided nothing else changed. Here no attempt is made to determine the PMA internal magnetic field variations with B_d. The potentially most serious difficulty is the variations with time and conditions of the air gaps in the assembly. This would clearly affect the magnetic field, but it is difficult to calculate these effects. Environmental tests of a prototype unit would be much more meaningful.

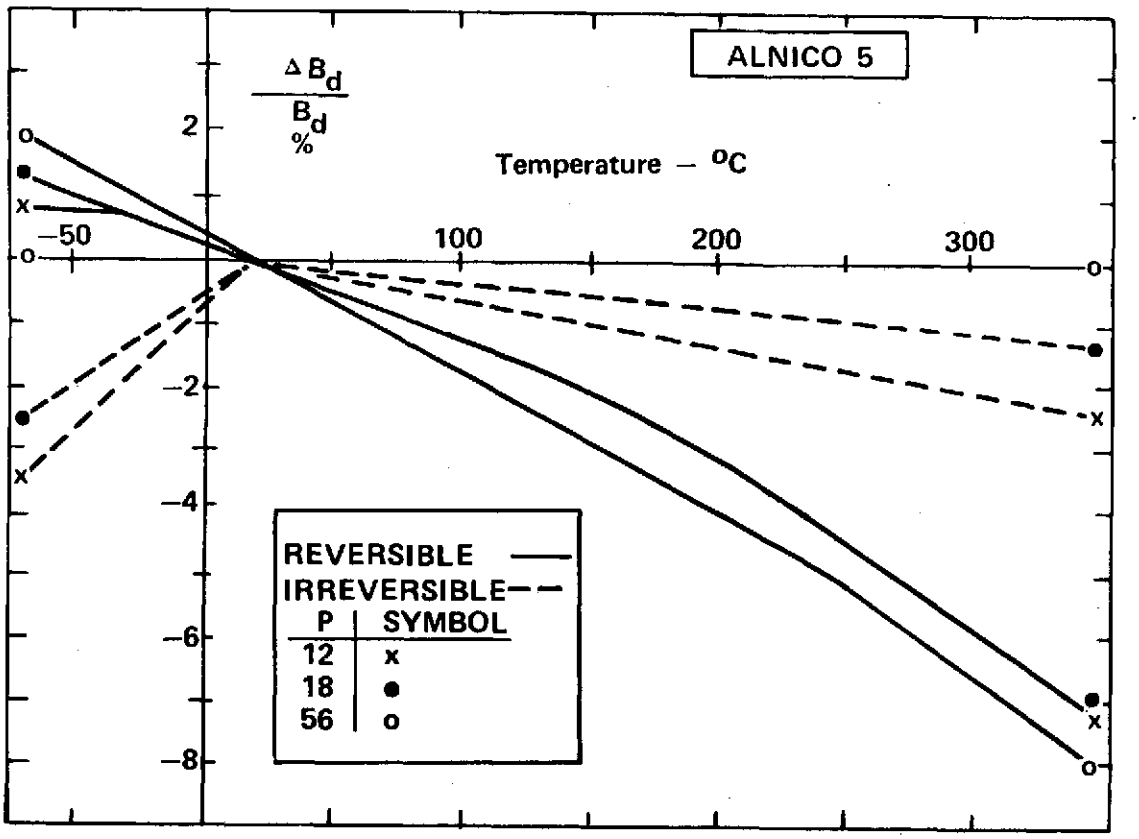

Changes in remanence of Alnico 5 magnets due to temperature.

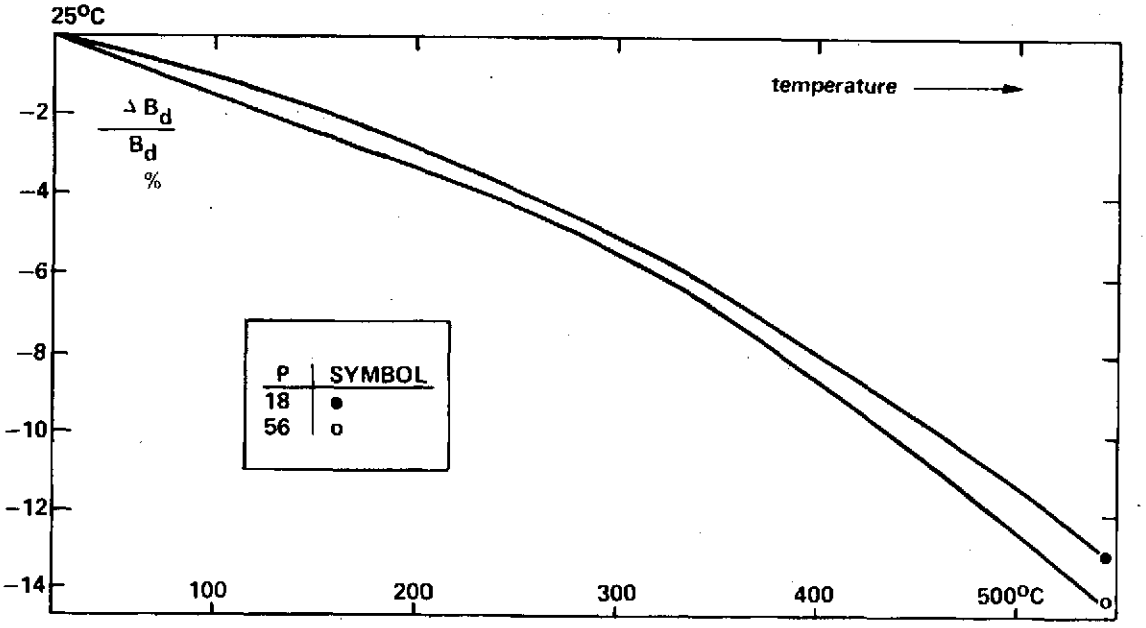

Reversible changes in remanence of Alnico 5 magnets after 1000 hours at 548°C.

Fig. 33 - Remanence Changes as a Function of Temperature for Alnico 5 Magnetic Material

The following excerpt from Indiana General data[21,22] summarizes the factors affecting magnetic stability.

FACTORS AFFECTING MAGNETIC STABILITY

Permanent magnets do not "run down". In this respect they fundamentally differ from batteries, radioactive materials, or the like. The magnetic field surrounding a magnet does not require energy to maintain it, therefore there is no theoretical reason for a permanent magnet to continually lose strength. In actual practice however, flux changes may occur as a result of several factors. Proper stabilization will eliminate or reduce these.

1. METTALURGICAL CHANGES

In the older permanent magnet materials, such as cobalt-steel, some metallurgical changes take place as a function of time. If such a magnet is magnitized before these changes have stabilized, flux changes superimposed on those to be described in the next section will occur. (This effect can be reduced to a negligible factor by artificial aging). In the newer materials, such as Alnico or Ceramic, metallurgical changes do not take place in any measurable degree at room temperature.

2. TIME

A freshly magnetized permanent magnet will lose a minor percentage of its flux, as a function of time. It has been shown that, if one plots flux loss linearly against time logarithmically, an essentially straight line results. Laboratory measurements on some materials are shown in the table below. All losses are based on measurements made starting at 0.1 hours after magnetizing.

Measurement accuracy by Indiana General was 1 part in 10,000

Material	Loss Per Log Cycle	Loss at 100,000 Hrs. (11.4 years)
Ceramic	Essentially zero	Essentially zero
Alnico 3 (Near Max. Energy)	0.4%	2.4%
Alnico 3 (Near Coercive	0.6%	3.6%
Alnico 5 (Near Residual)	0.01%	0.06%
Alnico 5 (Near Max. Energy)	0.15%	0.9%
Alnico 5 (Near Coercive	0.4%	2.4%

Alnico 8 - No Data (Expected to be less than Alnico 5)

In order to achieve a high degree of stability, it has become standard practice to sacrifice some useful flux. This reduces the remanence to a lower value which is more stable over long period of time. The relative amount by which the remanence is reduced through such a treatment is a controlled demagnetization. Temperature cycling or exposure to A.C. fields are methods used for demagnetization. Alnico 5 magnets have remanences at the knee of the demagnetization curve were found to be stable within ±0.03% when demagnetized 5 to 15%. The tolerance on the stability was limited by Indiana General's measuring ability for the sample size used.

3. TEMPERATURE

Temperature effects fall into three categories: Metallurgical, Irreversible and Reversible.

A. Metallurgical changes may be caused by exposure to too high a temperature. Such flux changes are not recoverable by remagnetization. The approximate maximum temperatures which can be used without experiencing metallurgical changes range from 550°C for Alnico 5 to 1080°C for the Ceramics. The effect of metallurgical changes, if present, can be avoided only by long-time exposure of the magnet to the temperature involved, prior to magnetizing.

B. Irreversible losses are defined as a partial demagnetization of the magnet, caused by exposure to high and low temperatures. Such losses are recoverable by remagnetization. Merely as examples, table below shows values measured on laboratory specimens, with percent flux losses measured at room temperature after exposure to the indicated temperatures. Percentages shown in the table are not additive for consecutive cycles above and below room temperature.

	662°F (350°C)	392°C (220°C)	-4°F (-20°C)	-76°F (-60°C)
Ceramic 5 (Pc 2 Above Max. Energy	0	0	0	0
Ceramic 6 (Pc 1.1 Near Max Energy	0	0	0	0
Alnico 5 (Near Max. Energy)	1.3%	0.8%	1%	2.5%
Alnico 6 (Near Max. Energy)	0.6%	0.4%	0.5%	1.3%
Alnico 8 (Near Max. Energy)	0.3%	0.3%	0.1%	0.1%
Alnico 8 (Near Coercive)	3.5%	2.0%	0.5%	0.8%

The ideal method for stabilizing magnets against temperature-induced irreversible losses, is installing them in the magnetic circuit for which they are intended, magnetize, then subject the assemblies to several temperature cycles which they are expected to experience in service. Alternatively, the magnetized assembly may be partially demagnetized by means of an AC field, following the procedure described in the last paragraph of Section 2, "TIME". A "Rule of Thumb" to follow is determining by experiment that temperature cycling will cause X% flux loss, then the AC field should be such as to cause a 2X% flux loss, to properly stabilize against temperature.

C. Reversible changes in flux are reversible with temperature. For example, if any of the ceramic grades are heated 1°C above room temperature, they will lose 0.19% of room temperature flux. However, this will be spontaneously regained upon the magnet's cooling back to room temperature. The Alnico materials have reversible variations on the order of 1/10 as great as the ceramics, depending upon the material and the operating point on the demagnetization curve. One cannot eliminate these reversible variations by stabilization treatments. However, use of proper temperature compensation material in parallel with the magnet will reduce the effect to a negligible factor. Among others, household watt-hour meter magnets and speedometer magnets are temperature compensated in this manner.

4. RELUCTANCE CHANGES

If a magnet is magnetized in a magnetic circuit and subsequently subjected to permeance changes (such as changes in air gap dimensions or open-circuiting of the magnet) it may be found that a partial demagnetization of the magnet has occurred. Whether or not such a loss is experienced depends upon material properties and upon the extent of the permeance change.

Stabilization against such change is accomplished either by several times subjecting the magnet to such reluctance changes after magnetizing, or by use of the previously described AC field.

In this section it should be mentioned that contacting the magnets with ferro-magnetic material (screw drivers, pliers, and the like), at points other than the poles, can cuase an appreciable drop in flux at the poles. It is difficult to stabilize against this type of abuse. The remedy is to avoid such practices.

5. ADVERSE FIELDS

If a magnet or magnet assembly is subjected to an adverse magnetic field, a partial demagnetization may result, depending upon material properties and upon the intensity and direction of the adverse field. Proper stabilization consists of subjecting the magnet or assembly to a DC or AC demagnetizing field of the same magnitude as it is expected to encounter in service. The direction should be the same as that of the anticipated demagnetizing field.

6. SHOCK, STRESS AND VIBRATION

The effects of shock, stress and vibration below destructive limits on most permanent magnet materials are so minor (a few tenths of a percent) that little consideration need be given to them. Proper stabilization as described in any of the preceding sections will also stabilize against shock and vibration.

7. RADIATION

The effects of radiation on permanent magnet materials varies widely by material classes. Current experiments indicate that all permanent magnet materials of a commercial nature can withstand irradiation to 3×10^{17} neutrons per CM^2 (neutron energies greater than 0.5 eV), without flux changes. A majority of the commercial materials (including Alnico and Ceramic can withstand 2×10^{18} neutron per CM^2 exposure, without flux changes, and show only minor changes (less than 10%) when the radiation level is increased to 3×10^{19} neutrons per CM^2. Radiation, like thermal demagnetization, is not applicable to calibration although some evidence indicates that secondary exposure to high neutron densities causing initial flux changes results in only negligible additional flux changes. This would indicate that stabilization of radiation effects by initial exposure is possible.

8. MAGNETIZED PERMANENT MAGNETS

If, for one reason or another, a permanent magnet is purchased magnetized, what does or can occur magnetically must be fully realized. The concept of magnetic behavior, or operating slope for maximum magnetic efficiency must be recognized. The accrued factor of self-demagnetization, or "Build-IN" stabilization must be evaluated. The problem of in-plant processing cannot be overlooked. The problem of multiplicity of magnetized magnets and their attractive forces, along with temperature extremes, must be considered.

This magnetized condition, and its associated problems, can be alleviated by specifying that keepers be attached. A keeper is simply one or more pieces of ferrous material usually placed across the gap of a magnetized permanent magnet interaction between magnets.

Manufacturing personnel who handle magnetized magnets and assemblies should receive special instructions. This instruction merely details what should or should not be done to the magnetized assemblies. As an example, the dropping of a permanent magnet structure may alter the gap dimensions. This could occur without any visible damage to the structure but would necessitate demagnetizing the permanent magnet, reworking the structure, and remagnetization. In many cases the removal of a magnetized permanent magnet from its structure will degrade the performance, resulting in a "Knock-Down" of the permanent magnet, a condition remedied only by remagnetization.

All of the above discussion for the two states of a permanent magnet-magnetized or not magnetized —are, of necessity, quite general. The user of this material will have specific problems, which in many cases will require a unique procedure. This information for maximum permanent magnet efficiency should be obtained from the technical staff of the supplier.

VII. INTERRELATIONSHIP OF PMA TO TUBE CONFIGURATION

The basic requirement on the permanent magnet design is to provide a radially symmetric field. It must be reasonably uniform axially as well, but the tolerance is greater. The overall length and diameter have a direct bearing on the weight of the permanent magnet assembly. In this respect the length of the image section is directly proportional to the focus field so that the length could be decreased if the focus field were higher, but this appears to be a poor tradeoff since the length of the electron gun is fixed by target-scanning-deflection angle considerations. A higher focus field would impose a higher deflection field for the same length gun section.

There would be a real advantage in decreasing the diameter of the image section, or in a design that allowed minimum clearance between the tube and the focus magnet assembly. One possibility for decreasing the diameter of the image section would be to put the high voltage electrodes inside the image section. This would save about 2 cm of the inside diameter of the PMA. Trajectory analysis near the inside diameter of the PMA indicates that the useful "magnetic" radius is approximately 75% of the inside radius of the profile cylinder. This means that the target diameter could be 8 cm diagonally or an 56.5 mm square based on the magnetic focus requirements. Therefore it is quite feasible from the magnetic assembly considerations to shrink the inside diameter of the PMA or alternatively to scan a larger image format. But this scheme is limited by features of the tube fabrication itself. There must be minimum flange annular surface areas for sealing the image section to the gun section and the window to the image section. Also, there must be annular space for mounting the target and field mesh inside the image section. Any

consideration of actually placing the high voltage electrodes and the resistor voltage divider inside the image section must take into account possible contamination of the photocathode from outgassing of the resistors during bake out while making the photocathode and over the long term. Also, as the electric field seen by the photoelectrons is affected by the potential of the walls of the image section, the closer the photoelectron comes to the wall the more it will be affected by any non-uniformities in the voltage gradient down the wall.

In summary:

(a) A reduction in the inside diameter of the focus assembly could make a large reduction in focus assembly weight.

(b) A reduction in inside diameter is possible by redesigning the tube so as to keep the high voltage electrodes in the image section inside the insulating walls of the image section.

(c) The feasibility of putting the electrodes inside the image section and other changes to reduce the diameter of the tube is not clear and would require detailed study by the tube manufacturers.

The electron gun length in the 2-inch return beam vidicon, which scans a 25 x 25 mm format, is 14.0 cm long compared with the 24.2 cm length of the comparable SEC tube. Redesigning the SEC tube to use this shorter gun would reduce the PMA length. The resultant weight would be less than 13 Kg.

Note that a reduction in tube diameter and/or length would reduce the weight and/or power dissipation of a solenoid electromagnet focus assembly also.

VIII. COMPARISON WITH BAR MAGNET AND SOLENOID FOCUS ASSEMBLY DESIGNS

Bar Magnet Assembly

Permanent magnet focus assemblies are used routinely to focus image intensifiers. Baum has described in detail a design using long bar magnets distributed uniformly around a cylinder.[13] This configuration is shown schematically in Figure 34 . In one specific design, a Leonard window image tube is focused with a 155 gauss field. The parameters are:

Length	36 mm
Diameter	22 mm
Useful Length	28 cm
Weight of Magnets[15]	7.5 Kg (Alnico 5)
Weight of Brass Cylinder	1.0 Kg

The magnetic shield for this permanent magnet focus assembly has the following parameters:

Length	76 cm
Diameter	56 cm
Material	Armco iron

The shield diameter to magnet assembly diameter ratio is approximately 40%. Using the shield reduces the field strength within the magnet assembly by approximately 30%. The external field outside the shield caused by the Alnico magnet assembly is reduced by a factor of about 45 by the shield. The weight of the image tube system including shield and supporting structure is approximately 100 Kg. The weight of a similar design for 80 gauss would be approximately 73 Kg. The useful diameter of this assembly is not stated as a function of length but is presumably large enough to accommodate the 35 mm format of a 75 mm diameter television camera tube. Its useful length of 28 cm is too short compared to an SEC tube's photocathode to electron gun length of 36.6 cm.

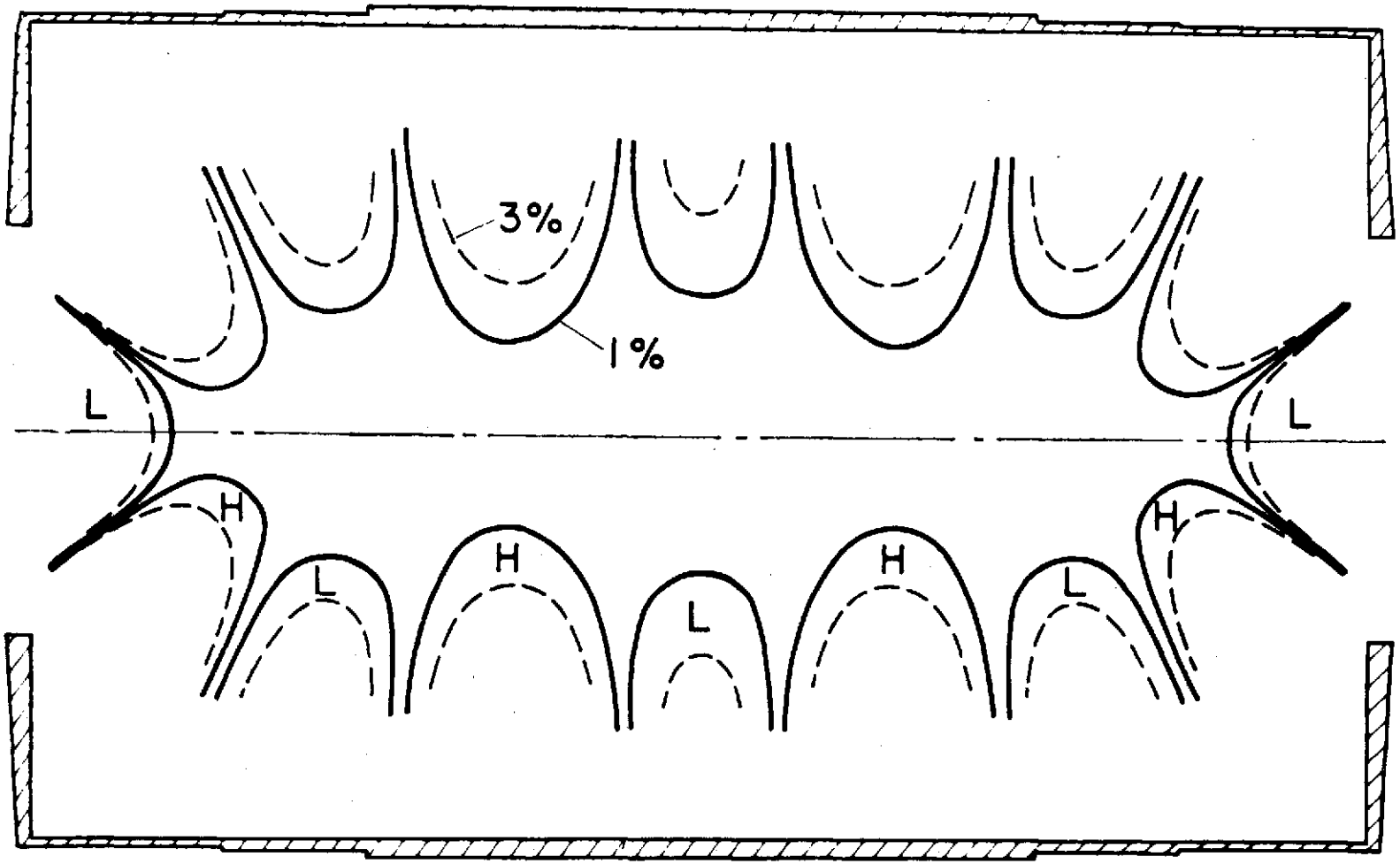

Fig. 34 - Bar Magnet Permanent Magnet Focus Assembly
Schematic and Volume of Uniformity.

A design to accommodate the greater length would be considerably heavier as its diameter must also increase so that the ratio L/D remains near 1.6; which is a condition for best magnetic field uniformity.[13] From these considerations one could conclude that the Mod 7 PMA design at 19 Kg is preferable to the bar magnet design from a weight standpoint.

In both the PMA and bar magnet focus assembly designs, the assembly weight is dominated by the components that provide the path for the external magnetic field. It is important that the assembly provide this low reluctance path for the external magnetic field for two reasons. In ground based applications the image sensor moves relative to the telescope and dome structure during an exposure as the telescope tracks. This means that the coupling of the magnet's external field, i.e., the reluctance of the external field path, is varying during exposure. This causes the internal magnetic field to vary since the flux of the magnet divides in proportion to the ratio of the reluctance of the internal and external paths.

The second reason for providing a low reluctance return path is that the television or image tube must also be shielded from the earth's magnetic field in those applications where its orientation to the magnetic field is changing during an exposure, or it is impractical to refocus for each new fixed orientation. To provide shielding from the earth's magnetic field a high permeability path around the tube is needed. This means that the magnetic material used for the shield must not saturate under the influence of extraneous external fields and the external field of the focus magnet. In the PMA this problem is solved by a two-layer shield. The inner cylinder carries the external field of the focus magnet and the outer cylinder provides the high permeability path for the earth's magnetic field. Bowen

has proposed a shield that consists of washer shaped rings that are sections of a cone.[16] These rings are placed perpendicular to the external field of the focus magnet such that they are an effective shunt for the earth's magnetic field but do not saturate on the focus magnet field. This allows a somewhat lighter weight assembly but is inadequate in those applications where, during an exposure, there is motion of the magnetic parts relative to the telescope or dome structure. It would be more feasible for satellite applications where there is no such relative motion. However, it may be necessary in satellite applications to restrict the extent of the external magnetic field for other reasons, such as interference with other instruments and the torque produced by the interaction of the magnetic field of the satellite and the earth's magnetic field.

Solenoid Focus Assembly

A solenoid design was investigated for comparison with the PMA. A parametric study of weight versus power dissipation was made to determine the power dissipation of a solenoid assembly comparable in weight to the Mod 7 PMA. Trajectory, magnification, image rotation and field characteristics were also studied.

The power dissipation and weight in the focus coil is a function of the cross-sectional area and length. For a long solenoid, (neglecting end effects) the power per unit length is given by the following equation[1]:

$$W' = \frac{H_o^2}{[G'(\alpha)]^2} \times \frac{\rho}{\lambda} \quad \text{watts/cm}$$

where: $$G'(\alpha) = \frac{2}{5}\left[\frac{\pi(\alpha-1)}{\alpha+1}\right]^{1/2}$$

and $$\alpha = \frac{a_1}{a_2}$$

where:

a_1 = inside radius

a_2 = outside radius

H_o = magnetic field in oersteds

ρ = resistivity in ohm-cm

($=2.83 \times 10^{-6}$ ohm-cm for aluminum)

λ = Space factor ($\simeq .7$)

The weight of the windings is given by:

$$W = (V)\ (D)\ (SF)$$

where

V = volume of windings, cm^3

$= \pi b\ a_1^2\ (\alpha^2 - 1)$

b = coil length

D = density of the winding material in gm/cm^3 ($= 2.7\ gm/cm^3$ for aluminum)

SF = stacking factor ($\simeq 0.85$)

The major consideration in a solenoid focus coil design for space use would be the power dissipation. Aluminum wire has a higher resistivity than copper by a factor of 1.67, but a lower density by a factor of 3.3. Thus, for a given weight, aluminum has a lower power dissipation.

Table VI, numbers 1, 2 and 3 show the effects of α on the weight and power dissipation for a 35 mm solenoid assembly. For an α of 1.625 the weight of the total solenoid assembly, which includes the bobbin and magnetic shield, is comparable to the weight of the Mod 7 PMA. The length of the solenoid

TABLE VI

EFFECT OF α ON THE WEIGHT AND POWER DISSIPATION FOR 35 mm and 70 mm SOLENOID FOCUS ASSEMBLIES

No.	α	DIMENSIONS - CM					WEIGHT - KILOGRAMS				POWER @ 25°C Watts	COMMENTS
		Length Total	Bobbin I.R.	Coil I.R.	Coil O.R.	Shield O.R.	Wire Alum	Shield	Bobbin	Total		
1	1.5	43.3	5.4	5.55	8.25	8.37	11.94	1.90	0.81	14.65	11.1	Single Solenoid for 35 mm SEC
2	1.75	43.3	5.4	5.55	9.13	9.85	19.70	3.02	0.95	23.67	8.1	Single Solenoid for 35 mm
3	1.625	43.3	5.4	5.55	9.02	9.14	15.67	2.72	0.89	19.28	9.3	Single Solenoid for 35 mm
4	1.625	43.3	5.4	5.55	9.02	9.14	15.67	2.72	0.89	19.28	9.8	Photocathode end of Solenoid has booster coil to flatten field at Photocathode (35 mm SEC)
5	1.625	50.0	6.6	6.75	10.97	11.20	27.0	3.82	1.25	32.07	11.3	Single Solenoid for 70 mm SEC
6	1.50	50.0	6.6	6.75	10.13	10.30	21.0	2.66	1.14	24.80	12.8	Single Solenoid for 70 mm SEC

winding was fixed at 43 cm for all comparisons, but because of the end effects of an uncompensated solenoid the magnetic field is not uniform at the photocathode location. Additional turns were added to the photocathode end of the coil. This "booster" section does not increase the coil's length, but increases the current density in the first 2 cm of the coil.

Table VI, number 3 lists the parameters for the 35 mm booster solenoid design. Also, in Table VI, numbers 4 and 5 show the effect of α on the weight and power dissipation for the 70 mm solenoid assembly.

The single energy trajectory focusing, magnification, rotation, and field strengths for the boosted design are listed in Table VII, number 1 and compares favorably with the PMA Mod 7 design. The power dissipation is 9.8 watts and the weight is 19.28 kg for the full length boosted design. Table VII, numbers 4 and 5 show the effect on the magnification and image rotation if the gun end of the solenoid is not energized during image section integration. When considering total system weight of the electromagnetic focus system the weight of the power source and electronic circuits to furnish and regulate the focus current must be included.

TABLE VII

IMAGE QUALITY CHARACTERISTICS FOR 35 mm SOLENOID WITH BOOSTER FOCUS ASSEMBLY

No.	α	TRAJECTORY On-Axis Start ΔX	TRAJECTORY On-Axis Start ΔY	TRAJECTORY Off-Axis Start ΔX	TRAJECTORY Off-Axis Start ΔY	Magnification	Rotation Degrees	Location from On Axis, Axial Magnetic Field Coil End-CM PC	Gun	PC	Target	Booster Length CM	COMMENTS
1	1.625	0	0	1	0	0.999	0.05	6.0	1.4	80.0g	80.2g	2.0	Solenoid with booster coil on PC end of coil. Length= 43 cms for 35 mm SEC. Z_f = 11.9 cm, *See Note 1
2	1.625	0	0	3	0	1.029	0.77	6.0	1.4	80.7g	74.7g	2.0	Same as 1 above except energized 17 cm less of gun end of solenoid. Z_f = 12.1 cm *See Note 2
3	1.625	0	0	7	0	1.053	1.87	6.0	1.4	81.7g	69.2g	2.0	Same as 2 above, except de-energized 21 cm of gun end. *See Note 3

Notes:

1. Trajectory Conditions: V_{xo} = ± 1 ev, V_{yo} = 0, V_{zo} = 1 ev; Off-axis start, X_o = 1.8 cm; and Δ X, Δ Y are in microns.
2. Power reduced from 9.8 watts to 7.1 watts. (Power length = 26.0 cm).
3. Power reduced to 6.8 watts. (Power length = 22.0 cm).

IX. CONCLUSIONS

The permanent magnet assembly design presented provides a uniform magnetic field of a volume adquate for the SEC television camera tube. The calculated point spread function for the image section is excellent for the application, and the design appears to be practical in terms of fabrication, stability and configuration.

The necessity to recess the tube several centimeters within the assembly so as to imbed it within the most uniform magnetic volume does limit the focal ratio of the unvignetted optical image to about f/2.7 for the 35 mm tubes and f/3.9 for the 70 mm tubes.

The weights of the optimal designs are 19.0 Kg and 31.5 Kg for the 35 mm and 70 mm tubes, respectively. Those weights are equivalent to an aluminum wire solenoid electromagnet designs with power dissipations of about 10 watts and 12 watts, respectively.

Comparison of the weights of the PMA designs with the bar magnet arrays employed to focus image intensifiers indicates that the PMA design is lighter when magnetic shielding is included. It also points up the fact that the weight in both permanent magnet designs is dominated by the return path for the magnet's external field.

There is a good possibility of reducing the length and weight of the PMA design by adding small low power electromagnets to extend the region of uniform magnetic field. The length is somewhat longer than necessary anyway. As a basis for overall camera system studies, one might presume an optimized 35 mm focus assembly weight of approximately 15 Kg.

The question of minimum weight-length as well as the accuracy of the computer program modeling the actual situation can best be answered by building a prototype unit as the next step in this development program.

ACKNOWLEDGEMENTS

The basic concept for the toroidal PMA design and the computer programs for calculating the magnetic field were conceived and developed by Ken Wakefield of the Plasma Physics Laboratory of Princeton University. George Scheffield, of Princeton's Plasma Physics Laboratory, developed the electron trajectory computer program. Much of the detailed computer programming was carried out by Dick Meckstroth. Paul Zucchino provided many invaluable suggestions throughout the study. Thomas Kelsall of the NASA Goddard Space Flight Center supplied the material found in Appendix B, which deals with focusing of photoelectrons with electric and magnetic fields that are spatially uniform and parallel.

X. REFERENCES

1. Montgomery, Bruce D., "Solenoid Magnet Design", Wiley-Interscience, New York, (1969).

2. Jones, R. Clark, "On the Point and Line Spread Function of Photographic Images". Journal of Optical Society of America, Vol. 48, pp. 934-937, 1958.

3. Hanson, Roger J., and Pipkin, Francis M., "Magnetically Shielded Solenoid with Field of High Homogeneily". In Review of Scientific Instruments, Vol. 36, pp. 179-188, (1965).

4. Wadey, W.G., "Magnetic Shielding with Multiple Cylindrical Shells". In Review of Scientific Instruments, Vol. 27, pp. 910-916, (1965).

5. Bhatia, M.K., "Core Selection Charts". In EDN., Cahners Publishing Co., (1964).

6. "Typical Properties and Characteristics of Vanadium Permendur", Technical Memorandum, No. TM-72-424, Allegheny Ludlum Research Center, (1972).

7. "Magnetic Shielding Electrical Materials", Alleghney Ludlum Steel Corp., (1972).

8. "Permanent Magnets Materials Manual No. 34", Indiana General, (1972).

9. Kueser, P.E., Pavlovic, D.M., Lane, D.H., Clark, J.J., and Spewock, M., "Properties of Magnetic Materials for Use in High Temperature Space Power Systems", Westinghouse Electric Corporation, NASA SP-3043,(1967).

10. Long, D.C., Zucchino, P., Lowrance, J.L., "Study of Magnetic Perturbations on SEC Vidicon Tubes", Princeton University Observatory. Final Report on NASA Contract No. NAS-5-23254, 1973.

11. Spicer, W.E., "J. Phys. Chem. Solids", Vol. 22, pp. 365-370. Pergamon Press, New York,(1961).

12. Kelsall, Thomas, "Letter on Results of Group Meeting at PUO on 8 Oct. 1974".

13. Baum, W.A., "Magnetic Focusing of Image Tubes", Advances in Electronics and Electron Physics, Vol. 22A, pp. 617-628, Academic Press,(1966).

14. Beurle, R.L. and Wreathall, W.M., "Aberration in Magnetic Focus Systems", Advances in Electronics and Electron Physics, Vol. 16, pp. 333-340, Academic Press,(1962).

15. Baum, W.A. (private communication).

16. Apparently unpublished work by Bowen at Hale Observatories.

17. Ando, K., (private communication).

18. Hall, J. (private communication).

19. Mende, S. (in press).

20. Schade, O.H. and Johnson, C.B., "Advanced Electron Optics", Technical Report AFAL-TR-69-293. Wright Patterson Air Force Base, Ohio, November,(1969).

21. "Temperature Effects on Permanent Magnets", Applied Magnetics, Indiana General, Vol. 16, Number 1,(1969).

22. "Stability of Permanent Magnets", Applied Magnetics, Indiana General, Vol. 15, Number 1,(1968).

APPENDIX A

STATEMENT OF WORK

Permanent Magnet Focusing for Astronomical Camera Tubes

Permanent magnet assemblies to provide focusing within the image section of candidate television sensors for the Large Space Telescope (LST) are being considered as a means to reduce the thermal and power load on the spacecraft support system. The purpose of this study is to prepare designs of focusing units utilizing state of the art magnetic materials and to analyze mathematically their predicted performance. The results of this study shall be substantial enough so they can be used later as a basis for the fabrication of laboratory devices for experimental verification in breadboarding configurations using actual detector prototypes. The combination of permanent magnet focusing with the needs to a) shield the camera from external perturbing fields and b) operate the camera at different gain (sensitivity) levels are recognized as significant problem areas to which this study should be addressed. The study is for a six month period.

Task 1

Perform the mathematical analysis and design of a focus assembly based on state of the art permanent magnets for use with the imaging sections of intensified television detectors. Design specifications shall be expressed in parametric form as a function of detector configuration (e.g., size, material, properties, operating and voltages). Imaging by both single loop and multi-loop electron trajectories shall be treated. The reference detectors are the Westinghouse WX 32193 and WX 31958 SEC Vidicons. For the former, use the 4.2 inch cathode window version. Methods shall be described if needed to provide fine tuning of the focus assembly by either permanent magnets and/or small trimming coils. The design shall be sufficiently detailed in terms of material and size specification to allow later the preparation of a fabrication procurement for the construction of assemblies to operate with the above two detectors.

Task 2

Perform an image analysis based on the design prepared in Task 1. Electron trajectories shall be calculated to demonstrate performance, spatial distortions, and aberration.

Task 3

Analyze and describe the expected long term properties of one magnet structure. Degradation of performance due to environmental conditions such as temperature variation or cycling, corpuscular radiation, and shock and vibration shall be treated explicitly.

Task 4

Describe the interrelationships among the imaging magnet structure design and typical fabrication procedures for the class of imaging detectors referenced above. What changes to these detectors can be suggested to optimize performance when utilizing a permanent image magnet focus design.

Task 5

Develop and analyze one or more conceptual designs of permanent magnet focusing assemblies to operate with a class of imaging detectors similar to those referenced above but incorporating variable gain features. It can be assumed that two or three discrete gain levels covering a total gain variation of 20:1 are to be achieved by discrete charges of the accelerating potential between the photocathode and target within the imaging section of the detector. The precise gain levels should be prescribed by the study to allow simplified but optimal performance of the imaging section. A SIT type of detector in the configuration given by the WX31958 detector above may be used for reference purpose for this task.

Task 6

Specify and analyze the shielding requirements for the designs developed. Shielding against external fields shall be considered in as much as it affects the design configuration. Material specification and relevant physical properties, e.g., saturability shall be discussed.

Documentation

Monthly technical progress reports due the 15th of each month beginning the 1st month after award of contract.

Final Report due one month after completion of all tasks.

APPENDIX B

FOCUSSING OF PHOTOELECTRONS WITH PARALLEL ELECTRIC AND MAGNETIC FIELDS THAT ARE SPATIALLY PERFECTLY UNIFORM

If in a TV tube's image section the focussing E and B fields are both spatially uniform and parallel, the equations of motion for the photoelectrons (pe) become most simple. Under these conditions the following three questions can be easily answered: (1) how sensitive is the focus on the form of the angular emission of pe's at the photocathode (PC); (2) what is the depth-of-focus; and, (3) what is the point spread function of the pe's at the target.

As is well known, for parallel, uniform E and B fields the equations of motion for a pe are easily decomposed into two independent components - one transverse to the fields (x,y plane), and one parallel to the fields (z-axis). Here the z-axis is taken perpendicular to the PC and runs parallel to the fields; and, without loss of generality, the point of emission on the PC is located at the origin. Thus, the equations (Gaussian units) of interest are:

Axial Equations

$$a_a = qE/m$$
$$v_a = qEt/m + v_o\cos\theta$$
$$z = \tfrac{1}{2}qEt^2/m + v_o t\cos\theta$$

Transverse Equations

$$a_t = (qBv_o\sin\theta)/mc$$
$$v_t = v_o\sin\theta$$
$$R_t = (mcv_o\sin\theta)/qB, \qquad (1)$$

where E is the electric field, B is the magnetic induction, t is the time, v_o is the initial total velocity, θ is the angle of emission of a pe from the PC ($\theta = 0^o$ along the z-axis), q and m are an electron's charge and mass, and c is the speed of light. The transverse spatial coordinate, R_t, is the radius of the Larmor circle executed in the x,y plane by a pe in a period

$$P = 2\pi cm/qB, \qquad (2)$$

and with center located at $(0,R_t,z(t))$.

At any distance L along the z-axis the above equations give the relationships:

$$\text{transit time} = T = (-v_o\cos\theta + (v_o^2\cos^2\theta + 2qEL/m)^{\frac{1}{2}})/(qE/m), \qquad (3)$$

and

$$\text{impact radius} = r_i = 2^{\frac{1}{2}}\cdot R_t\cdot(1 - \cos(2\pi T/P))^{\frac{1}{2}}, \qquad (4)$$

where the impact radius is the radial distance to the pe relative to the time-shifted origin (0,0,L). Eq.'s (1)-(4) are sufficient to numerically determine answers to the three questions posed. Assuming for representative operating conditions that B = 80 gauss and a potential difference of 8000 volts exists between the PC and a target at z = L, the above equations become:

$$R_t = 7.10219\times10^{-6}\cdot v_o \sin\theta \quad \text{microns} \tag{1'}$$

$$P = 4.42644\times10^{-9} \quad \text{seconds} \tag{2'}$$

$$T = ((-v_o\cos\theta + (v_o^2\cos^2\theta + 2.81409\times10^{19})^{\frac{1}{2}})/1.17791\times10^{18})\cdot L/L_o \quad \text{seconds} \tag{3'}$$

$$r_i = 1.41412\cdot R_t\cdot(1 - \cos(8.06734\times10^{10}\cdot T))^{\frac{1}{2}} \quad \text{microns} \tag{4'}$$

where L_o is 11.94526 cm and the argument of the cosine in (4') is in degrees.

The Eq.'s (1')-(4') are the basis for studying the pe's emitted from an UV PC for two assumed angular emission characteristics: Case 1 - the emission is Lambertian (probability of emission = $\cos\theta$); Case 2 - the probability of emission is independent of angle (= 1 for $0^o \leq \theta \leq 90^o$). The distribution of energies for the emitted pe's assumed is that shown in Figure III. For both cases 1 and 2 the sample angles and energies for the calculations are those at which the integrals of the respective probability distributions take on the values of 0.05, 0.15, .. , 0.95, for a total of one hundred 'trajectories'. Choosing the variables in this way means that each calculation for a given angle and energy of emission is a good representative of 1% of all the pe's emitted from the PC. A series of calculations were performed for different values of the PC-to-target separation (L) appropriate for single-loop focussing.

In Table I the percentage (= number) of pe's striking within various annuli centered at (0,0,L) on the target are given as a function of L. The results in Table I show that: (1) the focus is insensitive to the angular distribution of emission; and, (2) the depth-of-focus for both cases is approximately 1 mm.

By an approximate calculation best focuses should occur at the values of L = 11.94526 cm and L = 11.92515 cm for cases 1 and 2, respectively. The detailed points of impact on the target were printed out for these two cases. For case 1 the plots of the loci of the impact points on the target as θ varies for five energies are shown in Fig. I. For illustrative purposes the graph is constructed so that the negative-x impacts correspond to those pe's with T's less than P, while positive-x impacts are for pe's with T's greater than P. All impacts lie virtually along the x-axis, as the Larmor radii for all pe's are much larger than the impact radii (in Fig. I the y-axis is expanded by a factor of 100).

In Fig. II the details of the impacts for cases 1 and 2 are compared for an L = 11.92 cm. The plot of I versus impact radius shows that the half-width at half-maximum point in both cases is of the order of 1 micron, indicating a limiting resolution of approximately 500 lp/mm. The integrals of I are seen to take on the value of 0.5 at 2.75 and 4.25 microns for cases 1 and 2, respectively. This indicates that good resolution for the cases 1 and 2 can be obtained at 180 and 120 lp/mm, respectively.

Best focus is at that L where $\bar{T} = P$. Using Eq.'s (2) and (3) gives:

$$L \propto \bar{v}\bar{T}$$

$$L \propto V^{\frac{1}{2}}B^{-1}$$

or

$$L = \text{const.}V^{\frac{1}{2}}B^{-1}, \tag{5}$$

where V is the potential between the PC and the target. Eq. (5) shows that

the focus point shifts with variations in V and B according to the relation:

$$\delta L/L = \tfrac{1}{2}(\delta V/V) - (\delta B/B). \qquad (6)$$

During an exposure the obvious variational constraint is that the focus not move by more than half the depth-of-focus. The results of Table I give

$$\tfrac{1}{2}(\text{depth-of-focus})/L \sim 0.05/12 = 0.004. \qquad (7)$$

Comparison of Eq.'s (6) and (7) indicates that the focus fields must be held stable during an exposure to within 0.3%.

Acknowledgement: I wish to thank Mr. D. Hei of GSFC for his aid in programming the equations on the Tektronix 31 computer.

Thomas Kelsall
Code 601
Goddard Space Flight Center
Greenbelt, MD 20771

TABLE I

THE PERCENTAGE OF PHOTOELECTRONS FALLING WITHIN SELECTED ANNULI AS A FUNCTION OF THE TARGET DISTANCE (L) FOR THE OPERATING CONDITIONS OF B = 80 GAUSS AND V = 8000 VOLTS.

	Case 1: Photoelectron Emission Probability = Cosθ						Case 2: Photoelectron Emission Probability Independent of Emission Angle (θ)					
	Radii (microns) of the Annuli						Radii (microns) of the Annuli					
L (cm)	0 to 1.5	1.5 to 5.0	5 to 10	10 to 20	20 to r_{max}	r_{max}	0 to 1.5	1.5 to 5.0	5 to 10	10 to 20	20 to r_{max}	r_{max}
11.60	1	7	8	18	66	122.7	0	4	7	12	77	122.8
11.70	2	10	11	23	54	88.92	1	6	8	20	65	88.86
11.80	5	18	18	33	26	58.15	2	17	21	34	26	58.10
11.85	17	22	26	22	13	43.55	23	23	23	20	11	43.55
11.88	24	36	18	16	6	35.82	21	35	26	13	5	35.82
11.90	32	35	18	9	6	30.66	23	34	23	15	5	30.66
11.91	35	33	20	7	5	28.08	26	28	28	13	5	28.09
11.92	34	39	17	6	4	25.52	24	34	17	19	6	26.12
11.93	38	31	17	11	3	23.34	27	27	22	19	5	30.13
11.94	37	32	16	13	2	21.16	25	27	19	22	7	34.14
11.95	34	32	19	15	0	18.98	24	25	20	23	8	38.16
11.96	34	28	19	19	0	19.48	24	21	19	25	11	42.17
11.98	26	29	23	16	6	26.31	17	21	20	25	17	50.19
12.00	22	26	25	19	8	33.92	14	19	19	24	24	58.21
12.05	13	21	20	24	22	52.94	11	11	13	25	40	78.25
12.10	10	12	15	28	35	71.95	2	10	12	22	54	98.28
12.20	1	10	12	20	57	109.9	0	10	2	15	73	138.3
12.30	0	10	5	16	69	147.8	0	3	8	9	80	178.2

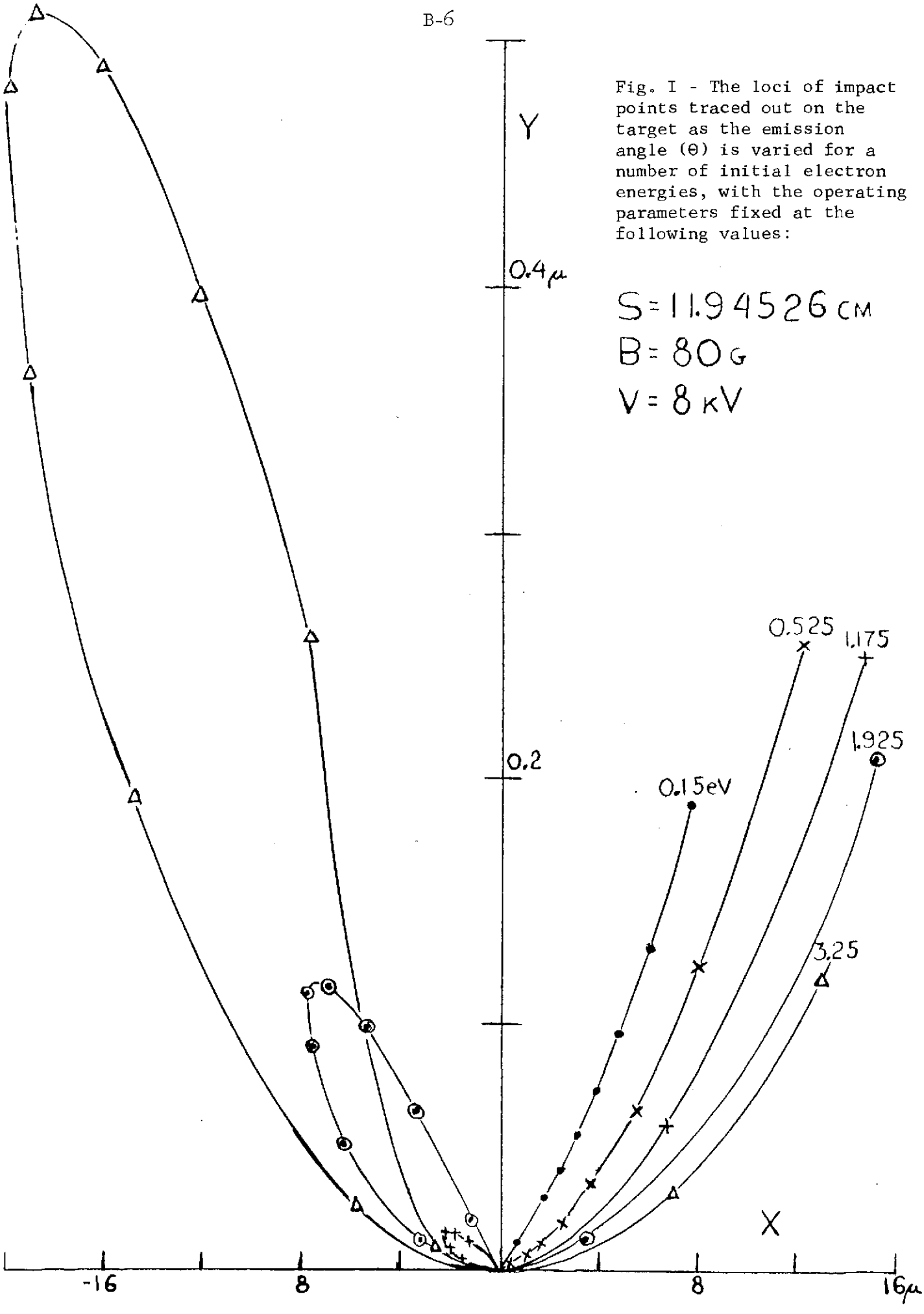

Fig. I - The loci of impact points traced out on the target as the emission angle (Θ) is varied for a number of initial electron energies, with the operating parameters fixed at the following values:

S = 11.94526 CM

B = 80 G

V = 8 KV

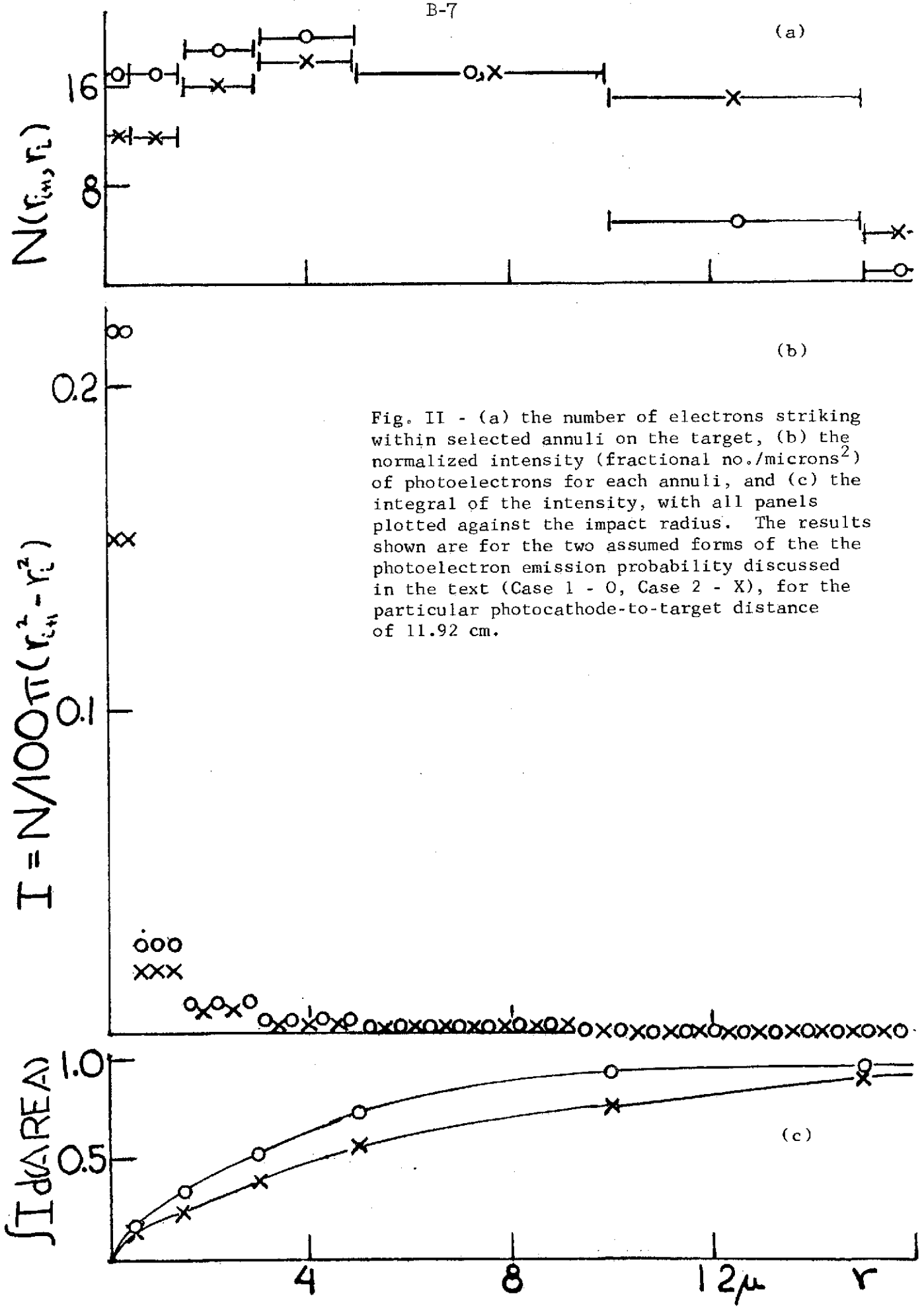

Fig. II - (a) the number of electrons striking within selected annuli on the target, (b) the normalized intensity (fractional no./microns^2) of photoelectrons for each annuli, and (c) the integral of the intensity, with all panels plotted against the impact radius. The results shown are for the two assumed forms of the the photoelectron emission probability discussed in the text (Case 1 - O, Case 2 - X), for the particular photocathode-to-target distance of 11.92 cm.

Figure III

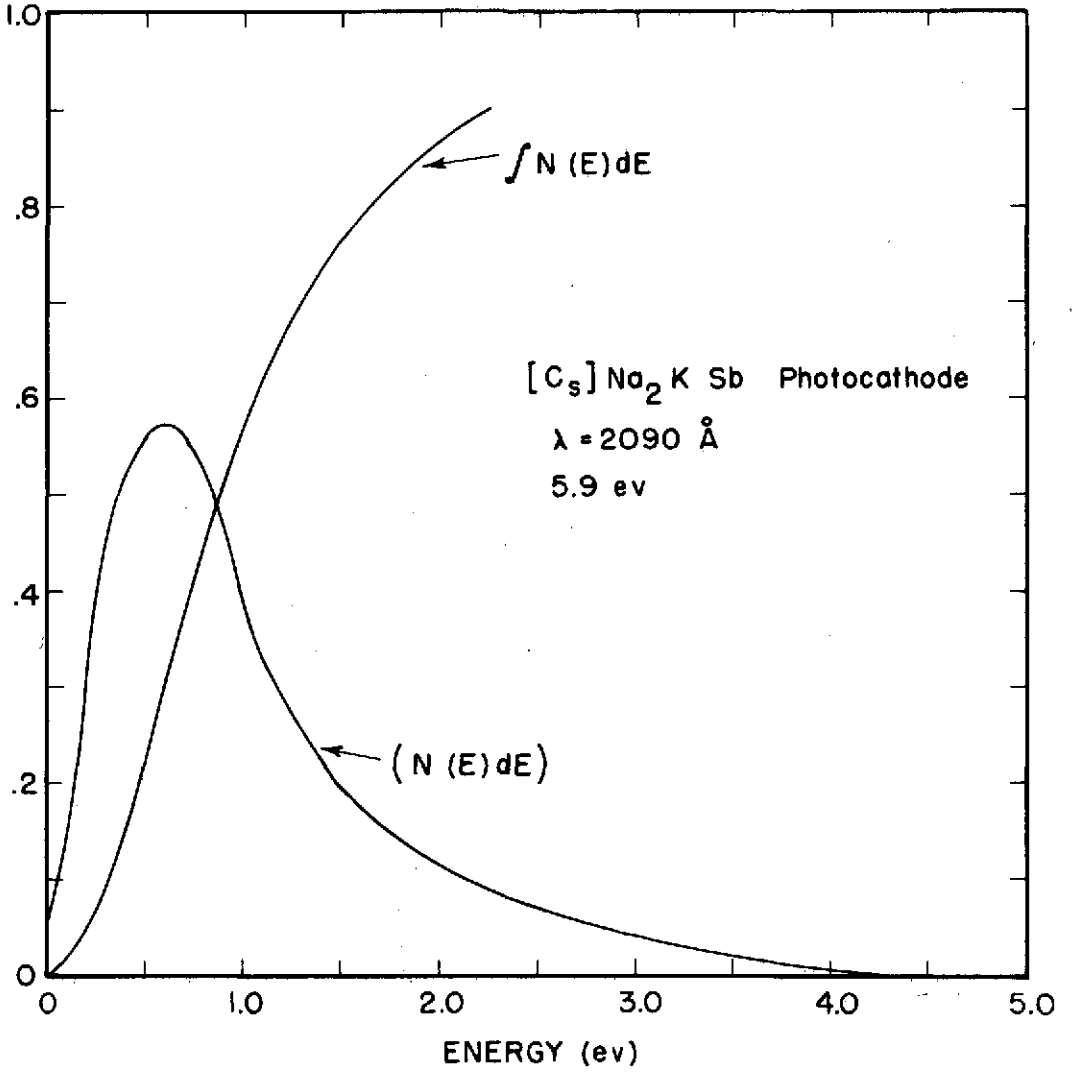
1.0
.8
.6
.4
.2
0
0
1.0
2.0
3.0
4.0
5.0
ENERGY (ev)
∫N (E)dE
(N (E)dE)
[Cs] Na2 K Sb Photocathode
λ = 2090 Å
5.9 ev